

The Promise of Transmutation

Los Alamos National Laboratory, Argonne National Laboratory
Oak Ridge National Laboratory, Pacific Northwest National Laboratory
Brookhaven National Laboratory, Lawrence Livermore National Laboratory
Idaho National Engineering and Environmental Laboratory, Idaho Accelerator Center
University of Nevada, University of Michigan, University of California, University of Texas
Burns & Roe, Enterprises, Inc., General Atomics, Westinghouse Savannah River Company

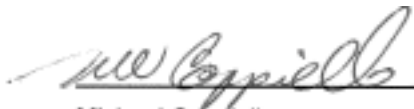
This page left intentionally blank

AAA Technical Quarterly Report October–December 2001

LA-UR-02-0724

AAA-PDO-GEN-02-0005

Approval



Michael Cappiello
LANL AAA Program Manager
Advanced Accelerator Applications

Date 2/13/02

This page left intentionally blank

Table of Contents

Major Contributors	ix
List of Figures	xi
Acronyms and Symbols	xiii
I. INTRODUCTION	1
II. HIGHLIGHTS	3
III. TECHNOLOGY DEVELOPMENT	5
1. FUELS DEVELOPMENT	5
Scope	5
Highlights	5
Fabrication Development	6
Metal Fuel.....	6
Nitride Fuel.....	6
Metal Fuels Irradiation Testing.....	7
ATW-1 Irradiation Test	7
ATW-3 Irradiation Test	8
Nitride Fuel Performance	8
Assessment of Radiation Tolerance	8
Radiation Damage	8
Fuel Qualification	10
Metal Fuel.....	10
Transmuter Fuel Development Workshop.....	10
Fuel Design.....	11
Nitride and Oxide Modeling	11
Atomic Scale Modeling of Nuclear Fuels.....	13
2. SEPARATIONS TECHNOLOGY	15
Scope	15
Highlights	15
LWR Spent Fuel Treatment — Optimized UREX Process Demonstration.....	16
Uranium.....	18
Technetium	19
Plutonium	21
Neptunium.....	22
Conclusions.....	22
Radiation Stability of Acetohydroxamic Acid.....	22
Dose Calculation.....	23
Irradiation Tests	23
Experimental Method.....	23
Results	24
Discussion.....	24
Treatment of UREX Raffinate Stream	25
Reference Flowsheet.....	25
Alternate Flowsheet.....	26
TRISO Fuel-Processing Development	26

3. TRANSMUTATION SCIENCE	28
3.1 Integration and Analytical Support.....	28
Scope	28
Highlights	29
Spallation Target and Materials Research Plan	29
LBE-Sodium Compatibility Experiments.....	30
Product Inventories for Na-Cooled Tungsten and LBE Targets.....	33
Scoping Calculation for the Neutron Yield Experiments.....	34
3.2 Materials	35
Scope	35
Highlights	36
High-Temperature Testing of Structural Materials.....	36
Hot-Cell Work	37
Materials Handbook	37
TEM Analyses of Irradiated Steel Samples.....	37
Tungsten Compression Testing.....	38
3.3 Lead-Bismuth Eutectic Technology	40
Scope	40
LBE Technology Development	40
DELTA Loop Operations	40
Highlights	41
DELTA Loop	41
Lead-Bismuth Eutectic Research	43
3.4 LANSCE Irradiation Experiments.....	43
Scope	44
Sodium Activation Tests.....	44
Neutron Yield and Spectrum Tests.....	44
Helium and Hydrogen Production Tests.....	44
Corrosion Studies	45
Highlights	45
Sodium-Activation Tests	45
Neutron Yield and Spectrum Tests.....	46
Foil Counting.....	47
Helium and Hydrogen Production Tests	48
Corrosion Studies	50
3.5 High-Energy Physics	51
Scope	51
MCNPX Code Development	51
Nuclear Data Evaluations.....	51
Highlights	52
MCNPX Code Development	52
Nuclear Data.....	53
CINDER90 Update	53
3.6 Reactor Physics.....	53
Scope	54
Experiment and Safety Analysis	54
Physics Needs and Methods Development	54
Physics Experiment Planning	54
Highlights	55

MUSE Benchmark	55
Uncertainty Assessment.....	55
3.7 International Support.....	64
Scope	64
Highlights	64
MEGAPIE.....	64
4. SYSTEMS TECHNOLOGIES.....	65
Scope	65
Accelerator-Driven Test Facility	65
ADS Preconceptual Reference Design.....	65
Accelerator-Driven Coupling Proof-of-Performance Experiments.....	66
Highlights	66
Target and Material Test Station.....	66
Subcritical Multiplier.....	66
Balance of Facility.....	66
Target and Materials Test Station.....	66
Target Design	69
Subcritical Multiplier — 100 MW	74
Accelerator-Driven Coupling Proof-of-Performance Experiments	74
ADTF Documentation	76
SCM Preconceptual System Design Description	76
SCM Target Design Completion and Documentation	78
Balance of Facility Design	78
International Support	79
5. PROJECT INTEGRATION.....	80
Scope	80
5.1 Systems and Technology Integration	80
5.2 University Programs	81
Scope	81
Highlights	81
American Nuclear Society Winter Meeting, Reno, NV	81
AAA University Participation Program	81
AAA Idaho Accelerator Center	82
AAA University Fellowship Program	82
AAA Directed University Research	82
Technical Progress.....	82
5.3 Collaborations.....	83
Scope	83
5.4 Report to Congress	83
Supplemental Analyses	84

This page left intentionally blank

Major Contributors

Fuels Development: D. Crawford (ANL)
K. Chidester (LANL)
M. Meyer (ANL)
S. Hayes (ANL)
R. Margevicius (LANL)
K. McClellan (LANL)

Separations Technology: J. Laidler (ANL)

Transmutation Science: K. Pasamehmetoglu (LANL)
E. Pitcher (LANL)
L. Waters (LANL)
M. James (LANL)
M. Chadwick (LANL)
N. Li (LANL)
V. Tcharnotskaia (LANL)
S. Wender (LANL)
S. Maloy (LANL)
B. Haight (LANL)
G. Morgan (LANL)
S. Lillard (LANL)
R. Klann (LANL)
G. Palmiotti (ANL)

Systems Technologies: M. Cappiello (LANL)
S. McConnell (LANL)
K. Pasamehmetoglu (LANL)
J. Roglans (ANL)
R. Guffee (LANL)
H. Cohen (BREI/GA)
J. Herceg (ANL)

Project Integration: G. Van Tuyle (LANL)
W. Davidson (LANL)
D. Beller (LANL)
A. Hechanova (UNLV)
F. Goldner (DOE-HQ)
R. Matthews (LANL)
D. Hill (ANL)

This page left intentionally blank

List of Figures

Fig. 1.	Void formation at the grain boundaries due to ion implantation.	8
Fig. 2.	Twin formation observed in Xe-implanted ZrN.	9
Fig. 3.	SEM image of Xe-implanted area (left side of micrograph) and masked area (right side) with the corresponding EDS line scan of Xe content (bottom).	9
Fig. 4.	Gibbs free energy of CeN, ZrN, UN, and PuN.	12
Fig. 5.	Gibbs free energy of formation of CeN, ZrN, UN, and PuN.	13
Fig. 6.	Gibbs free energy of PuO ₂ -x.	14
Fig. 7.	Revised preliminary Ce-O phase diagram.	14
Fig. 8.	As-run extraction, scrub, U-re-extraction, and Tc-strip sections for the UREX cold demonstration run completed in September.	17
Fig. 9.	As-run uranium strip section of the flowsheet for the UREX cold demonstration run completed in September.	17
Fig. 10.	Aqueous-phase concentration profile for isotope 238 in the extraction and scrub sections of the September 2001 UREX demonstration vs. AMUSE predictions as a function of stage efficiency. Uranium is removed from the aqueous solution as it passed from stage 12 to stage 1. Below stage 8, only Pu-238 is measured by ICP-MS.	19
Fig. 11.	Temperature profile calculated for the first 33 stages of the September 2001 UREX demonstration. The extraction section was stages 1-12; the scrub section was stages 13-16; the Tc-product U-re-extraction section was stages 17-25; and the Tc-strip section was stages 26-33.	20
Fig. 12.	Experimental and AMUSE-predicted aqueous-phase concentration profile for technetium in the extraction and scrub sections of the September 2001 UREX demonstration. Using the temperature profile for individual stages greatly enhances the fit of the AMUSE model to the experimental data.	20
Fig. 13.	Experimental and calculated stage-wise concentration profile for plutonium in the extraction (stages 1-12) and scrub (stages 13-16) sections of the September 2001 countercurrent demonstration of the UREX process.	21
Fig. 14.	Experimental and calculated stage-wise concentration profile for neptunium in the extraction (stages 1-12) and scrub (stages 13-16) sections of the September 2001 countercurrent demonstration of the UREX process.	22
Fig. 15.	AHA absorbance as a function of radiation dose.	25
Fig. 17.	Experimental facilities and programs to support the proof-of-performance phase of spallation target and materials development.	30
Fig. 18.	Experimental setup for the LBE-sodium compatibility tests.	31
Fig. 19.	Temperature traces for the 600°C mixing tests.	32
Fig. 20.	Spallation and activation products comparison for the LBE and sodium-cooled tungsten targets.	33
Fig. 21.	Image of surface flux of Pb-Bi target. (X axis is in degrees, y axis is in position along target. Color denotes neutron flux intensity).	34
Fig. 22.	Time necessary to get sufficient counts for adequate statistics at various energies.	35
Fig. 24.	Effect of dose on fractional percent of Frank loop size.	38
Fig. 25.	Compression testing of wrought tungsten.	39

Fig. 26.	Compression stress/strain curves tested at 25°C for tungsten manufactured by powder metallurgical (PM)-wrought, PM-wrought and annealed, chemical vapor deposition (CVD) and vapor plasma spray (VPS).	39
Fig. 27.	Pump power vs. flow rate curves.....	43
Fig. 28.	Foils mounted on the LBE target in the Blue Room.	47
Fig. 29.	Bismuth foil measured twice at about 20-hr interval in the 700–900-keV region.	48
Fig. 30.	Interactions of neutrons with materials produce charged particles that stop either in the material or in neighboring materials.	49
Fig. 31.	Identification of protons, deuterons, tritons, ^3He , and alpha particles from this quarter's experiment of neutron interactions with iron.	50
Fig. 33.	Uncertainties by isotopes on ϕ^* , where $\phi^* = 8.21\text{E-}1$	57
Fig. 34.	Uncertainties by isotopes on dpa at the boundary between the core and buffer.	58
Fig. 35.	Uncertainties by isotopes on helium production at the boundary between the core and buffer.	58
Fig. 36.	Uncertainties by isotopes on hydrogen production at the boundary between the core and buffer.....	59
Fig. 37.	Uncertainties by isotopes on helium production to DPA ratio at the boundary between the core and buffer, where $(n,\alpha)/\text{DPA} = 1.84\text{E-}01$	59
Fig. 38.	ADMAB benchmark R-Z model.	60
Fig. 39.	Uncertainty on reactivity level of the ADMAB benchmark, where $K_{\text{eff}} = 0.94930$	61
Fig. 40.	Uncertainty on source importance factor of the ADMAB benchmark, where $\phi^* = 0.8941$	61
Fig. 41.	Uncertainty on max DPA of the ADMAB benchmark, where $\text{dpa} = 4.48 \times 10^{-3}/\text{s}$	62
Fig. 42.	Uncertainty on max helium production of the ADMAB benchmark, where $(n,\alpha) = 1.16 \times 10^{-3}/\text{s}$	62
Fig. 43.	Uncertainty on max hydrogen production of the ADMAB benchmark, where $(n,p) = 3.49 \times 10^{-8}/\text{s}$	63
Fig. 44.	Uncertainty on max helium/dpa of the ADMAB benchmark, where $(n,\alpha)/\text{DPA} = 0.260$	63
Fig. 45.	TMT first floor plan view.	67
Fig. 46.	Irradiation chamber elevation view.	68
Fig. 47.	Target trolley isometric view.	68
Fig. 48.	(a) Proton and (b) fast (>0.1 MeV) neutron flux spatial distributions for an annular target.	70
Fig. 49.	Energy dependence of neutrons responsible for atomic displacements and helium production in stainless steel located in the fuel test region.	71
Fig. 50.	Softening of the neutron flux spectrum in the fuel test region through the use of a depleted uranium buffer.	72
Fig. 51.	Proton and fast neutron flux spatial distributions for a depleted uranium target and buffer.	73
Fig. 52.	SCM plan view.....	77
Fig. 53.	SCM elevation.	77
Fig. 54.	Time-dependent simulation of the shutdown of the installed capacity of the present fleet of commercial reactors and the buildup of waste in cooling ponds (a 60-year plant-life is assumed).	85

Acronyms and Symbols

AAA	Advanced Accelerator Applications
AC	Accelerating cavities
ADS	Accelerator-Driven System
ADTF	Accelerator-Driven Test Facility
ADMAB	Accelerator-Driven Minor Actinide Burner
AES	Advanced Energy Systems (formerly Northrup-Grumman Corp.)
AET	Ability Engineering Technology
AFM	Atomic Force Microscopy
Ah	Ampere-Hour
AHA	Acetohydroxamic acid
Am	Americium
AMUSE	Argonne Model for Universal Solvent Extraction, the generic TRUEX model expanded to include UREX and PUREX processing
ANL	Argonne National Laboratory (Chicago)
ANL-W	Argonne National Laboratory-West (Idaho Falls)
ANRC	Amarillo National Research Center
ANS	American Nuclear Society
ANSYS	structural analysis modeling code
appm	atomic parts per million
APT	Accelerator Production of Tritium
ASME	American Society of Mechanical Engineers
ATR	Advanced Test Reactor (INEEL)
ATW	Accelerator Transmutation of Waste
Ba	Barium
BCM	Beam-Current Monitor
BCP	Baseline Change Proposal
BCP	Buffered Chemical Polishing
Be	Beryllium
Beta (β)	Ratio to the speed of light
Bi	Bismuth
BISTRO	Two-Dimensional Discrete Ordinates Code
BNFL	British Nuclear Fuels, Ltd
BNL	Brookhaven National Laboratory
BOF	Balance of Facility
BOL	Beginning of Life
BOP	Balance of Plant
BOR-60	Sodium-Cooled Fast Reactor (Dmitrovgrad, Russia)
BPM	Beam-Position Monitor
CCDTL	Coupled-Cavity Drift-Tube Linac
CCL	Coupled-Cavity Linac
Ce	Cerium
CEA	Commissariat à l'Energie Atomique (France)
CEM	Cascade Exciton Model code (Model-based Monte-Carlo particle transport code)
CERCA	Compagnie Pour L'Etude Et La Realisation De Combustibles Atomiques
cercer	Ceramic-Ceramic
cermet	Ceramic-Metal
CFD	Computational Fluid Dynamics
CINDER90	Computer Code
CLWR	Commercial Light-Water Reactor
Cm	Curium
CMPO	Neutral Extractant
CMR	Chemistry and Metallurgy Research (facility at LANL)
CONCERT	Combined Neutron Center for European Research and Technology

Cs	Cesium
Cu	Copper
CVD	Chemical Vapor Deposition
cw	Continuous Wave (100% duty factor)
DACS	Data Acquisition and Control System
DAS	Data Acquisition System
DCR	Design Change Request
DDN	Design Data Need
DIAMEX	Aqueous Solvent Extraction Process for TRU Recovery
DOE	Department of Energy
dpa	Displacements per Atom
EBR	Experimental Breeder Reactor
ED&D	Engineering Development and Demonstration
EDS	Energy Dispersive Spectrometry
EPFD	Effective Full-Power Day
EFTTRA-T4	Radiation Test Sponsored by the European Union
EIS	Electrochemical Impedance Spectroscopy
EIS	Environmental Impact Statement
ENDF	Evaluations that can be used in MCNPX for more accurate predictions of fission, criticality, transport, and radiation damage
EOI	End of Irradiation
EOL	End of Life
EPICS	Experimental Physics and Industrial Control System
ERANOS	Computer modeling code
ERC	External Review Committee
ES&H	Environmental, Safety, and Health
ESS	European Spallation Source
ESSAB	Energy System Acquisition Advisory Board (DOE)
Eu	Europium
FDD	Facility Design Description
Fe	Iron
FFTF	Fast Flux Test Facility
FMF	Fuel Manufacturing Facility
FODO	Focus-Drift-Defocus-Drift
FPY	Full-Power Year
FWHM	Full Width Half Maximum
FZJ	Forschungs Zentrum Jülich (German Laboratory)
FZK	Forschungs Zentrum Karlsruhe (German Laboratory)
g/L	Grams per Liter
GA	General Atomics Inc.
GNASH	Nuclear Reaction Code
GSI	Gesellschaft für Schwerionenforschung (Darmstadt, Germany)
GT-MHR	Gas Turbine Modular Helium Reactor
H	Hydrogen
HAN	Hydroxylamine
HCP	Hazard Control Plan
He	Helium
HEBT	High-Energy Beam Transport
HEU	Highly Enriched Uranium
Hf	Hafnium
HFIR	High Flux Isotope Reactor (ORNL)
HFR	High Flux Reactor (Petten, Netherlands)
HIP	Hot Isostatic Process (for bonding materials)
HM	Heavy Metal
HPRF	High-Power Radio Frequency
HS/WS	Halo-Scraper/Wire-Scanner (diagnostic device)

HX	Heat Exchanger
I&C	Instrumentation and Control
IAC	Idaho Accelerator Center
IAEA	International Atomic Energy Association (Vienna, Austria)
ICP-MS	Inductively Coupled Plasma-Mass Spectrometry
ICS	Integrated Control System
IFMIF	International Fusion Materials Irradiation Facility
IFR	Integral Fast Reactor
IHX	Intermediate Heat Exchanger
IMS	Information Management System
INEEL	Idaho National Engineering and Environmental Laboratory
IPBT	In-Pile Beam Tube
IPPE	Institute of Physics and Power Engineering, Obninsk, Russia.
ISABEL	Physics Modeling Code
ISTC	International Science and Technology Centre (Moscow)
ITER	International Thermonuclear Experimental Reactor
ITU	Institute for Transuranium Elements (Karlsruhe, Germany)
JAERI	Japan Atomic Energy Research Institute
JCNNM	Johnson Controls Northern New Mexico
JLAB	Jefferson Laboratory (VA)
K	Potassium
KAERI	Korean Atomic Energy Research Institute
KEK	National Laboratory for High-Energy Physics (Tsukuba, Japan)
keV	Kiloelectron Volt
LA150n	Los Alamos generated nuclear data library, extending up to 150 MeV
LAHET	Los Alamos High-Energy Transport
LANL	Los Alamos National Laboratory
LANSCE	Los Alamos Neutron Science Center
LBE	Lead-Bismuth Eutectic
LBHM	Low- β Hot Model
L/d	Length-to-Diameter Ratio
L/hr	Liter per Hour
LEBT	Low-Energy Beam Transport
LEDA	Low-Energy Demonstration Accelerator
LINAC	A computer code based on PARMILA that has been modified to include CCDTL and SCRF elliptical cavities as options
LLFP	Long-Lived Fission Product
LLNL	Lawrence Livermore National Laboratory
LLRF	Low-Level Radio Frequency
LMR	Liquid-Metal Reactor
LWR	Light-Water Reactor
<u>M</u>	Molar
MA	Minor Actinide
mb	Millibarn
MCA	Multi-Criteria Analysis
mCi	Millicurie
MCNP	Monte Carlo N-Particle Transport Code
MCNPX	Merged code—Los Alamos High-Energy Transport (LAHET) and Monte Carlo N-Particle Codes (MCNP)
MDD	Modified Direct Denitration
MEGAPIE	MEGAwatt Pilot Experiment
MFM	Magnetic Flow Meter
MIT	Massachusetts Institute of Technology
mL	Milliliter
Mo	Molybdenum
MOX	Mixed oxide fuel

mR	Millirad (a measure of radiation)
MT	Metric Ton
MTL	Materials Test Loop
MW	Megawatt
MWD/T	Megawatt Days per Ton (standard unit for burnup)
MWth	Megawatt Thermal
N	Nickel or Nitride
Np	Neptunium
n/p	Neutrons per Proton
NDA	Nondestructive Analyses
NEA	Nuclear Energy Agency (Paris)
NEPA	National Environmental Protection Agency
NERAC	Nuclear Energy Research Advisory Committee
NERI	Nuclear Energy Research Initiative
NFC	Nuclear Fuel Cycle
NFF	Nonfertile Fuel
O	Oxygen or Oxide
O&M	Operations and Maintenance
OECD	Organization for Economic Cooperation and Development (Paris)
ORIGEN	A computer code system for calculating the buildup, decay, and processing of radioactive materials
ORNL	Oak Ridge National Laboratory
P&ID	Piping and Instrumentation Diagram
PACS	Personnel Access Control System
PARMTEQM	RFQ simulation code
Pb	Lead
PCM	Pulse Control Modulation
Pd	Paladium
PFD	Process Flow Diagram
PHA	Preliminary Hazards Assessment
PHENIX	Fast Reactor in France
PIE	Post-irradiation examination
PNNL	Pacific Northwest National Laboratory
POP	Proof of Performance, Proof of Principle
PRAD	Proton Radiography
PRISM	Power Reactor Innovative Small Module
PSAR	Preliminary Safety Analysis Report
PSS	Personnel Safety System
PSI	Paul Scherrer Institute (Switzerland)
Pu	Plutonium
PUREX	Plutonium-Uranium Extraction
PWR	Pressurized Water Reactor
PYRO	Pyrochemical process
Q	Quality factor
QA	Quality Assurance
QAC	Quick ATW Costing
R	Rad (a measure of radiation)
RAMI	Reliability, Availability, Maintainability, and Inspectability
RBS	Rutherford Backscattering Spectrometry
RERTR	Reduced Enrichment for Research and Test Reactors program
RF	Radio Frequency
RFQ	Radio-Frequency Quadrupole
RCCS	Resonance-Control Cooling System
RIA	Rare Isotope Accelerator
RIAR	Russian Institute of Atomic Reactors
rms	root mean square

RRR	Residual Resistance Ratio
RSICC	Radiation Safety Information Computational Center
RTD	Surface Temperature Detector
RTH	Royal Institute of Technology (Stockholm, Sweden)
Ru	Ruthenium
SAA	Systems Approaches Analysis
SANEX	Aqueous Solvent Extraction Process for Am and Cm Recovery
SAR	Safety Analysis Report
SC	Superconducting
SCM	Subcritical Multiplier
SCRF	Superconducting RF
SDD	System Design Description
SEM	Scanning Electron Microscopy
SFT	Stacking-Fault Tetrahedral
SHR	shutdown heat-removal
SINQ	Spallation Neutron Source at Paul Scherrer Institute (Switzerland)
SNF	Spent Nuclear Fuel
SNL	Sandia National Laboratory
SRS	Savannah River Site
SRTC	Savannah River Technology Center
Star-CD	Computational fluid dynamics code
STAYSL2	A computer code used to analyze the results of the activation foil measurements in both a proton and neutron flux
STP	Standard Temperature and Pressure
STIP	Spallation Target Irradiation Program (at PSI)
T/p	Tritons (nucleii of tritium atoms) per Proton
T/B	Target / Blanket
Ta	Tantalum
TBP	Tri- <i>n</i> -butyl Phosphate or Tributylphosphate
Tc	Technitium
TEM	Transmission Electron Microscopy
TESLA	International Collaboration on a TeV Superconducting Linear Accelerator
TGA	Thermal Gravimetric Analysis
TJNAF	Thomas Jefferson National Accelerator Facility
TMT	Target and Materials Test Station
TRAC	Transient Reactor Analysis Code
TRACE 3-D	Interactive computer code that calculates the envelopes of a bunched beam through a user-defined transport system
TREAT	Transient Reactor Test Facility
TRISO	Tri-isotropic, referring to a multi-layered fuel-particle coating consisting of pyrolytic carbon and silicon carbide
TRISPAL	Refers to the French APT Program
TRL	Technical Readiness Level
TRU	Transuranics (americium, curium, neptunium, and plutonium)
TRUEX	Aqueous solvent extraction process for TRU recovery
U	Uranium
UFP	University Fellowship Program
UNLV	University of Nevada Las Vegas
UPP	University Participation Program
UREX	Uranium Extraction (an aqueous partitioning process)
URP	University Research Program
USQD	Unreviewed Safety Question Determination
V	Vanadium
VPS	Vapor Plasma Spray
VARIANT	Three-Dimensional Nodal Transport Code
W	Tungsten

WBS	Work Breakdown Structure
WNR	Weapons Neutron Research (facility at LANL)
WPPT	Working Party on Partitioning and Transmutation
WSRC	Westinghouse Savannah River Company
Xe	Xenon
XRD	X-ray Diffraction
Y	Yttrium
ZPPR	Zero Power Physics Reactor
Zr	Zirconium

Advanced Accelerator Applications

Quarterly Report

October–December 2001

I. INTRODUCTION

The Advanced Accelerator Applications (AAA) Program, a Department of Energy (DOE) program commissioned by Congress in FY2000, is a national effort consisting of DOE laboratories (Los Alamos, Argonne, Savannah River, Livermore, Oak Ridge), industry (Burns and Roe Engineering Inc, General Atomics) and universities (UC-Berkeley, Texas, Michigan, Nevada). The primary mission of the AAA Program is to develop the technology base for the transmutation of nuclear waste and to demonstrate its practicality and value for long-term waste management.

The AAA Program was constituted by combining two programs: The Accelerator Production of Tritium (APT) Program and the Accelerator Transmutation of Waste (ATW) Program. The APT Program was established in 1995 with a commercial light-water reactor (CLWR) program as part of a dual-path strategy for development of a new tritium-production technology for the nation. From 1995 through 2001, DOE-Defense Programs invested in the design and development of an accelerator to produce tritium, including a full-scale prototype of the front end of the accelerator. In December 1998, the DOE chose the CLWR as the primary technology for tritium production, leading to the closeout of APT at the end of FY01. The ATW Program, which was investigating the feasibility of accelerator-driven systems to transmute long-lived toxic components of spent nuclear fuel. Together, benefit from the technology development of APT.

The goal of the AAA Program is to evaluate the effectiveness of transmutation of spent nuclear fuel against the following criteria:

- (1) Reduce the long-term radiological impact of waste;
- (2) Enable development of a simpler, cheaper repository;
- (3) Reduce proliferation risk; and
- (4) Improve long-term prospects for nuclear power.

Improving the long-term prospects for nuclear power means not only demonstrating through proof-of-performance the practicality of the transmutation of nuclear waste and its meaningful impact on nuclear materials, waste management, and economics, but also defining and executing activities designed to support the country's nuclear science and engineering infrastructure.

For the short term, the AAA Program has focused its efforts on

- (1) Evaluating the most effective systems for transmutation of spent nuclear fuel,
- (2) Developing separations technologies to partition long-lived radioactive waste from reusable nuclear material,
- (3) Developing and testing potential transmutation fuels,

- (4) Developing a spallation target to provide an effective environment for transmutation,
- (5) Establishing and supporting a national university program to re-energize development and training in nuclear-related fields, and
- (6) Collaborating in international research efforts with nations involved in evaluating nuclear waste management.

Through these focused efforts, the AAA Program is defining the key experiments, analyses, and facilities needed to demonstrate the technical viability of partitioning and transmutation of long-lived nuclear wastes.

A key future objective of AAA is the construction of an accelerator-driven test facility (ADTF). The goal of the facility would be to demonstrate the transmutation of nuclear waste and to function as a national nuclear science and engineering user facility.

II. HIGHLIGHTS

Fuels Development

- A workshop on Transmuter Fuel Development was hosted at Argonne National Laboratory (ANL). Participants included Germany (ITU), Russia (IPPE), Switzerland (PSI), Korea (KAERI), Japan (JAERI), Sweden (KTH), and the United States (INEEL, ANL, LANL, and MIT).
- A draft long-term fuel development plan was completed, indicating the number, test types, and schedule of irradiation tests required for fuel development and qualification.
- The preliminary Fuel Specification for the Na-bonded ATW 1A–1D experiments was nearly completed.
- Free energies for CeN, ZrN, UN and PuN, as well as for some Pu- and Ce-oxide compounds were modeled, providing values necessary for the detailed thermodynamic modeling in a mono-nitride-structured transmutation fuel.

Separations Technology

- A detailed analysis was completed of the results of the UREX cold demonstration, showing that recovery of technetium can be improved significantly and decontamination of plutonium brought into target ranges.
- An evaluation of the radiation stability of acetohydroxamic acid (AHA) was completed, showing that this reagent is sufficiently stable under irradiation that the performance of the UREX process will not be impacted by high-radiation fields associated with spent LWR fuel.

Transmutation Science

- A successful collaboration meeting between DOE and the French CEA was held in Phoenix, Arizona. The progress and status for physics and materials work were discussed and new agreements reached for additional international support.
- Construction and initial checkout of the DELTA loop was completed and operational testing started.
- An LBE target was irradiated in the LANSCE WNR Blue Room, providing an abundance of neutron yield and spectrum data that are being analyzed. Also, a commissioning test for the production of helium and hydrogen was conducted, with all detectors performing well.
- MCNPX version 2.3.0 was released to the Radiation Safety Information Computational Center (RSICC).
- An uncertainty assessment quantifying the impact of nuclear data on integral parameters relevant to the neutronic design of an Accelerator-Driven System (ADS) was completed for systems with fuels having high content of minor actinides.

Systems Technologies

- Simulations have confirmed that the innovative annular geometry concept for the ADTF Target and Materials Test (TMT) Station produces a peak neutron flux in the central core region that is about a factor of two greater than other conventional target geometries.

University Programs

- A total of 32 presentations based on AAA-sponsored university programs were given at the ANS Winter Meeting and student mini-conference held in Reno, NV, in November.
- UNLV hired a research scientist in the Center for Environmental Studies to develop a new laboratory to conduct scientific studies in support of AAA R&D missions.
- The Idaho Accelerator Center (IAC) of Idaho State University (ISU) submitted a draft plan, statement of work, milestones, and deliverables for ISU-IAC participation in the AAA Program.
- Argonne technical staff conducted AMUSE training at UNLV (training on the Argonne Model for Universal Solvent Extraction separations process modeling).
- The Amarillo National Research Center (ANRC) issued an announcement and call for applications for ten fellowships available in the 2002 AAA University Fellowship Program.

III. TECHNOLOGY DEVELOPMENT

1. FUELS DEVELOPMENT

Scope

AAA fuels development activities are directed toward the development and qualification of fuels for safe transmutation of actinides at maximal rates. The objective of the effort is to provide one or more transmutation fuel forms at Technical Readiness Level (TRL) 6 at the time that transmutation technology overall is to begin integral demonstration. Thus far, requirements for such fuels include nonfertile compositions in forms suitable for fast-spectrum transmuters and a homogenous fuel cycle (i.e., all minor actinides would be maintained in the same fuel and processing stream). However, the AAA transmutation program is considering additional transmuter architectures, the use of which would imply different requirements for fuels; therefore, the fuel development program is evolving as the nature of and approach for the overall transmutation mission evolves.

The specific R&D activities include development of techniques to fabricate transmutation fuels from LWR fuel-derived actinide feed and from actinide feed recycled from transmuters. As-fabricated samples are chemically and micro-structurally characterized to evaluate the success of fabrication processes and to better understand the nature of the fuel materials. Evaluation of proposed fuel forms (nitride, oxide, metal, carbide, dispersion, etc.) requires irradiation testing, so near-term irradiation tests are being planned and will be performed through the course of this program. Finally, the understanding of in-service fuel behavior is best demonstrated through the development and validation of fuel behavior models that are eventually incorporated into fuel performance codes. Such models are being developed, concurrent with an effort to develop thermal models that allow calculation of fuel and cladding temperatures in service and during testing.

Highlights

- A draft of the *AAA Fuel Functions and Requirements* document was prepared, defining the direction for fuel development and qualification.
- A workshop on Transmuter Fuel Development was hosted at ANL. Participants included Germany (ITU), Russia (IPPE), Switzerland (PSI), Korea (KAERI), Japan (JAERI), Sweden (KTH), and the United States (INEEL, ANL, LANL, and MIT). Discussions focused on issues and solutions for transmuter fuel.
- A draft long-term fuel development plan was completed, indicating the number, test types, and schedule of irradiation tests required for fuel development and qualification.
- The preliminary fuel specification for the sodium-bonded ATW 1A–1D experiments was nearly completed.

- Candidate sintering aids for nitride cold press/sinter processing have been identified and experiments initiated. The use of sintering aids is anticipated to reduce Am volatilization.
- Void formation, often detrimental to fuel performance, was observed in ZrN irradiated at low temperatures with He and Xe; however, any tendency for swelling will be dependent on details of fission gas release at elevated temperatures.
- Free energies for nitrides of Ce, Zr, U, and Pu, as well as some Pu- and Ce-oxide compounds, were modeled, providing values necessary for the detailed thermodynamic modeling in a mono-nitride-structured transmutation fuel.

Fabrication Development

Metal Fuel

Weld qualification was started on the irradiation-specimen closure welds for the ATW-1 fuels-irradiation experiment, and a final end-plug design selected. The document specifying general weld and weld inspection requirements for ATW-1 hardware, *Welding Program for Welding Fuel Elements and Containment Capsule*¹ was completed and approved. Another document, *Orbital Welding System General Operating Procedure*² was drafted and is undergoing revision.

Lower end-plug weld qualifications are in progress. Specimens required for destructive and nondestructive evaluation have been fabricated. Independent chemical certification of cladding and end-plug stock to be used for ATW-1 was completed.

Physical installation of an arc melter in the casting laboratory glovebox was completed. This arc melter will be used to fabricate metal fuel specimens for the ATW-1 irradiation test. An operational readiness review is underway. In preparation for fabricating TRU-bearing materials, Np, Pu, and Am feedstock have been identified and partially staged. A list of the fuel-material sample requirements was established and a draft process sample-transfer plan prepared. The process material and safeguards material tracking systems have been integrated.

Nitride Fuel

Cold Press/Sinter Processing of Nitride Pellets — ZrN with an L/d (length-to-diameter ratio) ~0.5 can typically be cold pressed to a “green density” of 75% of theoretical density, and additional densification can be achieved with sintering above ~1600°C for fine mesh powders (sieve size –325). However, with the anticipated L/d~1.5 for fuel pellets for the ATW-1 irradiation, we will not be able to reach the desired final density of 85% without use of a sintering aid to allow significant densification at ≤1400°C. A sintering aid study was initiated, with three classes of sintering aids being identified as having promise for providing densification at ≤1400°C while still providing a stable microstructure during irradiation.

¹ ANL-West Document Control Number W7520-0474-ES-00.

² ANL-West Document Control Number W0650-0053-OP.

Specifically, the three classes can be categorized as noble metals, mono-nitride-forming rare-earth-type metals, and oxides. The noble-type metals and alloys such as palladium, nickel, and copper have melting points on the order of 1400°C, are easily handled, and are anticipated to have a limited solubility in PuN.

The rare-earth-type metals such as yttrium, Zr, and Ce can have melting points below and above 1400°C, but can be reacted under nitrogen to form mono-nitrides, which are predicted to have 100% solubility in PuN. These metal powders, however, are extremely reactive, either with oxygen or water. Alloys within the rare-earths (e.g., Zr-V) or between rare-earths and noble-type (e.g., Y-Pd) may provide easier handling.

Published reports on sintering of nitrides (typically silicon and aluminum) use oxides as sintering aids. It is typically possible to sinter oxides at lower temperatures than the strongly covalently bonded nitrides. Therefore, it may be possible to add small quantities of oxides, such as ZrO_2 or Y_2O_3 , to enhance densification while providing a microstructure that will be thermally stable during service.

Cold press and sinter processing of ZrN matrix pellets has been conducted using some noble-type and rare-earth-type sintering aids.

Metal Fuels Irradiation Testing

ATW-1 Irradiation Test

Several iterations of the physics analysis and design of the ATW-1 fuels-irradiation experiment were completed in collaboration with the Advanced Test Reactor (ATR) experimental staff. These analyses indicated that a borated aluminum neutron filter will be as effective in controlling experiment fission power as the initially planned Hf shroud. The borated aluminum filter has been adopted as the reference design. The ATR outer experiment holder (basket) will be constructed using this material, thus satisfying the requirement for a neutron filter and basket in a single assembly. The material is available commercially with no problem. The borated aluminum basket allows the experiment power to be adjusted during irradiation by varying basket wall thickness or boron enrichment.

Several improvements to the physical design of the experiment assembly were incorporated. Based on early information supplied by the ATR, the original outer capsule design contained both an upper and a lower gas plenum. Based on new information about the flux-trap-experiment hole geometry, the capsule design was simplified by removing the lower plenum. The upper plenum was enlarged to further reduce the potential for capsule pressurization as a result of fuel failure.

Staff from Argonne National Laboratory-West (ANL-W) noted a potential deficiency in power generation calculations for Am-bearing fuels. Power generation calculations for the high-Am fuels in the ATW-1 fuels test showed a rate of power increase with burnup much lower than that shown in calculations published for the EFTTRA-T4 test (radiation test sponsored by the European Union). The need to benchmark or validate ATR power generation calculations is thus identified.

The preliminary fuel specification for the Na-bonded ATW 1A–1D experiments was drafted and reviewed, and is largely complete. The working copy will allow the ATW-1 experimental safety analysis to be completed.

ATW-3 Irradiation Test

Arrangements were made for a January meeting of ANL, LANL, and CEA (French) fuel-development personnel at Cadarache and Marcoule to define the ATW-3 test matrix and schedule.

Nitride Fuel Performance

Assessment of Radiation Tolerance

Various techniques have been used to evaluate the radiation damage in ZrN under heavy-ion and fission-product implantation. Using both cross-section and plan-view transmission electron microscopy (TEM) samples, irradiation damage from Xe- and He-ion implantation (300 keV and 50 keV, respectively, both at 5×10^{16} fluence) has been characterized. Surface topography characterizations using scanning electron microscopy (SEM) and atomic force microscopy (AFM) have been used to study swelling effects due to inert gas implantations. The presence of implanted gas was confirmed using energy dispersive spectrometry (EDS). Contamination and phase-relations have been studied by changes in crystal structure characterized by x-ray diffraction (XRD). Element implantation depth has been characterized by resonant Rutherford backscattering spectrometry (RBS).

Radiation Damage

TEM studies show that under high fluence (5×10^{16} ions/cm²) of both Xe and He, some void formation exists at the grain boundaries (Fig. 1). Twin formation has also been observed, but it is not yet known if this is a direct result of irradiation (Fig. 2). Further characterization on unimplanted and differently implanted ZrN is necessary to determine whether twinning is being caused by ion-implantation.

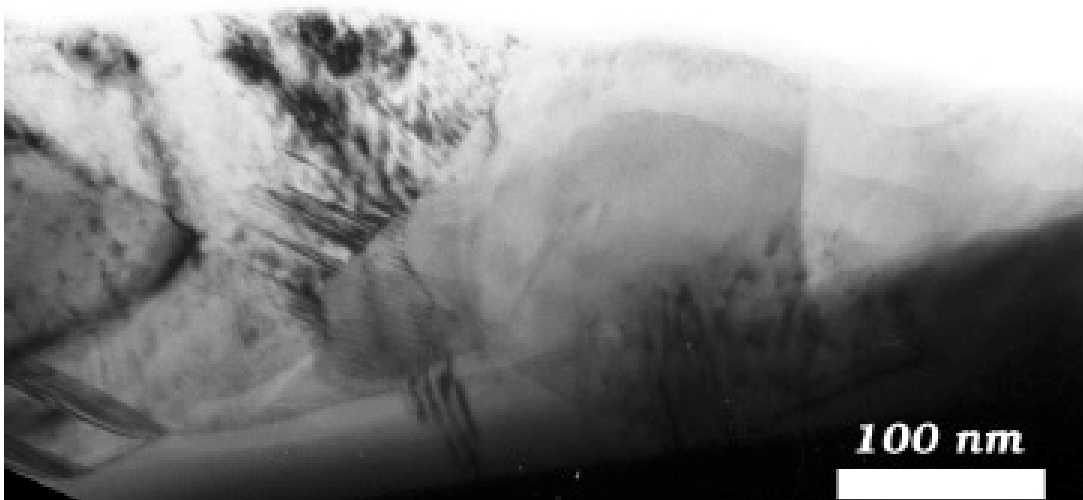


Fig. 1. Void formation at the grain boundaries due to ion implantation.

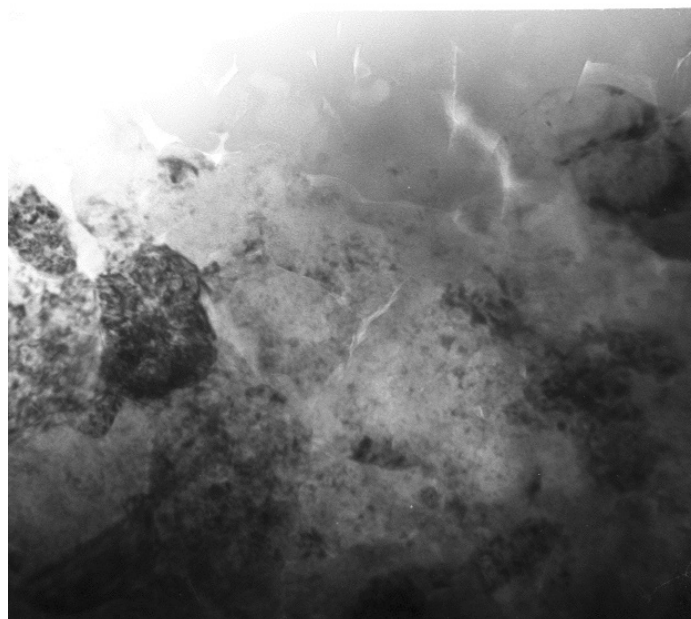


Fig. 2. Twin formation observed in Xe-implanted ZrN.

Swelling due to inert gas implantation, either from void formation or integration into the crystal structure, has not been observed. Masking was used to create an interface of implanted and nonimplanted ZrN so that swelling would produce a “ridge.” An EDS line scan was used to show the Xe-implanted area (Fig. 3). Although the line scan showed that the left side of the sample has a higher Xe content, both SEM and AFM showed no change in topography at the interface where the ZrN sample had been masked, indicating that ZrN is accommodating Xe without swelling.

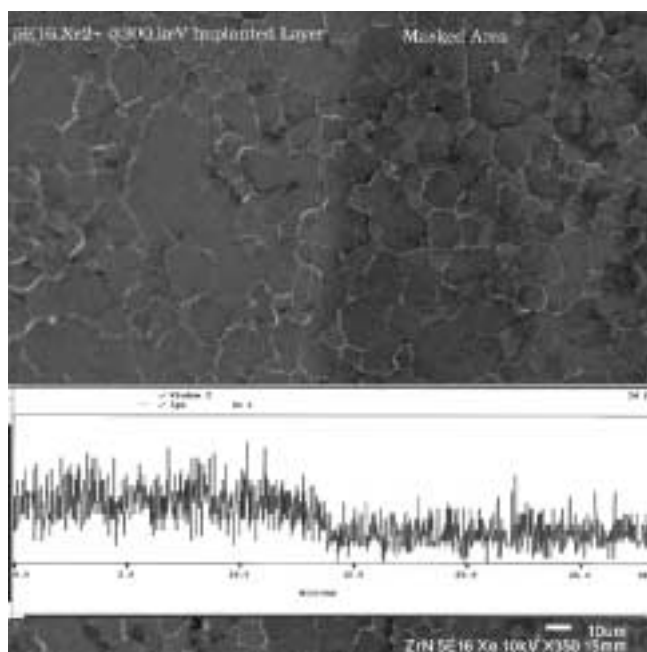


Fig. 3. SEM image of Xe-implanted area (left side of micrograph) and masked area (right side) with the corresponding EDS line scan of Xe content (bottom).

Fuel Qualification

Metal Fuel

Discussions were held with Dr. Lioudmila Zaboudko from the Institute of Physics and Power Engineering (Obninsk, Russia) to obtain a (somewhat) independent assessment of BOR-60 (RIAR, Dmitrovgrad) fuel testing capabilities. Dr. Zaboudko is familiar with fuel testing in BOR-60, being intimately involved with the current French-Russian BORA-BORA experiment. Dr. Zaboudko was confident about the future availability and suitability of the BOR-60 reactor for tests subsequent to ATW-3.

Work continued on incorporating reviewer comments into the document, *Transmutation Fuel Development for the Advanced Accelerator Applications (AAA) Program: Objectives, Functions, Requirements, and Approach*. This document defines functional requirements for transmuter fuel to aid in defining and developing fuel test plans.

A long-range, conceptual, fuel test plan was drafted. The test plan defines general irradiation test requirements for fuels qualification for a demonstration facility based on three scenarios of reactor availability for testing. The number of tests and test conditions were identified (this early test plan is mostly theoretical); however, it should be recognized that the actual number of required irradiation vehicles will be dependent on performance, reliability, safety issues, and phenomena to be identified through the early stages of development activities. A test schedule was mapped based on the three reactor-availability scenarios. The test plan will be used to develop a detailed testing schedule, identify specific reactors, estimate material quantities, and set dates by which agreements for collaboration or contracts should be in place.

Transmuter Fuel Development Workshop

A Transmuter Fuel Development Workshop was held in Idaho Falls, hosted by ANL-W during November. The workshop was successful in bringing to light the current status of transmuter fuel developments worldwide; it also served as a forum for discussing research and development work that should be performed to advance the state of knowledge.

The meeting opened with a session on the relationships between fuel, core design, safety, and recycle processes. This session was designed to lay the groundwork for considering fuel as part of an integrated system. Other sessions included fuel performance, fuel modeling, fabrication and properties, irradiation testing, national transmuter fuel programs, and opportunities for collaboration. A panel of speakers was convened after each session to discuss issues raised during workshop presentations. A final panel of experts presented views on technical issues facing development of fuels and the actions necessary for successful fuel development efforts. Summary conclusions from the workshop are as follows:

- Workshops or meetings specific to transmuter fuel development should be held on a regular basis, either in conjunction with an existing meeting or as a separate meeting.
- The United States and the European Union should submit a joint proposal on transmuter fuel development to the European 6th Framework program. A joint

US/European working group should be formed soon to begin work on this proposal. This working group should investigate the possibilities for joint irradiation tests in both Phenix and BOR-60.

- The US and the partners for the CONFIRM irradiation experiment should explore the possibility of cooperation. The level of cooperation would likely be limited to an information exchange at this point, because the programs have plans to irradiate nitride fuels under different conditions. The US and partners of the EFTTRA irradiation test should likewise explore the possibility of cooperation in the area of oxide fuel development.
- A successful fuel development effort will require sustained funding at a level of tens of millions of dollars per year for up to 15 years.
- The enhanced safety benefit of adding fertile material to first-generation transmuter fuels should be considered. The quantity of material required to significantly enhance core safety and the impact on transmutation rate should be explored.

Fuel Design

Nitride and Oxide Modeling

Modeling Free Energy — Thermodynamic data for nitrides have been collected from the literature and from the available commercial databases, e.g., Barin,³ JANAF,⁴ CODATA,⁵ Pankratz⁶ and other sources. The modeling process consisted of analyzing the data using an uncertainty evaluation procedure based on Bayesian statistics. A polynomial function in temperature was used as a model for the heat capacity:

$$C_p(T) = A + BT + CT^2 + DT^{-2} \quad (1)$$

A set of computer programs was developed that is capable of checking the self-consistency of the data set by verifying the fundamental thermodynamic relationships. These relationships involve the heat capacity at constant pressure, C_p , the entropy, S , the enthalpy, H , and the Gibbs free energy, G . If the pressure is constant, then:

$$C_p(T) = f(T) \quad (2)$$

$$H(T > T_1) = H_{T_0} + \int_{T_0}^{T_1} C_{p1}(\tau) d\tau + \Delta H_{T_1} + \int_{T_1}^{T_2} C_{p2}(\tau) d\tau \quad (3)$$

³ Barin, I., *Thermochemical Data of Pure Substances*, Part II, VCH Verlags Gesellschaft, Weinheim, 1993.

⁴ JANAF, "Thermochemical Tables," 3rd ed., Chase, M.W. et al., eds., *J. of Phys. and Chem. Ref. Data*, Vol. 14, Suppl. 1, pp. 1-1856, 1985. Chase, M.W., Jr., Davies, C.A., Downey, J.R., Jr., Frurip D. Journal, McDonald, R.A., Syverud.

⁵ Cox, J.D., Wagman, D.D., and Medvedev, V.A., *CODATA: Key Values for Thermodynamics*, Hemisphere Publishing Corporation, New York, p. 271, 1989.

⁶ Pankratz, L.B., *Thermodynamic Properties of Carbides, Nitrides, and Other Selected Substances*. U.S. Dept. of the Interior, Washington, DC, p. 957, 1995.

$$S(T > T_1) = S_{T_0} + \int_{T_0}^{T_1} \frac{C_{p1}(\tau)}{\tau} d\tau + \frac{\Delta H_{T_1}}{T_1} + \int_{T_1}^T \frac{C_{p2}(\tau)}{\tau} d\tau \quad (4)$$

$$G(T) = H(T) - T \cdot S(T), \quad (5)$$

where T_1 is the temperature of the phase transformation (if any) and T_0 is the reference temperature for enthalpy and entropy. Additional terms have been included to describe subsequent phase transformations. In many commercial databases, T_0 equals 298.15 K because only high-temperature properties are of interest. The LANL program also models properties situated below room temperature.

The study of PuN, UN, CeN, and ZrN was started. Figure 4 shows the Gibbs free energy of each compound, which is critical for the phase-stability calculations. It is important to note that this free energy is different from the Gibbs free energy of formation (from metal and nitrogen) that is required for modeling kinetics of chemical reactions. Figure 5 shows the Gibbs free energy of formation for the same compounds.

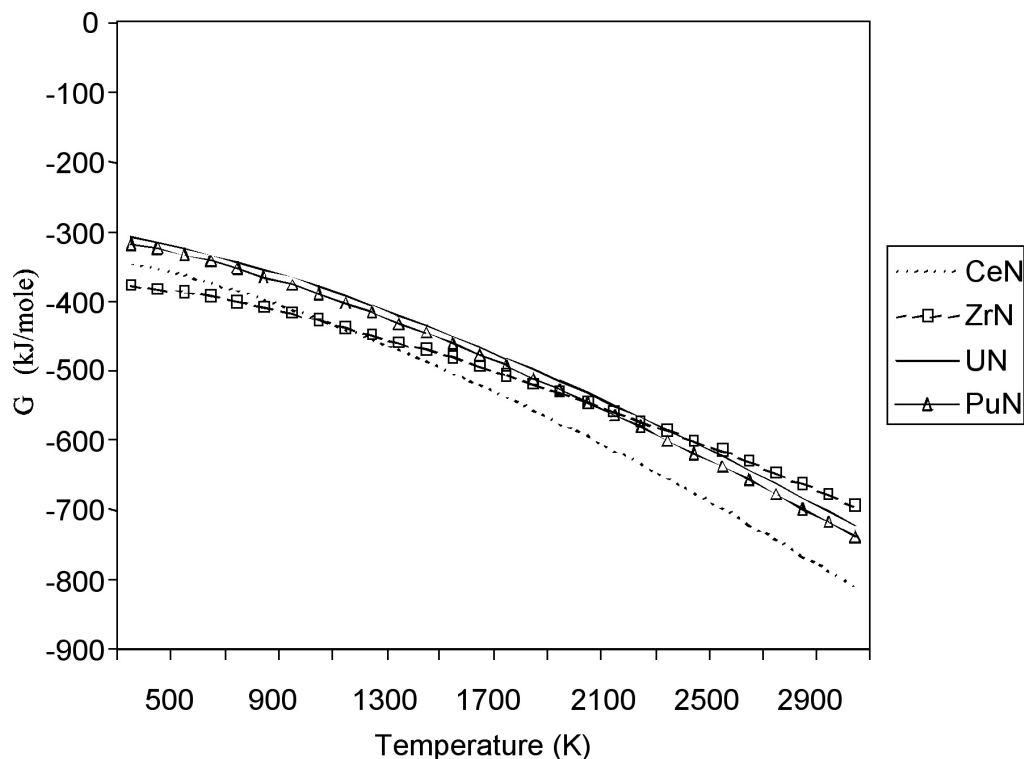


Fig. 4. Gibbs free energy of CeN, ZrN, UN, and PuN.

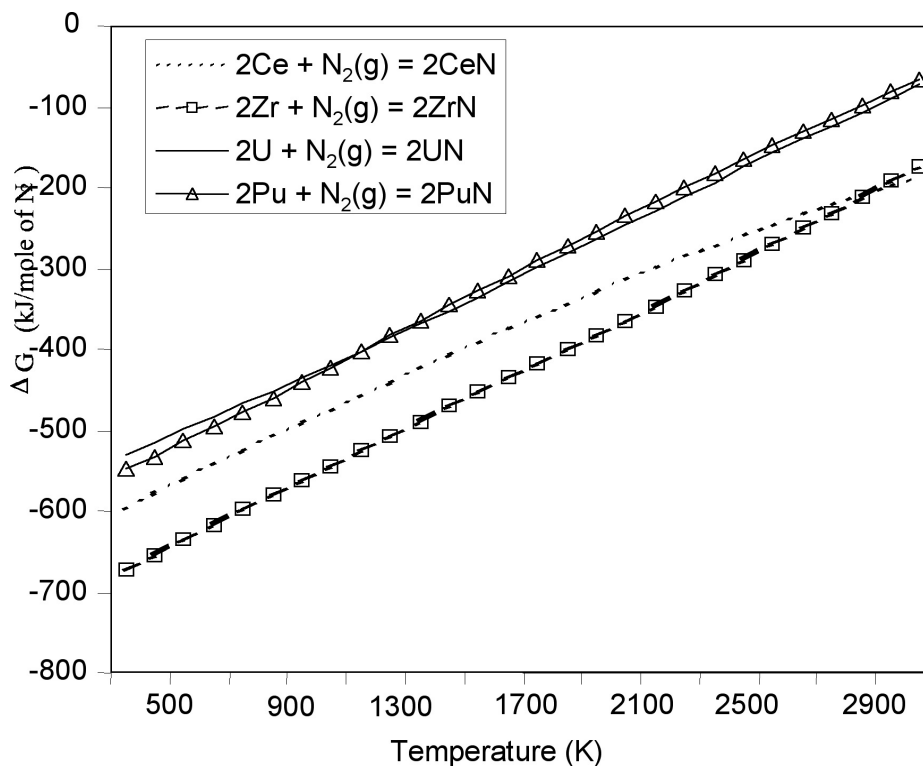


Fig. 5. Gibbs free energy of formation of CeN, ZrN, UN, and PuN.

A more complex problem is the modeling of the Gibbs free energy of solutions and nonstoichiometric compounds, which involves not only knowledge of the thermodynamic properties of the components, but calculations regarding interaction parameters. We decided to restrict the number of parameters in the excess free energy to two (a subregular model). The procedure was applied to CeO_2 , CeO_{2-x} , Ce_2O_3 , PuO_2 , PuO_{2-x} , and Pu_2O_3 . Figure 6 shows the Gibbs free energy of PuO_{2-x} , as a function of composition, for three different temperatures.

Phase Stability Calculations — The Ce-O system was used to tune up the phase stability modeling process. Important progress was made on the assessment of the Ce-O phase diagram (see Fig. 7), which will be submitted for publication soon.

The assessment of the Pu-O and Pu-N phase diagrams was initiated. The cumbersome modeling process involves numerous iterations to adjust the parameters of the free energy of compounds and solutions and will continue during the year.

Atomic Scale Modeling of Nuclear Fuels

Electronic structure calculations for ZrN were started in collaboration with the Theory Division at LANL. The plan is to eventually calculate the free energy of formation for compounds such as NpN, AmN, and CmN for which it is difficult, if not impossible, to get accurate equilibrium experimental data. The calculated free energy will be used in modeling the phase stability of TRU-nitrides.

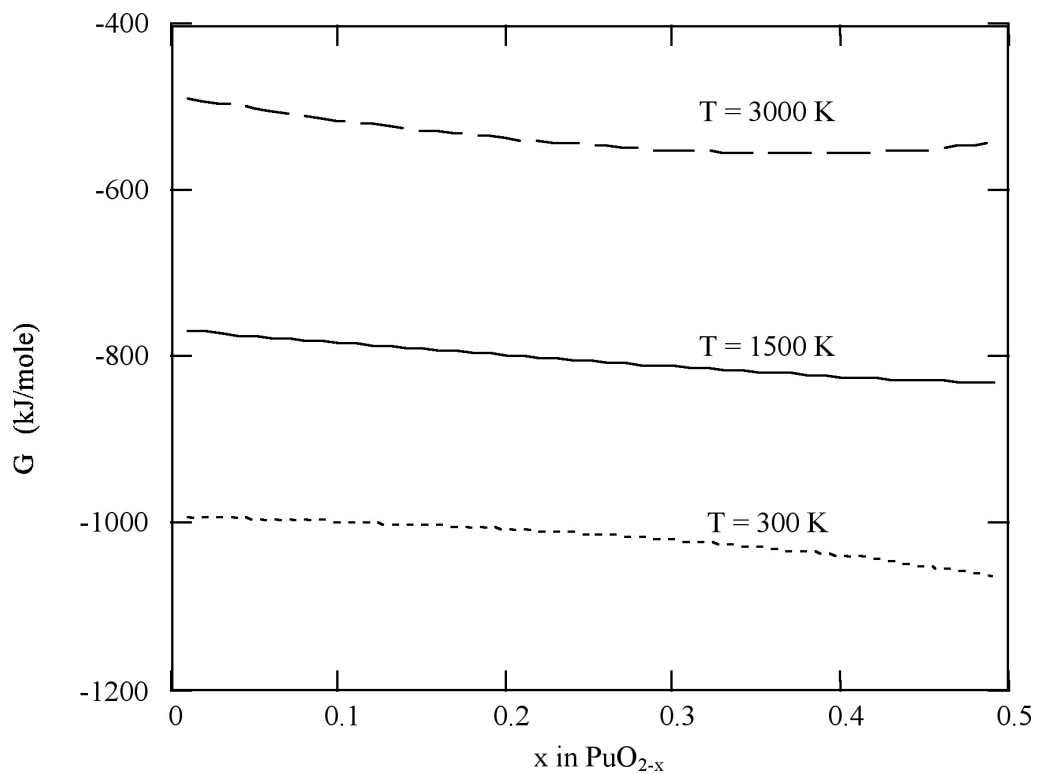


Fig. 6. Gibbs free energy of PuO_{2-x} .

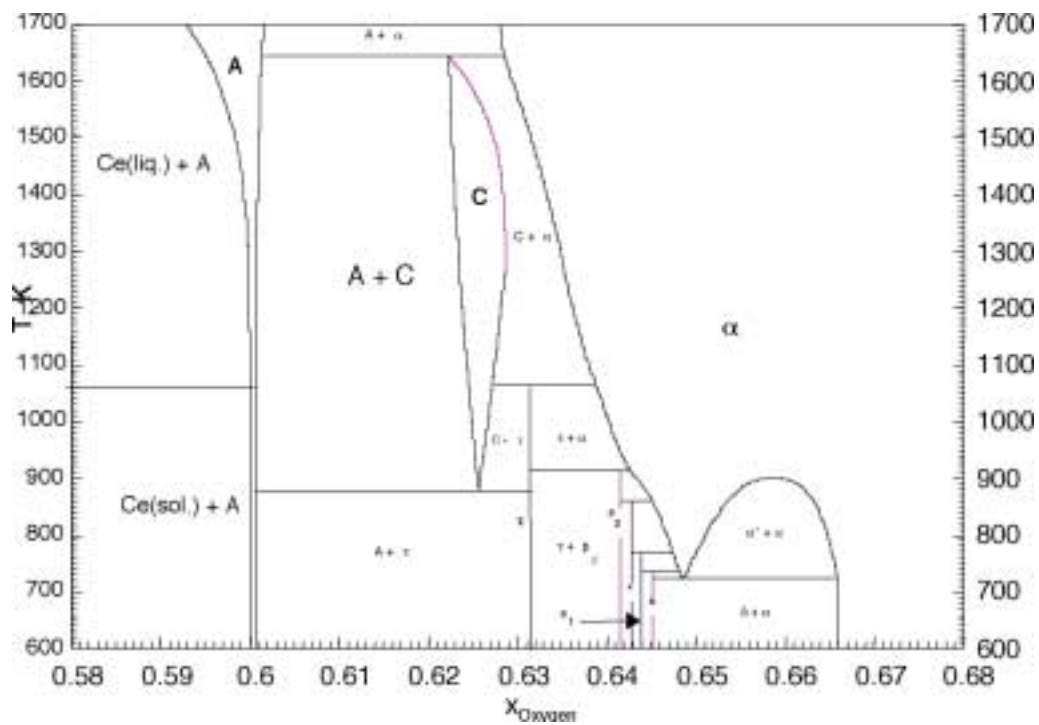


Fig. 7. Revised preliminary Ce-O phase diagram.

2. SEPARATIONS TECHNOLOGY

Scope

The AAA separations technology activity consists of three tasks addressing the various stages in the process of partitioning irradiated fuels for subsequent fissioning of transuranic elements and transmutation of long-lived fission products. The tasks are as follows:

- **Light-Water Reactor Spent Fuel Treatment** – This task involves the development and demonstration of efficient and economic means for the separation of uranium, transuranic elements, specific long-lived fission products, and other fission products from LWR spent fuel. An aqueous partitioning process (UREX) is envisioned for the initial treatment of LWR fuel, involving the extraction of uranium for disposal as a low-level waste. A pyrochemical process (PYRO-A) will follow to separate the transuranic elements from fission products.
- **Transmuter Blanket Fuel Treatment** – Nonfertile blanket fuel that has been irradiated in the AAA transmuter to fission transuranic elements must be processed to recover and recycle the unburned transuranics and to extract newly generated, long-lived fission products for transmutation. This task accomplishes the development and demonstration of the means for processing that blanket fuel. A pyrochemical process (PYRO-B) is planned for the separation of unburned transuranics and long-lived fission products. Such processes are favored because the reagents are stable under high-radiation fields, and because the processes are normally operated at elevated temperatures with the use of molten salts and can thus accommodate high levels of decay heating.
- **Waste Form Production** – One of the overarching criteria for AAA separations technology development is the minimization of high-level waste generation. Design of the LWR fuel-treatment process has been oriented toward the elimination of liquid high-level waste streams, and the pyrochemical processes are similarly being designed to minimize high-level waste volumes. This task involves the development and qualification of durable high-level waste forms to accommodate the two principal waste streams (salt and metal) that emanate from the separations process as well as the waste form for the disposal of the pure uranium extracted from the spent LWR fuel.

Highlights

- A detailed analysis was completed of the results of the UREX cold demonstration performed in September 2001, showing that the recovery of technetium can be improved significantly by taking into account the temperature sensitivity of its extraction behavior. The analysis also showed that the decontamination of plutonium could be brought into target ranges by adding one or two more scrub stages.
- An evaluation of the radiation stability of acetohydroxamic acid (AHA) was completed, showing that this reagent is sufficiently stable under irradiation that

the performance of the UREX process will not be impacted by high-radiation fields associated with spent LWR fuel.

LWR Spent Fuel Treatment — Optimized UREX Process Demonstration

The major tasks performed this quarter were to:

- (1) Collect additional analytical data from the September UREX demonstration,
- (2) Compare the data to the AMUSE (Argonne Model for Universal Solvent Extraction, the generic TRUEX model expanded to include UREX and PUREX processing) predictions,
- (3) Build an understanding of the differences, and
- (4) Improve AMUSE calculations based on this understanding.

All this effort is directed to developing an improved flowsheet for the hot demonstration with actual dissolved LWR fuel. As a result of this analysis, we are confident in our ability to design a flowsheet for the UREX process and to successfully demonstrate it at the Savannah River Technology Center (SRTC) later this fiscal year.

Figures 8 and 9 show the UREX flowsheet, which was demonstrated in a 49-stage, 2-cm centrifugal contactor during September. Flowsheet detail is described below:

- The clean solvent entered the extraction section in stage 1.
- The simulated feed (containing nitric acid, nitrate salts of U, Pu, and Np, and HTcO_4) entered at stage 12, where it mixed with the scrub solution, which contained a mixture of nitric and acetohydroxamic acids.
- The scrub solution entered the contactor bank at stage 16.
- The solvent flowed countercurrent to the aqueous solution, moving from stage 1 to stage 16. In the extraction section, uranium and technetium partitioned to the solvent and were mostly removed from the aqueous solutions; most of the uranium and technetium exited the contactor with the loaded solvent at stage 16.
- Most of the plutonium and neptunium exited the contactor in the raffinate at stage 1.
- The loaded solvent re-entered the contactor at stage 26, where it flowed countercurrent to the technetium strip solution, stripping technetium and a small fraction of the uranium from the solvent. The strip feed entered the contactor at stage 33.
- Before the technetium-product stream exited the contactor, it was purified from the small fraction of uranium that was also stripped from the loaded solvent. This was done by passing it countercurrent to the flow of clean solvent that entered the contactor in stage 17. The purified Tc-product exited the contactor at stage 17, while the now U-loaded solvent that entered stage 17 was mixed with the loaded solvent that entered stage 26.

Hydraulic performance of the flowsheet was outstanding. However, the behaviors of Pu and Tc were not as good as predicted. Table 1 shows the predicted and actual behavior of U, Pu, Np, and Tc during the September demonstration in terms of the fraction of material reporting to each effluent stream. The results found in Table 1 are mixed. Uranium extraction as measured by inductively coupled plasma-mass spectrometry (ICP-MS) was as expected until the amount removed from the aqueous phase appeared to go to zero at a concentration of 1 μM ; the residual mass-238 material was later found to be ^{238}Pu , not ^{238}U . Although Tc met the specification of $\geq 95\%$ recovery, it extracted more poorly than expected. Neptunium behavior was predicted well by AMUSE. Plutonium extraction was far greater than expected in the extraction section and high enough to contaminate the Tc and U product streams. In the following sections, the extraction behavior of each component is discussed in more detail.

**Table 1. Predicted and Measured Component Recoveries
for the Demonstration Run Completed in September 2001**

	U		Pu		Np		Tc	
	Model (%)	Experiment (%)	Model (%)	Experiment (%)	Model (%)	Experiment (%)	Model (%)	Experiment (%)
Raffinate	10^{-5}	$<3.3 \times 10^{-4}$	100	99.7	100	>99.7	0.07	3
Tc Strip	0.01	3.9×10^{-4}	10^{-7}	0.16	10^{-5}	$<3 \times 10^{-3}$	99.7	>97
U Strip	99.99	99.999	10^{-4}	0.13	10^{-5}	<0.3	0.01	<0.1

Uranium

Uranium behavior was good (and well modeled) in the extraction section. Figure 10 shows the predicted and experimental aqueous-phase uranium concentration in each stage of the extraction and scrub sections of the process. The concentration profile in stages 8-12 was useful in establishing that the stage efficiency for the 2-cm centrifugal contactor was 100%, indicating that the organic and aqueous phases were thoroughly mixed in each stage and, therefore, completely equilibrated. Even with this superior behavior, the ICP-MS results led us to believe that no more ^{238}U extracted from the aqueous solution when its concentration dropped to 1 μM . However, using a combination of alpha-pulse and gamma-ray analysis, we have determined that the 238 isotope seen by ICP-MS analysis at $\leq 1 \mu\text{M}$ was actually ^{238}Pu . (Note the line at the bottom of Fig. 10, which shows the concentration of ^{238}Pu found in the raffinate and early extraction stages.) Therefore, we are not able to measure uranium concentrations below 1 μM . Also shown in Fig. 10 is the AMUSE predictions for uranium behavior as a function of stage efficiency.

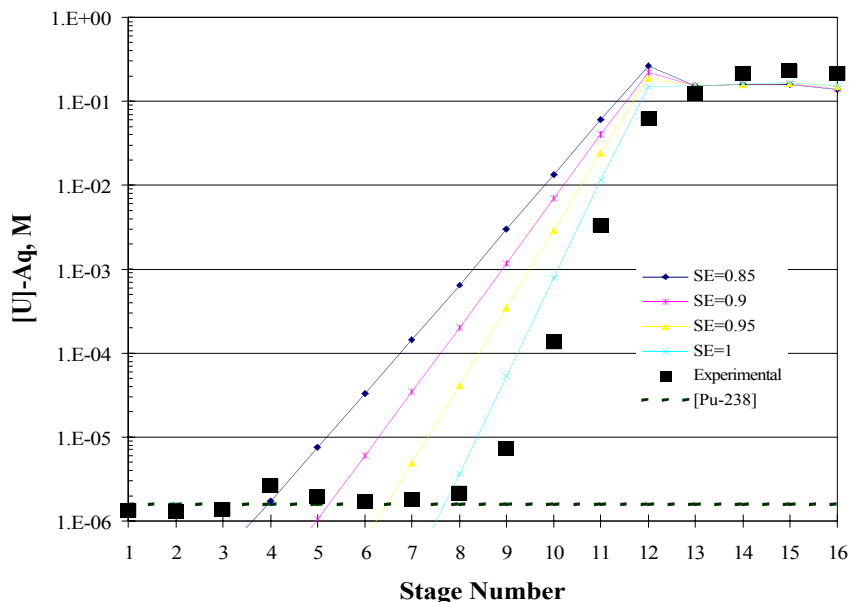


Fig. 10. Aqueous-phase concentration profile for isotope 238 in the extraction and scrub sections of the September 2001 UREX demonstration vs. AMUSE predictions as a function of stage efficiency. Uranium is removed from the aqueous solution as it passed from stage 12 to stage 1. Below stage 8, only Pu-238 is measured by ICP-MS.

Technetium

As stated earlier, the Tc extracted more poorly than expected. The poor fit of the AMUSE model (using a process temperature of 25°C) to the actual extraction behavior for pertechnetate is explained by (1) the high temperature-dependence of Tc extraction on process temperature, and (2) the heating of contactor stages during the demonstration, which raised the temperature of the solutions in the stages. The extent that the temperature of the solutions in each stage is increased is a function of the heat capacity and flow rate of each phase and their temperatures entering that stage. To estimate the stage-wise temperature profile in the demonstration, a heat balance was calculated on the first 33 stages based on the flow rates of influents, the temperatures of effluents, and the fraction of the 12 W of power from each contactor-stage motor that heated the solutions in a stage. In the demonstration, all influents were at 18°C. At steady state, the raffinate exited the extraction section at 25.3°C±0.3, the Tc-product stream exited at 31.2°C±0.2, and the loaded solvent exited stage 33 at 22.7°C±0.2. The best fit to the effluent temperatures was made by assuming 7% of the motor power went into heating the solutions. The stage-wise temperature profile calculated is shown in Fig. 11.

To take advantage of the temperature-profile results, the AMUSE code was enhanced to allow the user to specify the process temperature in each stage. With this new feature, AMUSE could better predict Tc behavior. Figure 12 compares the actual and predicted Tc behavior in the September demonstration. The benefit of using the temperature profile in AMUSE calculations is clear. Effects of the temperature profile on the extraction behaviors of U, Np, and Pu is insignificant.

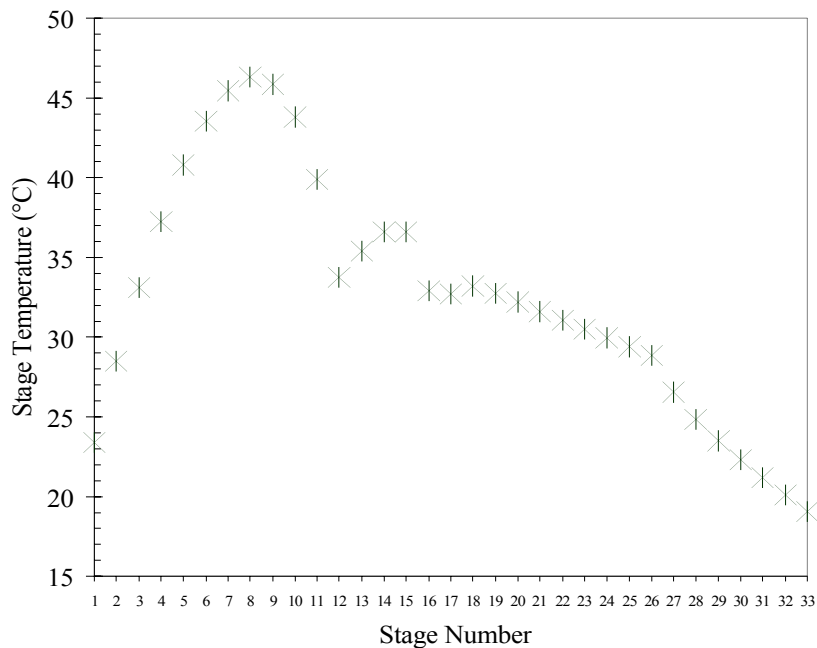


Fig. 11. Temperature profile calculated for the first 33 stages of the September 2001 UREX demonstration. The extraction section was stages 1-12; the scrub section was stages 13-16; the Tc-product U-re-extraction section was stages 17-25; and the Tc-strip section was stages 26-33.

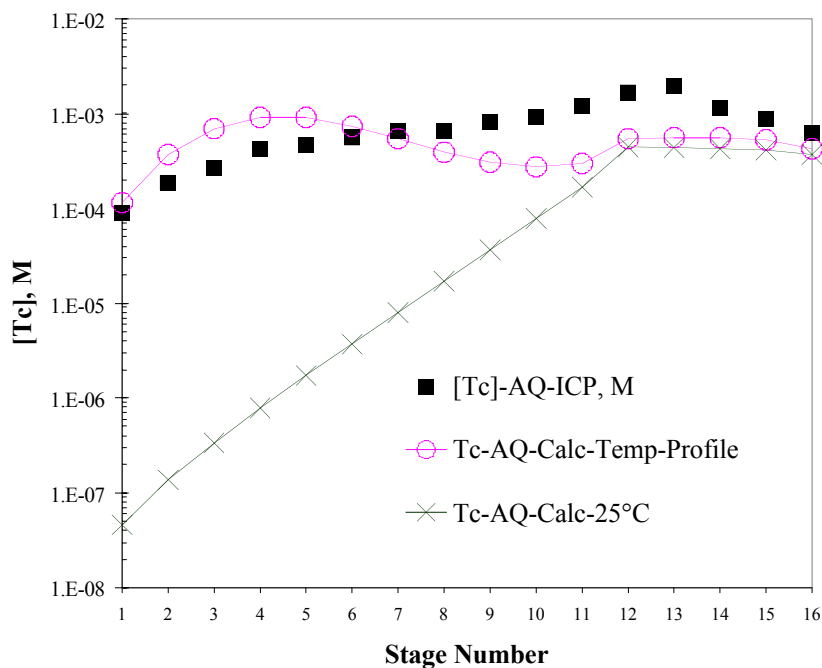


Fig. 12. Experimental and AMUSE-predicted aqueous-phase concentration profile for technetium in the extraction and scrub sections of the September 2001 UREX demonstration. Using the temperature profile for individual stages greatly enhances the fit of the AMUSE model to the experimental data.

Plutonium

Figure 13 shows the aqueous- and organic-phase concentration profiles of Pu in the extraction (stages 1-12) and scrub (stages 13-16) sections of the process. Plutonium concentrations in the aqueous and organic phases were measured by counting the ^{239}Pu gamma ray at 129 keV. Aqueous-phase concentrations were also measured by ICP-MS. The AMUSE fit to the data is also shown. Analysis of the demonstration results showed that the complexation of Pu by AHA was not as strong as predicted. To improve AMUSE predictions for Pu(IV) extraction with AHA present, the demonstration data were used to provide a better complexation constant for AHA ($\beta\text{-Pu/AHA}$). With this improvement, the AMUSE fit to the experimental data is much closer. The fit to the experimental data could be improved further by lowering the value for $\beta\text{-Pu/AHA}$ and adding a term for complexation of Pu(IV) by two AHA ($\beta\text{-Pu-AHA}^2$). We plan to collect distribution ratio data for Pu(IV) under conditions of low acid, low nitrate, and high AHA concentrations to obtain independent experimental values for $\beta\text{-Pu/AHA}$ and $\beta\text{-Pu-AHA}^2$.

Note how well plutonium is being scrubbed for the solvent in stages 13-16. These data show that one or, conservatively, two additional scrub stages would have allowed us to reach the decontamination goal for plutonium in the uranium product. Based on this knowledge, two additional scrub stages will be used for the hot demonstration at SRTC.

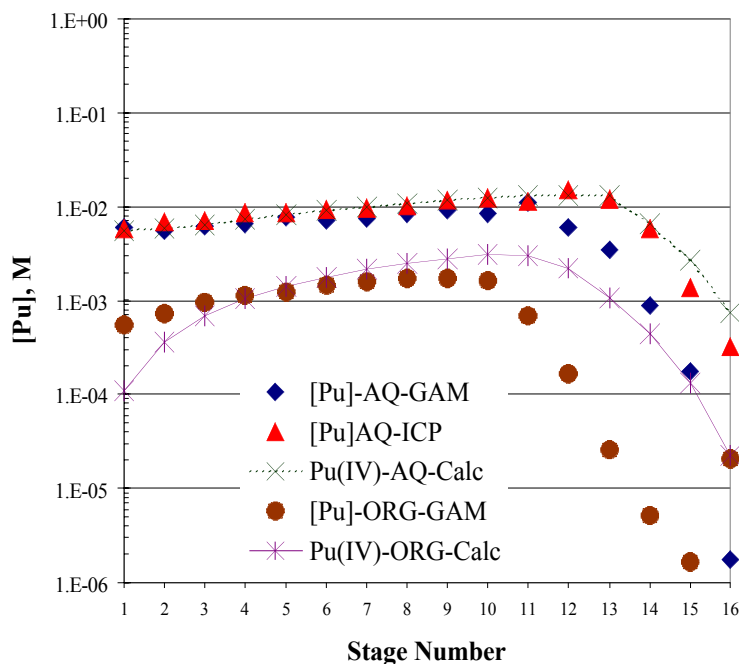


Fig. 13. Experimental and calculated stage-wise concentration profile for plutonium in the extraction (stages 1-12) and scrub (stages 13-16) sections of the September 2001 countercurrent demonstration of the UREX process.

Neptunium

The fit of AMUSE calculations for Np is shown in Fig. 14. Neptunium was measured in both the organic and aqueous stage samples by counting the ^{233}Pa daughter of the ^{237}Np .⁷ Aqueous-phase stage samples were also measured by ICP-MS. The AMUSE fit for neptunium is best fit by assuming Np(V) behavior.

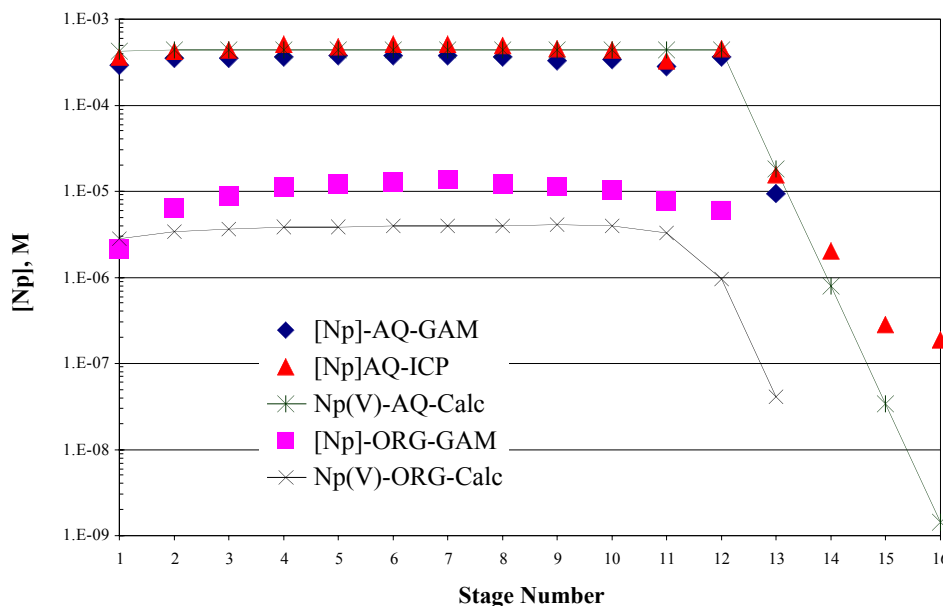


Fig. 14. Experimental and calculated stage-wise concentration profile for neptunium in the extraction (stages 1-12) and scrub (stages 13-16) sections of the September 2001 countercurrent demonstration of the UREX process.

Conclusions

Based on (1) our analysis of the results of the extraction and scrub sections and (2) the superb operation of the remaining sections in the September UREX demonstration, we are confident in our ability to design and perform a hot demonstration during FY02 at SRTC. The results of the September demonstration have given us a better understanding of important processing parameters and allowed us to enhance the accuracy of AMUSE predictions. Because the SRTC 33-stage contactor can be used thermostatically to control temperature in the extraction and scrub stages, Tc behavior should be well controlled. Further, our results also show that adding one or two more scrub stages will provide sufficient Pu decontamination.

Radiation Stability of Acetohydroxamic Acid

The UREX process is based on recovery of uranium by tributyl phosphate (TBP) while rejecting fission products and other actinide elements to the aqueous waste raffinate. Plutonium and neptunium are rejected to waste, along with fission products,

⁷ Gamma counting was performed three months after the demonstration to allow secular equilibrium to be established between ^{237}Np and ^{233}Pa ($t_{1/2} = 27$ d).

Am, and Cm, by reduction/complexation with AHA. Np and Pu are prevented from extracting by AHA, which complexes Np(IV) and Pu(IV) and reduces Np(VI) to inextractable Np(V). The AHA is readily decomposed to gaseous products during waste evaporation.

Dose Calculation

No studies of the radiation stability of AHA have been found in the literature. Therefore, a study was initiated with the calculation of expected dose (Table 2) during processing. The calculation assumes a Pu isotopic distribution taken from a text on nuclear engineering for 30,000 MWD/T (megawatt days per ton—standard unit for burnup) irradiation.⁸

Table 2. Data for Calculation

Isotope	% at discharge	% after 40 yr decay	mCi/g × 1.6g/mL
²³⁸ Pu	0.02	1.6	449
²³⁹ Pu	61.3	70.4	70
²⁴⁰ Pu	13.1	15.0	55
²⁴¹ Pu	17.7	5.4	9220 (beta)
²⁴² Pu	6.6	7.6	0.4
²⁴¹ Am	—	0.13g/g Pu	717

These values were converted to mCi/g, multiplied by 1.6 g/mL (extraction feed flow rate of 100 L/hr containing 2.9 g/L actinides diluted by the scrub feed rate of 65 L/hr) and the radiation dose calculated for each isotope from

$$\text{Dose (R/sec)} = 0.5927 \times C \times E,$$

where *C* is mCi and *E* is MeV/disintegration, taken to be 5.4 MeV for alpha emitters and 0.07 MeV for ²⁴¹Pu.⁹ For 1290 mR/sec alpha emitter, the dose calculated is 4132 R/sec; for the 9220 mCi/sec beta emitter, the calculated dose is 38 R/sec. The total dose of 4170 R/sec exposed in the stage-10 extraction section, at 6 sec/stage, is 2.5×10^5 R.

Curium isotopes, ²⁴³Am, and fission products were not included in the calculation. The calculation has considerable uncertainty because the ²³⁸Pu content is not considered reliable. Since it is a major contributor to the total dose, its uncertainty becomes a major source of error.

Irradiation Tests

Experimental Method

Solutions were prepared from reagent-grade chemicals and ordinary distilled water. Vials used to contain samples were heated to 500°C to destroy possible organic

⁸ Benedict, M., Pigford, T.H., and Levi, H.W., *Nuclear Chemical Engineering*, McGraw-Hill, 1981.

⁹ Spinks, J.W.T., and Woods, R.J., *Introduction to Radiation Chemistry*, John Wiley, p. 89, 1976.

impurities; otherwise, the extreme precautions against impurities normally taken in radiation chemistry were not employed.

AHA was analyzed by the absorbance at 505–515 nm of the tris-AHA-Fe(III) complex. The absorbance was linear on standard samples, but the position of the maximum was shifted by the characteristics of the spectrophotometer. An optical density of 0.300 in the 1-cm cell is equivalent to 7.5×10^{-4} M AHA. The error in the measurement is estimated to be $\pm 10\%$.

Aliquots (0.1 mL) of the irradiated samples and an unirradiated control were diluted a factor of 100 into 0.1 M Fe(III)-1 M HNO₃ and the absorbance measured on a Hewlett-Packard diode array spectrometer. A comparison of the absorbances of the irradiated sample and the unirradiated control determined the effect of the irradiation.

Results

The results of the irradiations are shown in Tables 3 and 4 as optical densities of the control and the samples. All samples were initially 0.1 M AHA. The control values reflect the hydrolysis of AHA during the time between sample make-up, irradiation, and analysis. Samples were irradiated in a ⁶⁰Co source at a dose rate of 9.5×10^5 R/h. The time for irradiation was a maximum of 50 minutes of the total of ~24 hours between make-up and analysis.

Table 3. Effect of Radiation on 0.1 M AHA Solutions at Low Doses

Solution	Control	Radiation Dose, R	
		1.91E+05	3.81E+05
0.5M H+	0.246	0.144	0.133
0.4M H+	0.276	0.185	0.174
0.2M H+	0.463	0.382	0.358

Table 4. Effect of Radiation on 0.1 M AHA Solutions at Higher Doses

Solution	Control	Radiation Dose, R	
		7.59E+05	1.14E+06
0.5M H ⁺	0.201	0.093	0.080
0.4M H+	0.292	0.162	0.135
0.2M H+	0.407	0.315	0.305
0.2M H+	0.413	0.312	0.324

Discussion

The radiation level in the extraction section of the UREX process is estimated to be ~4200 R/sec from Pu isotopes and ²⁴¹Am. Assuming a residence time of 6 sec/stage for the 10-stage extraction section, the total dose is estimated to be 2.5×10^5 R. The major contributors to the dose are ²³⁸Pu and ²⁴¹Am.

AHA is hydrolyzed in acid solutions to acetic acid and hydroxylamine (HAN); the radiolysis of these species is also a factor to be considered. Figure 15 shows the effect on AHA absorbance as a function of radiation dose. The y-axis is the difference between the control for that sample and the irradiated sample. The difference between control and irradiated samples increases slowly with a 6-fold increase in

dose, a puzzling result that could have one of several explanations. An obvious explanation is a back-reaction of the hydrolysis products to re-form AHA. However, no AHA was detected in several irradiations of acetic acid-HAN mixtures at doses up to 1.14×10^6 R.

Another possible explanation is that irradiation of AHA (CH_3CONHOH) converts AHA to formohydroxamic acid (HCCONHOH) by replacing a CH_3 - group with an H atom, and that the resulting hydroxamic acid analyzes as if it were AHA. Analysis of the radiation products is in progress, as well as further radiation studies at higher acidities.

Irradiated samples with no acid/0.2 M AHA and no acid/1 M NaNO_3 /0.1 M AHA were the same (within the error of measurement) as the control samples. On average, 0.012 M AHA were destroyed during irradiation with $G(-\text{AHA}) = -0.28$ molecules/100 eV absorbed radiation.

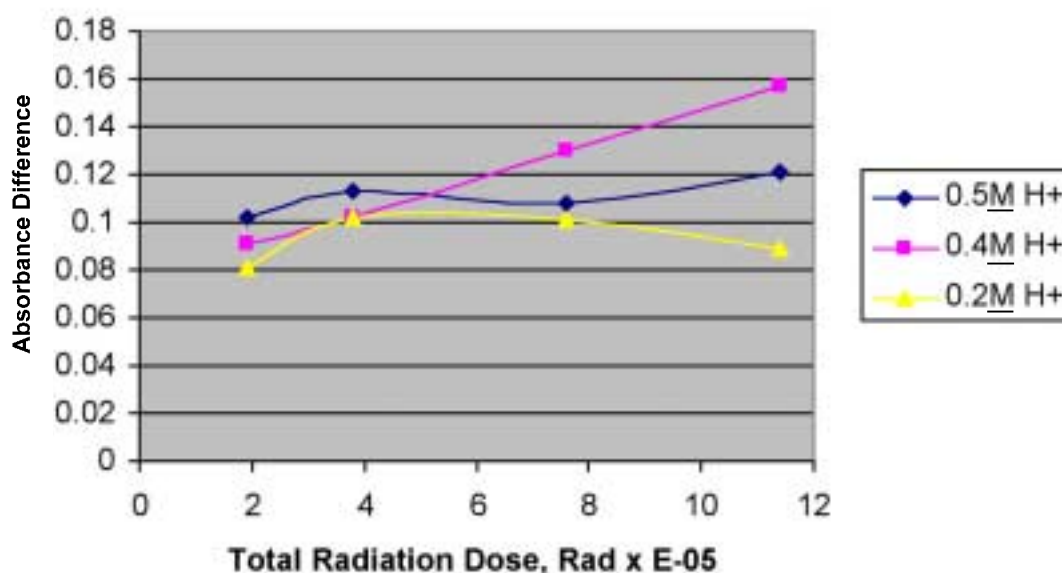


Fig. 15. AHA absorbance as a function of radiation dose.

The results obtained thus far do not indicate that radiation will have a significant effect on the UREX process.

Treatment of UREX Raffinate Stream

Reference Flowsheet

In the reference flowsheet, following the UREX step, the stream containing the minor actinides (Pu, Np, Am, Cm) and fission products must be converted from a liquid nitrate form to a solid oxide form prior to delivery to the PYRO-A process. Direct conversion by means of the modified direct denitration (MDD) process is planned. Tests of this process in a lab-scale rotary furnace will be made—first with nonradioactive simulants, and then, after installation of the test equipment into a glovebox, tests will be made with actinide elements Pu and Np. If the tests are successful, the

equipment will be moved into a hot cell and tested further with all actinides (Am, Cm, Np, Pu) and actual fission products.

Equipment design was begun and is in progress. The test equipment will be purchased and/or procured from a vendor. The simulant elements to be tested will include Ba, Ce, Cs, Eu, Mo, Pd, Ru, Tc, and Zr.

Alternate Flowsheet

The direct denitration process may encounter processing difficulties with the evolution of potentially volatile fission products, such as Cs, Mo, Ru, and Tc. Thus, a pretreatment step such as TRUEX solvent extraction or a cation exchange loading/calcination process is being considered. A recent hot test of the cation exchange resin-loading/calcination process was made using irradiated Pu samples containing all minor actinides and fission products except Np. A diagram of the process and the results of the tests are shown in Fig. 16.

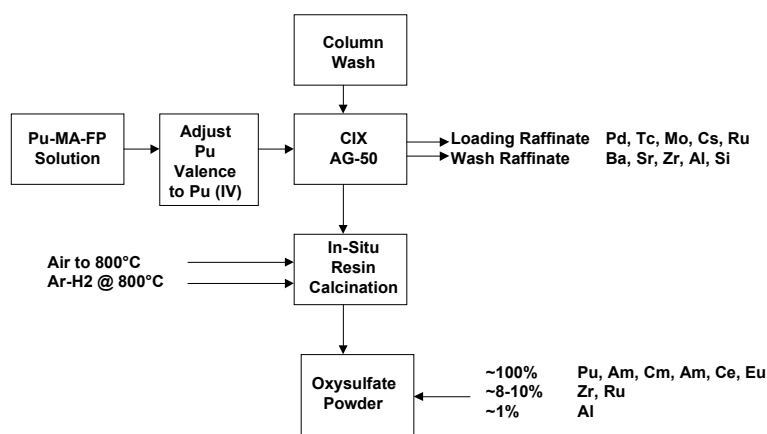


Fig. 16. Resin-loading/calcination process test.

The test results indicated that removal of the potentially volatile fission products was accomplished successfully prior to calcination of the actinide/lanthanide-loaded resin to the oxide form. In fact, removal of most nonlanthanide fission products, including the noble metals, was accomplished. Thus, this process can be considered a replacement for the MDD process.

TRISO Fuel-Processing Development

In the TRISO fuel-processing flowsheet, an actinide/lanthanide separation step must be used to prepare the Am and Cm for transmutation in a thermal flux gas turbine modular helium reactor (GT-MHR). European studies have been focused on next-generation solvent extractant agents. The process is called SANEX and several classes of new reagents are being considered. SANEX II reagents are the di-alkyl-triazin-pyridine-type compounds, and SANEX IV reagents are the dithiophosphinic acids. Both classes of reagents have shown promising results for efficient separation

of the actinides and lanthanides. Exploratory and confirmatory testing of these reagents are being planned for the AAA TRISO fuel-processing flowsheet.

One of the process difficulties noted in the European studies was the tendency of the noble metal fission product, Pd, to follow the actinides through prior process steps (PUREX, DIAMEX, TRUEX) and then to load irreversibly into the SANEX extractants. All of the prior process steps use neutral extractants, such as TBP and CMPO. A significant finding in our cation exchange process test described above was that, with a cationic extractant, Pd and other noble metal fission products were successfully removed from the actinide-lanthanide stream. Thus, it appears that the appropriate pretreatment step for the SANEX process is a cationic solvent extraction or ion exchange step.

3. TRANSMUTATION SCIENCE

Transmutation science research is divided among seven major categories:

- Integration and Analytical Support
- Materials
- Lead-Bismuth Eutectic (LBE) Technology
- Irradiation Experiments
- High-Energy Physics
- Reactor Physics
- International Support

The quarterly progress in each area is presented in the subsections that follow.

3.1 Integration and Analytical Support

The major objective of the integration and analytical support activities is to define and implement a consistent research plan for transmutation science.

Scope

Integration and analytical support activities include project management and integration of activities under transmutation science. The specific technical scope includes the following:

- Implement/maintain the 10-year research plan for transmutation science (experiments and supporting analyses);
- Maintain and coordinate international work packages (DOE international coordination agreements) relevant to transmutation science topics;
- Assist AAA program management in generating other international collaboration work packages; and
- Participate in safety and hazard control plan (HCP) reviews for project experiments.

In general, analytical support tasks involve defining and designing the experiments, defining the test requirements and the data quality objectives, and converting the test data into technology readiness input. Defining and designing experiments involve scaling analyses, assessment of the facility limits and parametric ranges, and comparing those to the technology development needs. During this process, the specific requirements for tests as a function of a Technology Readiness Level also are defined in terms of data quality objectives (with emphasis on accuracy requirements). Generated data must be analyzed and assessed in terms of TRL achievements and used to define design parameters or the need for supplementary and complementary tests. Specifically, tasks include:

- Integration of the Weapons Neutron Research (WNR) facility gas production test results with Blue Room neutron yield results to map out buffering effects;

- Assessment of the data provided through international collaboration in terms of its impact on the TRL and definition of US experiments;
- Input to international test plans; and
- Completion of LBE-sodium compatibility experiments begun in FY01.

Highlights

- A large fraction of the test matrix for the LBE-sodium compatibility experiments has been completed. Tests show that lead, bismuth, and LBE all react exothermically with sodium. Bismuth reactions are the most exothermic. The equilibrium temperature rises are consistent with the pre-test predictions. Kinetic effects on the temperature spikes are being investigated.
- A summary of a 10-year research plan for the spallation target and materials has been drafted.
- A successful collaboration meeting between DOE and CEA was held in Phoenix, Arizona. The progress and status for the physics and materials work packages were discussed and new agreements reached for additional collaborative work.

Spallation Target and Materials Research Plan

A summary of a 10-year research plan was prepared, outlining research details for the spallation target and materials. The spallation target is a major research topic because a compact target with a 5-10 MW continuous beam power coupled with a subcritical multiplier has never before been deployed. The fact that the target resides inside a subcritical reactor also imposes additional lifetime and efficiency constraints. At present, LBE is the leading spallation target technology being developed under this research plan. In addition to the spallation target materials, which are exposed to very-high-energy irradiation, the materials in the subcritical blanket also require additional research to maximize the lifetime. The transmutation efficiency depends strongly on burnup levels that can be achieved by dedicated fuels without recycling. At present, even if fuels that can achieve very high burnup levels can be developed, the fluence on the cladding would limit the fuel life.

In the 10-year research plan, major issues are identified and a high-level solution strategy is outlined. Major issues include:

- Liquid metal corrosion;
- Radiation damage;
- Liquid metal embrittlement;
- Thermal fatigue;
- Neutronic cross-sections and benchmark; and
- Window cooling.

The resolution of these issues is mapped into a Technical Readiness Level concept. Starting at TRL 3, the objective is to achieve TRL 6 within six years, which covers the proof-of-principle period. In the summary document, the main emphasis is on identification of the facilities and programs that will support the 10-year research objectives.

A summary of the facilities and programs mapped into the TRL levels is shown in Fig. 17.

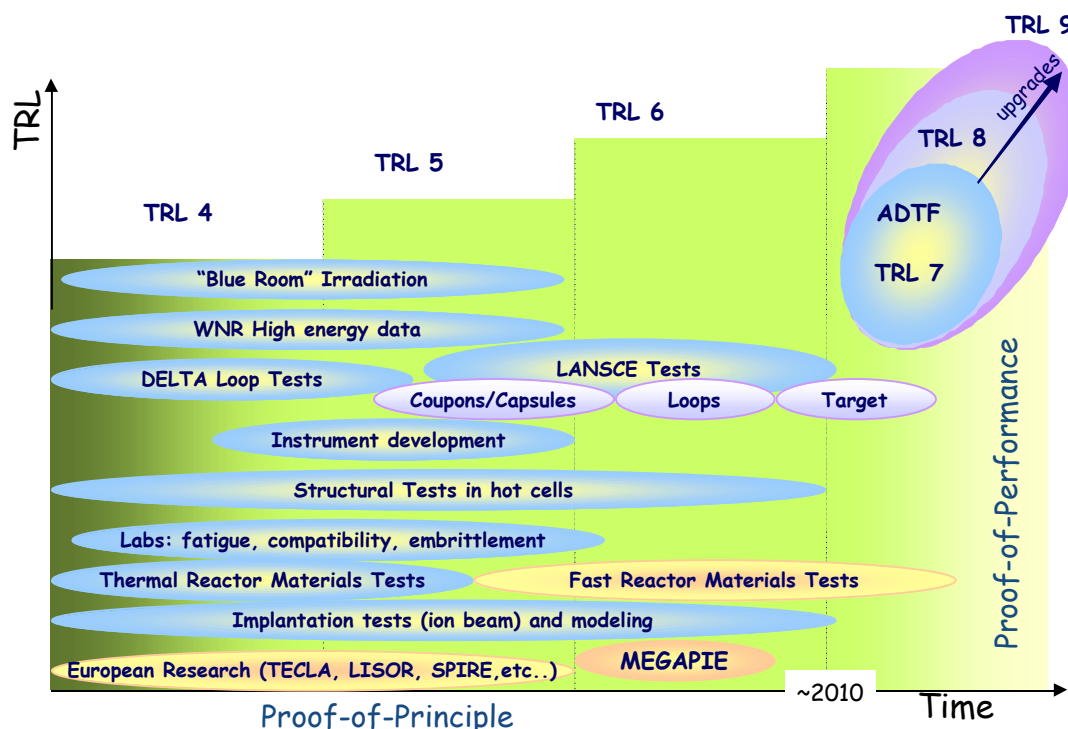


Fig. 17. Experimental facilities and programs to support the proof-of-performance phase of spallation target and materials development.

Specific experiments to achieve the desired objectives and incorporate the international collaboration more closely with the 10-year plan need to be defined. This effort is ongoing, and a first draft of the research plan is expected in the second quarter.

LBE-Sodium Compatibility Experiments

For transmutation scenarios in which an LBE target is used inside a sodium-cooled subcritical blanket, the compatibility of the two coolants are of interest in the event of accidental mixing. A less likely scenario in which the two fluids can be used together is when a sodium-bounded metallic fuel is deployed inside an LBE-cooled blanket. A series of calorimetric experiments were completed to investigate the thermal energy and reaction product yields when sodium is mixed with lead, bismuth, and LBE.

The experimental setup is shown in Fig. 18. As shown, a small volume of lead, bismuth, or LBE is contained above the mixing chamber filled with sodium. A diaphragm is ruptured to inject the lead, bismuth, or LBE into the sodium. For fast injection tests, the puncture area is $\sim 2 \text{ cm}^2$. A smaller size lance is used for the slow injection tests when the puncture area is $\sim 2 \text{ mm}^2$. The mixture temperature is recorded by thermocouples. For selected tests, mixed samples are obtained for analyzing reaction products. The test matrix is shown in Table 5, along with the peak

[illegible]

The temperature spikes typically occur near the bottom of the mixing chamber. One unexpected result was that the temperature spike for the only slow injection test was larger than the equivalent fast injection tests. However, in analyzing the peak temperature data, one must remember that those are obtained by discrete thermocouples, and it is difficult to assume that the initial reaction always occurs where the thermocouple is located. The most meaningful data would be equilibrium temperatures. Nonetheless, detailed analyses of the discrete thermocouple data continue. We will perform at least two additional slow injection tests in the second quarter.

Table 5. Test Matrix for the LBE-Sodium Compatibility Experiments

Test	Initial Temp. (°C)	Injection Speed (Area)	Sodium Volume (cm ³)	Heavy Metal		Max. Temp. Increase (°C)
				Injection Material	Vol. (cm ³)	
011023	600	Fast (2 cm ²)	50	Pb	2.5	110
011026	600	Fast (2 cm ²)	50	Bi	2.5	285
011102	600	Fast (2 cm ²)	50	LBE	2.5	165
011018	400	Fast (2 cm ²)	50	Pb	2.5	115
011012	400	Fast (2 cm ²)	50	LBE	1.25	105
011115	200	Fast (2 cm ²)	50	LBE	2.5	60
011120	400	Slow (2 mm ²)	50	LBE	2.5	310
	200	Slow (2 mm ²)	50	LBE	2.5	
	600	Slow (2 mm ²)	50	LBE	2.5	

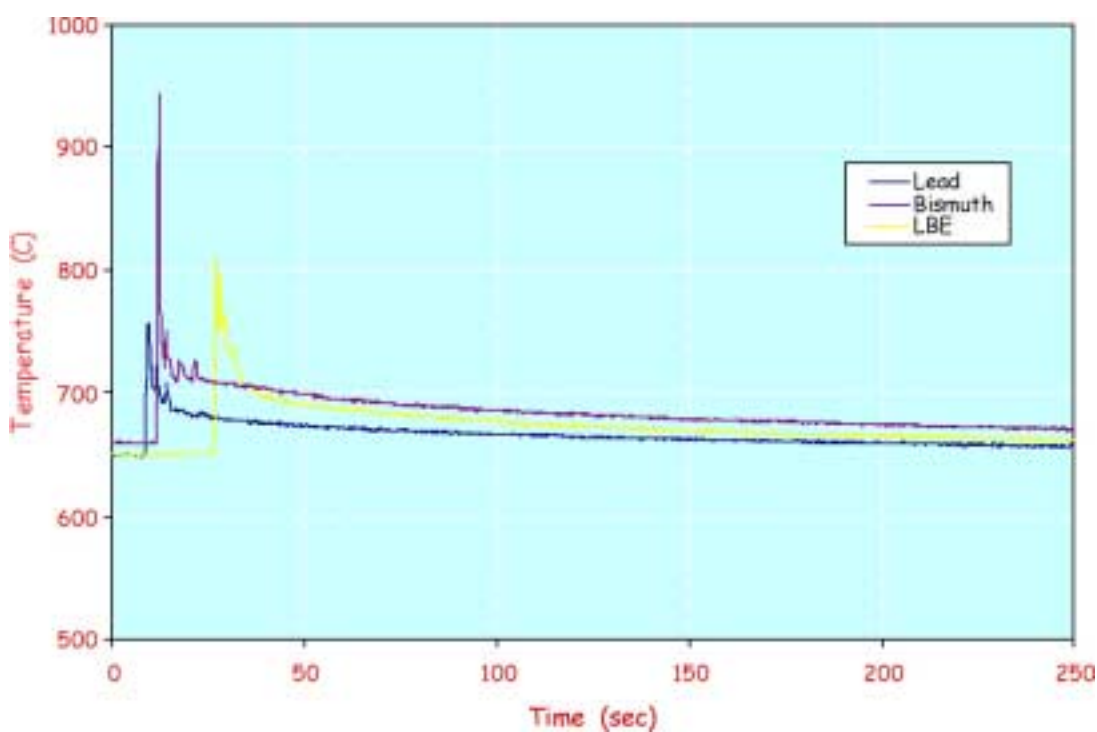


Fig. 19. Temperature traces for the 600°C mixing tests.

Product Inventories for Na-Cooled Tungsten and LBE Targets

We completed a series of calculations to compare the waste stream from the two spallation target concepts—LBE and sodium-cooled tungsten. For this comparison, we assumed a nine-month irradiation of the targets using a 600-MeV, 15-mA proton beam. Within the target region there is either 510 kg of tungsten with 25 kg of sodium (50% tungsten volume fraction) or 540 kg of LBE. The total loop volume is not used for the coolant for simplicity. This is primarily motivated by the fact that the secondary reactions are negligible and the final radioactive material inventory is nearly independent of the total coolant volume. The final results are shown in Fig. 20 for the total activity and for the ratio to Category III limits, used as a measure of the material's toxicity. It is important to note that not all spallation products have dose conversion factors (or Category III limits) available. Those products, which typically have low activity, are ignored in this calculation. However, once the dose conversion factors are developed for these isotopes, the curves in Fig. 20 may be considerably different.

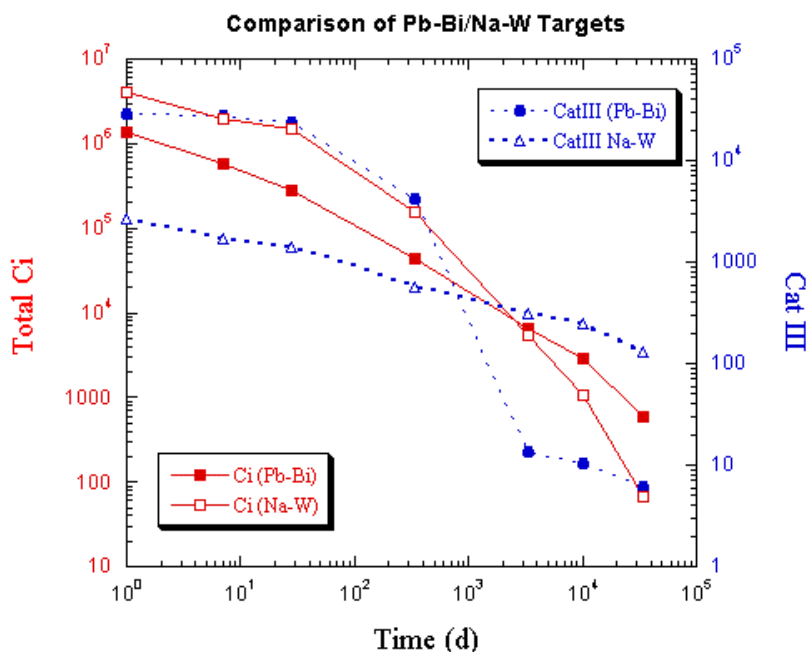


Fig. 20. Spallation and activation products comparison for the LBE and sodium-cooled tungsten targets.

Figure 20 shows that total activity of the sodium-cooled target is higher than the LBE target during the first ~3000 days of cool-down, primarily due to tungsten isotopes (W-187 specifically). However, LBE is more toxic than the sodium-cooled target during the first ~1000 days, because of polonium-210 production in the LBE system. It is important to note that, in these calculations, we used a beryllium reflector on one side of the target, resulting in a large thermal neutron population. Consequently, thermal neutron capture results in polonium production that is larger than one would get in a truly fast system.

Scoping Calculation for the Neutron Yield Experiments

We performed a number of scoping calculations using MCNPX (merged code that includes both Los Alamos High-Energy Transport (LAHET) and Monte Carlo N-Particle (MCNP) codes) to assess the data quality in the LBE target neutron yield experiments (see section entitled “LANSCE Irradiation Experiments”). The impact of the support structure on the activation foil measurements of flux was small, but the effect was not negligible. The estimated impact from the aluminum support plate was to increase the lower surface flux by ~10%. Foils were placed around the target at the 10-cm location to compare symmetry effects. The calculated neutron flux intensity around the target is shown in Fig. 21.

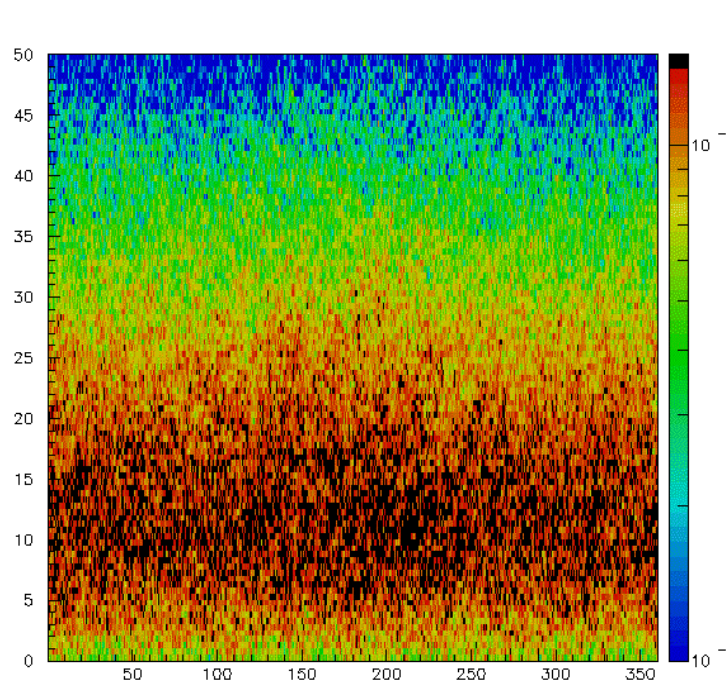


Fig. 21. Image of surface flux of Pb-Bi target. (X axis is in degrees, y axis is in position along target. Color denotes neutron flux intensity).

The expected count rates at the detectors down the flight paths were also calculated with MCNPX (Fig. 22) to determine what, if any, changes needed to be made on the collimator configuration. It was determined that the count rates were not excessive, and the existing configuration was used in the experiment.

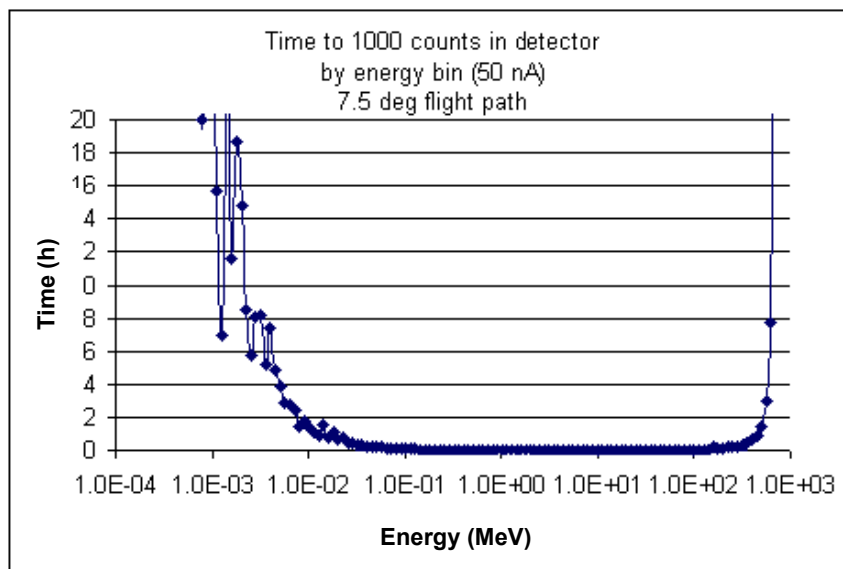


Fig. 22. Time necessary to get sufficient counts for adequate statistics at various energies.

3.2 Materials

The major objective of the materials activities is to test and quantify materials properties under proton and neutron irradiation.

Scope

The major activities in this area are continuation of the high-temperature testing of irradiated materials, irradiation test plans, collaborations with the Paul Scherrer Institute (PSI) materials program, and updating and maintaining the *Materials Handbook*. Specifically, testing in hot cells will support the AAA Program by determining the mechanical properties of structural materials at prototypic temperatures after irradiation in a proton beam. This will involve testing some materials irradiated at LANSCE at low temperatures and testing materials irradiated at PSI at high temperatures. The following are the activities in support of this mission:

- Receive and test irradiated rods from PSI;
- Order and install a high-temperature furnace for performing mechanical tests on specimens in vacuum or argon at temperatures up to 700°C;
- Perform bend tests at 300°C, 400°C, and 500°C on F82H, 9Cr-1Mo, and 316L;
- Perform compression tests on tungsten at 600°C;
- Perform mechanical tests on tantalum at high temperature;
- Continue high-temperature testing of 9Cr-1Mo at PNNL;
- Complete and publish new chapters of the *Materials Handbook*, including 9Cr-1Mo, tungsten, tantalum, mercury, LBE, and corrosion on various steels;

- Prepare an irradiation test plan (mostly in reactors) for cladding duct materials; and
- Review the reactor irradiation database as applicable to transmutation applications.

Work in the materials area has been curtailed due to budget uncertainties.

Highlights

- Strong collaboration between LANL and PSI materials teams continued. AAA staff member Robert Rutherford returned from PSI in November after successfully completing TEM analyses of irradiated steel samples as part of the Spallation Target Irradiation Program.

High-Temperature Testing of Structural Materials

One irradiated¹⁰ and two unirradiated tensile tests were performed at 600°C on Mod9Cr-1Mo (T91). Results plotted in Fig. 23 (along with previously obtained data at lower temperatures) show little difference when compared to unirradiated data; however, we can see a decrease in yield strength and uniform elongation when compared to tests performed at 500°C. A report that summarizes the tensile properties of candidate AAA structural materials was revised to include the new data.

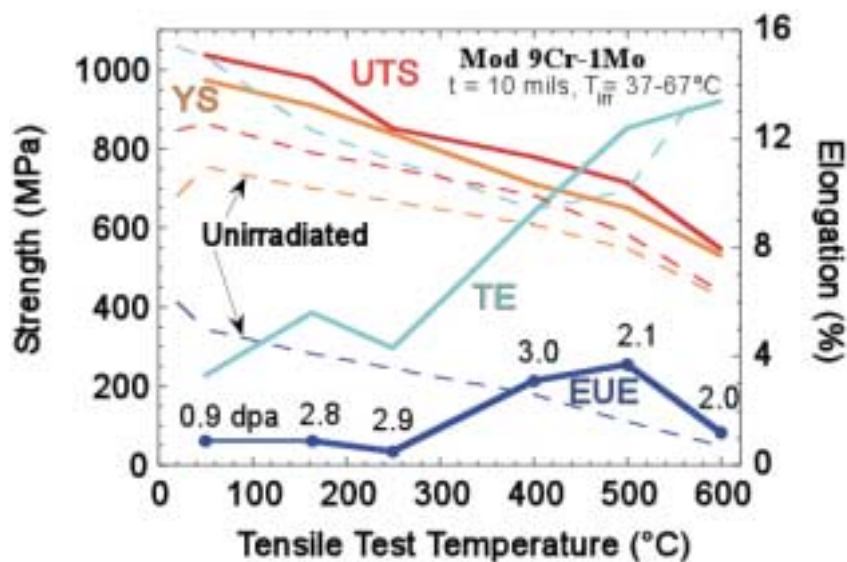


Fig. 23. Mechanical properties of Mod 9Cr-1Mo after irradiation in a proton beam at 37°C to 67°C and tested at temperatures from 50°C to 600°C (new data are at 600°C).

¹⁰ 2 dpa exposure at 37°C–60°C.

Hot-Cell Work

No hot-cell work was performed during this quarter due to upgrades being performed on hot-cell facilities. Related activities, however, included the following:

- Four certified, Type A, 55-gallon drums were bought for transporting materials irradiated by the SINQ accelerator at PSI to LANL and for returning specimens from ORNL and PNNL to LANL.
- Quotes were obtained for buying a high-temperature furnace for performing tests up to 1000°C in argon in a hot cell.

Materials Handbook

In the short timeframe worked during this reporting period, the following activities were ongoing or completed by the Handbook Coordinator:

- A Foreign Travel Report was provided to DOE covering the two weeks spent by the Coordinator at Forschungszentrum in Jülich, Germany, initiating cooperation with the European Spallation Source (ESS) Project and with PSI in Switzerland on additional chapters for the *Materials Handbook*.
- A slide presentation entitled "Radiation-Induced Stress Relaxation in Austenitic Alloys Exposed to Environments Anticipated in the Accelerator Production of Tritium Target/Blanket System" was prepared for the embedded topical AccApp01 meeting at the American Nuclear Society (ANS) winter meeting.
- Confirmation was sought and received from ESS that they intend to provide handbook chapters on tantalum and mercury; similarly, PSI is to provide a chapter on lead-bismuth eutectic.
- Drafting of sections of Chapter 19 on 9Cr-1Mo-V ferritic/martensitic continued.

TEM Analyses of Irradiated Steel Samples

Analysis was performed on SS-316L at PSI after irradiation in the SINQ accelerator. Microstructures of materials were studied after exposure to an environment of high-energy protons plus spallation neutrons. The material studied received a maximum total charge of 6.8 Ah of protons with a peak fluence of 3.2×10^{25} p/m², which correlates to a dose between 2.5 and 9.7 dpa. The temperature range for the specimens studied was between 70°C and 300°C. As shown in Table 6 and Fig. 24, the mean size of Frank loops grew with increasing dose while the density remained constant. The density and mean size of small-defect clusters and stacking-fault tetrahedral (SFT) remained relatively constant with increasing dose. These results show a good agreement with previous measurements on stainless steels irradiated to a similar dose.

Table 6. Dose Dependent Irradiation Defects in SS-316L, Including Small-Defect Clusters, Frank Loops, and Stacking-Fault Tetrahedral (SFT)

Dose (dpa)	Irradiation Temperature (C)	Small Cluster		Frank Loop		SFT	
		mean size (nm)	density (m ³)	mean size (nm)	density (m ³)	mean size (nm)	density (m ³)
2.5	74-87	1.6	3.7×10^{23}	6.5	9.8×10^{22}	1.5	5.6×10^{22}
5.8	188-222	1.6	4.0×10^{23}	14.1	6.9×10^{22}	1.5	4.0×10^{22}
9.7	262-305	1.7	4.1×10^{23}	17.4	6.0×10^{22}	1.5	6.5×10^{22}

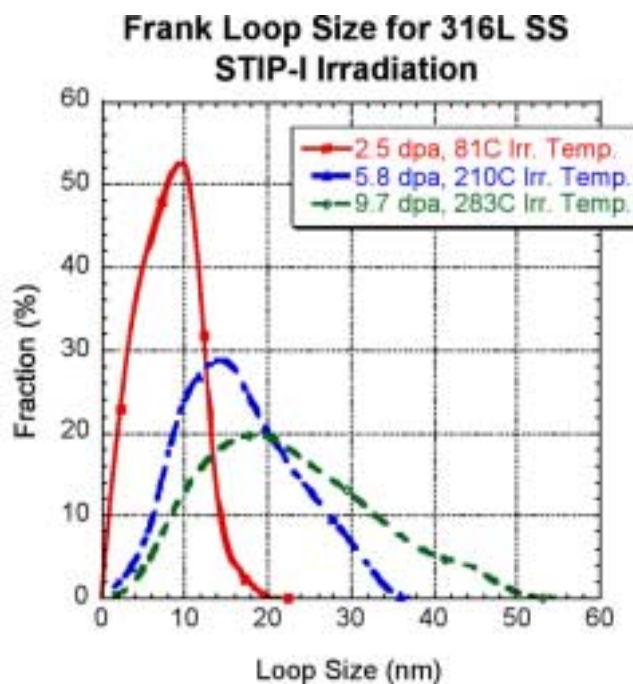


Fig. 24. Effect of dose on fractional percent of Frank loop size.

Tungsten Compression Testing

Compression testing of tungsten was conducted to 20% plastic strain using a strain rate of 10^{-3} at temperatures of 25°C, 150°C, and 300°C. Testing was performed on the tungsten manufactured in the following ways:

- Drawn wrought tungsten,
- Drawn wrought tungsten/annealed at 1800°C for 15 hours,
- Vapor plasma spray (VPS),
- Chemical vapor deposition (CVD) tested parallel to growth direction (radial), and
- CVD perpendicular to the growth direction (axial).

The results are shown in Figs. 25 and 26.

Wrought tungsten tested in compression had a yield strength of ~1150 MPa, ~750 MPa, and ~425 MPa when tested at 25°C, 150°C, and 300°C, respectively.

Although the decrease in percent yield strength from increasing temperature varied between the different types of processed tungsten, all forms exhibited a substantial decrease in yield strength with increasing temperature.

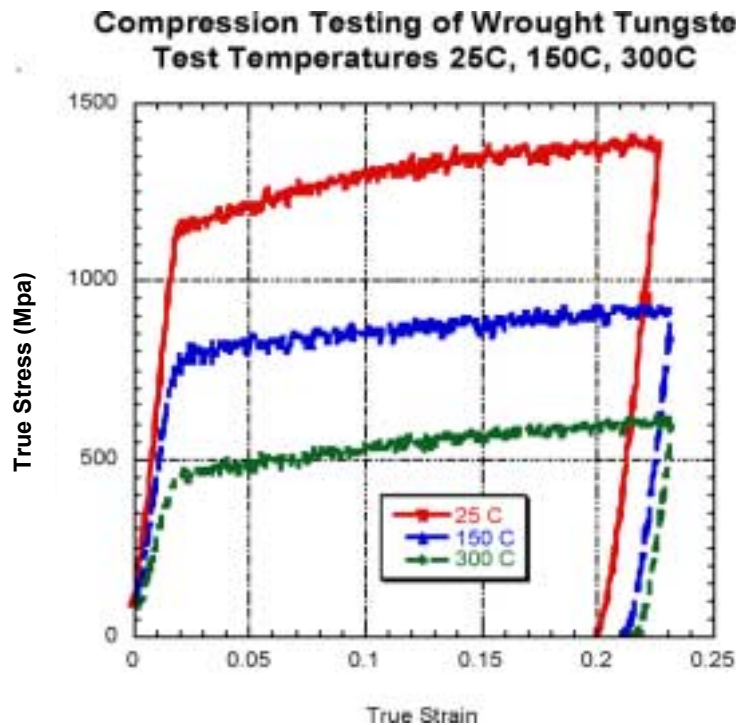


Fig. 25. Compression testing of wrought tungsten.

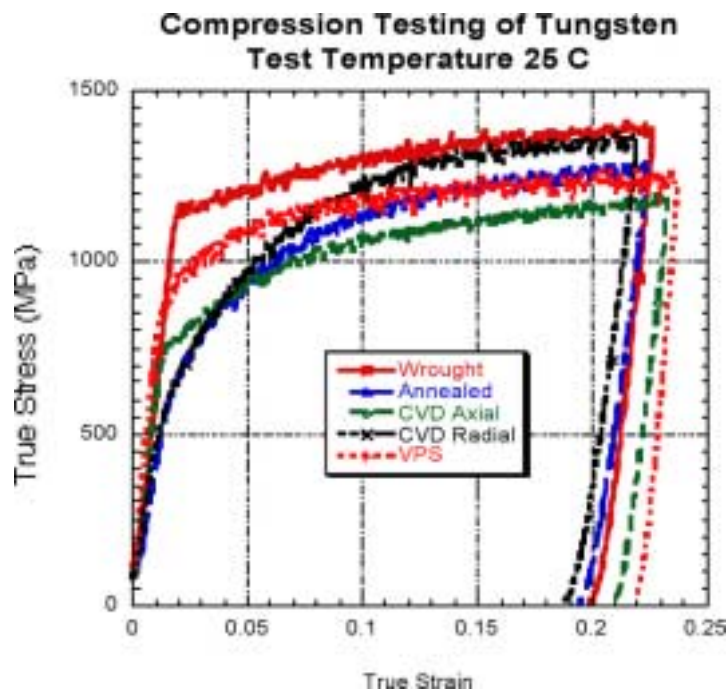


Fig. 26. Compression stress/strain curves tested at 25°C for tungsten manufactured by powder metallurgical (PM)-wrought, PM-wrought and annealed, chemical vapor deposition (CVD) and vapor plasma spray (VPS).

Wrought tungsten exhibited the highest yield strength of ~1150 MPa, followed by VPS at ~800 MPa. CVD axial showed a yield strength of ~750 MPa. CVD radial and annealed tungsten both revealed a yield strength of ~600 MPa.

3.3 Lead-Bismuth Eutectic Technology

The major objective of LBE research activities is to develop a fundamental understanding of LBE performance parameters and measurement techniques when used as a nuclear coolant, with primary emphasis on spallation target applications.

Scope

LBE Technology Development

The safe and reliable implementation of the LBE technology requires additional developments for the oxygen sensors. Development of other nonintrusive flow measurement and online corrosion measurements would significantly improve the reliable operations of an LBE target. The development will be carried out in collaboration with international partners (e.g., CEA and FZK) under DOE agreements. By collaborative testing, the objective is to achieve in 3-4 years a TRL-4 level where a parametric (velocity, temperature, materials, thermal gradients, etc.) is developed to lead into the spallation target conceptual design.

The scope of this work package involves developing new sensor technologies and corrosion data analyses with the long-term objectives listed above. Some of the actual tests will be performed in the DELTA Loop (Materials Test Loop), and testing must be closely coordinated with loop-operations work-package activities. The FY02 activities are as follows:

- Fabricate oxygen probes to be tested in the DELTA Loop;
- Develop a calibration standard in conjunction with international partners;
- Cross-calibrate oxygen sensors;
- Develop gas and solid-phase oxygen control methodology;
- Develop concepts for low-temperature oxygen probes;
- Develop ultrasonic laser velocimetry technique;
- Analyze corrosion data;
- Develop and design components for FY03 testing (with international collaboration); and
- Revise the DELTA Loop test plan according to international collaboration work packages.

DELTA Loop Operations

The DELTA Loop will be operated to validate key Russian LBE nuclear-coolant technology, to perform corrosion and thermal-hydraulic testing, and to develop diagnostics and probes for application in a high-powered spallation-target system. Again, the tests will be carried out in collaboration with international partners.

The scope of this work package involves operating, maintaining, and upgrading the DELTA Loop in accordance with the long-term objectives listed above. The actual test

plans will be developed under the LBE technology work package, and operations must be closely coordinated with activities under that work package. The FY02 activities are as follows:

- Complete construction for operational and instrumentation testing;
- Address all post-start findings;
- Perform operational tests;
- Test oxygen control techniques and procedures;
- Update data acquisition and control (DAC) system and hazard control plans for unmanned operations;
- Install new instruments (e.g., improved oxygen sensors and ultrasonic velocimetry) as delivered from the LBE technology team; and
- Perform 1000-hr corrosion tests (two different materials and/or two different velocities).

Highlights

- The DELTA Loop construction and initial checkout was completed. Operational testing began in December 2001. Official opening was also in December when the loop was dedicated to the memory of Joe King.
- The LBE team authored and co-authored six papers presented at the ANS Annual Winter Meeting in November (Reno, Nevada).

DELTA Loop

The main emphasis during the first quarter was to complete construction and initial checkout of the DELTA Loop and to start operations. A small amount of technology development work was performed on a magnetic flow-meter concept.

The DELTA Loop was operated for the first time. In preparation for operation, the following activities were undertaken:

- Doors on the loop enclosure were equipped with switches interlocked with the DAC system. If any door is opened, the system turns power to the heaters and pump off.
- SCRAM buttons were installed at every door and at the computer station. In case of emergency, a worker can press a SCRAM button to shut down power to the heaters and to the pump.
- Additional independent temperature sensors were installed on the piping. These devices are independent of the DAC system. If any of these temperature measurements is higher than the maximum allowed, power to the heaters and the pump is shut down.
- Additional critical conditions such as maximum temperature (500°C), minimum temperature (130°C), or maximum pressure (100 psig) are described in a "DAC Critical Controls" document that is kept with the HCP. The DAC system interprets these conditions and acts according to the Critical Controls document.
- SCRAM and interlock systems were finished and tested before the first run.

- All heating, cooling, data acquisition, and control equipment were installed and checked. The loop has 30 trace-heater zones, nine main heater zones, more than 200 thermocouples, pressure transducers in lead-bismuth and in the gas volumes, and water flow sensors, as well as gas, water, and lead-bismuth actuated valves. All these components were installed, connected to the DAC system, and tested.
- The DAC system was finalized, and many of its functions were checked. Some functions will be finalized after running the loop with lead-bismuth.
- The hazard control plan and operating procedures were finalized and approved.
- Piping and vessels were insulated.
- Lead-bismuth eutectic (8000 pounds) was loaded into the melt tank and melted.
- In December, liquid lead-bismuth was transferred from the melt tank into the sump tank and then into the loop piping using cover gas pressure. After the liquid metal reached the top pipes, we started the pump and ran liquid lead-bismuth flow through the loop for several hours.
- We achieved different flow speeds with an estimated maximum speed of about 3.3 m/s in a 1-inch test section or 29 gpm. We first ran the loop with uniform temperature distributions of up to 350°C. Heating zones were operated, and initial heating rates recorded.
- Next, we used the water-cooled heat exchanger to create temperature gradient in the loop. Heat exchanger capacity was varied to investigate its effect on temperature changes in the loop. To achieve a steady state, the lead-bismuth flow rate was set to ~2 m/s in a 1-inch test section and 4 of 9 main heater zones set to full power (27 kW). By adjusting the heat exchange area, we achieved steady state. Table 7 shows the temperature change in all heat exchanging areas.

Table 7. Temperature Profile Around the DELTA Loop

ΔT in Recuperator (Cold Side)	31°C
ΔT in Main Heater	14°C
ΔT in Recuperator (Hot Side)	-31°C
ΔT in Heat Exchanger.	-14°C

We used a magnetic flow meter (MFM) on the loop to measure liquid metal flow. MFM readings along with the calibration formula provided by IPPE, the manufacturer, gave us values for flow speed that we expected. In addition, we compared pressure measurements to the pressure drop calculations to calculate flow speed during the tests. Flow speed values based on these two measurements are shown on the plot in Fig. 27. Thus, the MFM measurements and pressure drop calculations were confirmed.

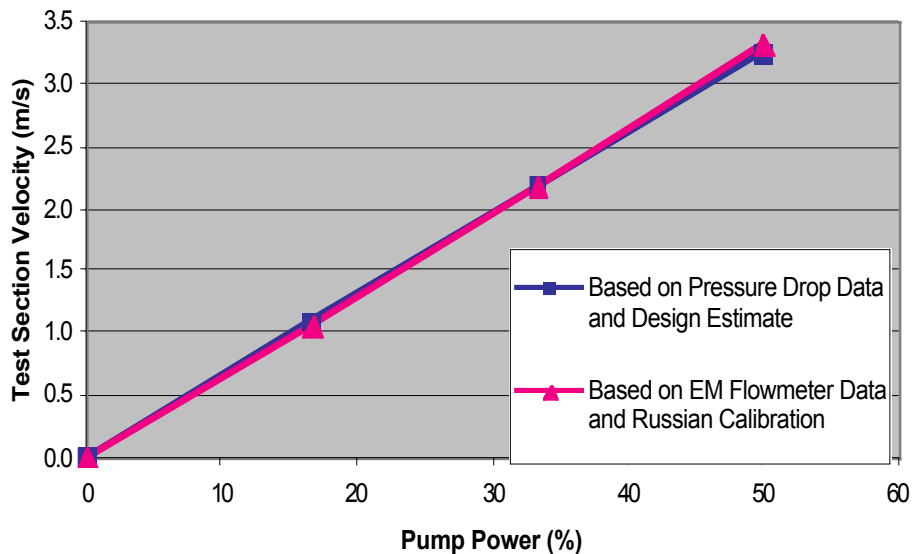


Fig. 27. Pump power vs. flow rate curves.

We tested several SCRAM conditions, and the DAC system reacted as expected. Several improvements were made to the DAC system to make it easier to use and to allow more user input during operation. The loop total running time for the first cycle was 15 hours.

Lead-Bismuth Eutectic Research

The main effort was to test the DELTA Loop instrumentation. A noteworthy achievement is installation of an external magnetic flowmeter. The initial experiment indicated good signal output within the desired range of LBE flow velocity, and the performance should not be adversely affected by the change of contact resistance that plagues conventional electromagnetic flow meters. Future calibration and tests of repeatability are planned.

3.4 LANSCE Irradiation Experiments

The major objective of the LANSCE irradiation experiments is to advance the TRL for transmutation in various areas up to TRL 6 by performing small-scale proton and neutron irradiation to investigate various phenomena. Four specific experiments planned for FY02 are as follows:

- Sodium activation tests;
- Neutron yield and spectrum tests;
- Helium and hydrogen production tests; and
- Corrosion studies.

Scope

Sodium Activation Tests

If a sodium-cooled spallation target is used, accurate prediction of coolant activation is important for operational and safety reasons. In the summer of FY01, we performed a series of activation tests using an 800-MeV beam. Subsequent tests at other energies were postponed because of budget reduction. FY02 activity is limited to completing the final data report.

Neutron Yield and Spectrum Tests

Spallation neutron sources create high-energy neutrons whose energies extend up to the incident proton energy. In the design of accelerator-driven waste transmuters, the high-energy neutrons that leak from the spallation target have three practical implications:

- (1) They dominate the shield design because they have long attenuation lengths (18 cm in steel);
- (2) They lead to the production of source neutrons in the fuel region, which generates a spatially dependent neutron source that influences the power density distribution in the blanket; and
- (3) They dominate the production of helium and hydrogen atoms in the steel structural elements that reside in the multiplier region near the target, while gas production limits the lifetime of structural materials near the target.

As a means of reducing gas production in structural materials in the multiplier region, a buffer region consisting of high-atomic-mass material may be placed between the target and the multiplier. This buffer attenuates high-energy neutrons that leak from the target into the multiplier. Additionally, the configuration of the buffer and the associated beam rastering parameters are variables available to the ADTF designer for adjusting the multiplier power distribution. The objective of these experiments is to provide benchmark data for the analysis tools. The data from these tests will be combined with the gas-production test results and structural properties test results to optimize the target and buffer design (which impacts the multiplier design). To evaluate the effectiveness of a buffer in reducing the leakage of high-energy neutrons, we propose making these measurements of high-energy neutron distributions a function of target radius.

Helium and Hydrogen Production Tests

Currently, considerable uncertainty exists in predicting the helium and hydrogen production at high energies. The objective of these experiments is to provide data to improve helium and hydrogen production cross-sections in materials near the spallation target. The data from these tests will be combined with data from spectrum tests and structural properties tests to optimize the target and buffer design (which impacts the multiplier design). Optimizing the design with large uncertainty in the design tool is not adequate and will result in a waste of time and money in the long run. Hydrogen and helium production on materials proposed for the AAA Program in the neutron energy range up to 100 MeV will be measured. Measurements of the double differential cross-sections for proton and alpha-particle emission will provide not only data for the total hydrogen and helium production by neutrons in these materials, but also data for transport of these elements by recoil into or out of zones

of different composition in AAA designs. We will take the measurements for iron (Fe). As an integral test and to provide data quickly, an alloy of stainless steel such as SS-316 will also be studied.

Corrosion Studies

Liquid-metal corrosion is the major issue when LBE is used as a nuclear coolant or as a spallation target. If oxygen control is used to control the corrosion, it must be shown that stable oxide layers can be developed and maintained on the surfaces. This is affected by the initial conditioning of the surfaces, as well as changes in thermodynamic conditions during operations. For spallation target applications, we must also show that direct proton irradiation does not cause a drastic change in oxide layer properties adversely affecting corrosion rates. Finally, a more reliable operation is possible if a capability for online corrosion monitoring during actual operations can be developed for the loops. By collaborative testing, the objective is to achieve in 3 to 4 years a TRL 4, where a parametric is developed to lead into the spallation target conceptual design. The scope of this work package involves oxide film characterization, Blue Room irradiation of oxidized surfaces, and conceptual design of corrosion probes to be used in the test loop

Highlights

- In December, an LBE target (50 cm long \times 25 cm dia) was irradiated in the Blue Room, providing an abundance of neutron yield and spectrum data that are being analyzed.
- The commissioning test for the helium and hydrogen production was performed at WNR (LANSCE); all the detectors performed well, providing some initial data with iron.

Sodium-Activation Tests

A draft of the final report of the sodium-activation tests is being reviewed internally at Los Alamos National Laboratory. The report will be issued as a LANL Technical Report.

The measured activities were corrected for the decay after irradiation and branching ratios, and then converted to cross-sections using the measured proton fluence and sample thickness. Data for the cross-sections derived from the four different counts were used to form a weighted average using the statistical uncertainties associated with each separate measurement. The statistical uncertainty on the average value was then combined with the various systematic uncertainties to produce the final overall uncertainty. The derived cross-sections and their estimated total uncertainties are listed in Table 8.

MCNPX (version 2.1.5) was used to model the experimental geometry. The calculated yields of isotopes were then used to determine production cross-sections. Additional MCNPX calculations were then performed to estimate production cross-sections for proton energies 100–800 MeV using the standard high-energy physics model in MCNPX (Bertini without a pre-equilibrium phase). Further calculations were performed using the ISABEL (physics modeling code) and CEM (Cascade Exciton

Model code) high-energy physics models available in MCNPX. Results are shown in Table 9. Results indicate that the Bertini model most closely calculates the ^7Be production cross-section, although the C/E is only 0.65. The ISABEL physics model is slightly better than the Bertini model for the ^{22}Na production cross-section (C/E=1.47). However, improvement in the estimate is only ~5% over the Bertini model.

Table 8. Measured Cross Sections and Uncertainties

Isotope	Cross Section (mb)	Uncertainty (mb)
^7Be	6.50	0.24
^{22}Na	29.45	1.00

Table 9. MCNPX Calculations of ^7Be and ^{22}Na Production Rates in Sodium Sample

High-Energy Physics Model	Proton Energy (MeV)	Be-7 Production				Na-22 Production			
		(atoms/proton)	error	cross-section (barns)	error (barns)	(atoms/proton)	error	cross-section (barns)	error (barns)
Bertini	100	3.05E-07	0.378	2.40E-05	9.09E-06	8.52E-04	0.0072	6.71E-02	4.83E-04
	200	2.87E-06	0.1078	2.26E-04	2.43E-05	6.98E-04	0.0069	5.50E-02	3.80E-04
	300	6.43E-06	0.072	5.07E-04	3.65E-05	6.44E-04	0.0072	5.07E-02	3.65E-04
	400	1.38E-05	0.0491	1.09E-03	5.35E-05	6.32E-04	0.0073	4.97E-02	3.63E-04
	500	2.27E-05	0.0383	1.79E-03	6.86E-05	6.21E-04	0.0073	4.89E-02	3.57E-04
	600	3.67E-05	0.0302	2.89E-03	8.72E-05	6.14E-04	0.0074	4.83E-02	3.58E-04
	700	4.51E-05	0.0272	3.55E-03	9.67E-05	5.96E-04	0.0075	4.70E-02	3.52E-04
	800	5.39E-05	0.0249	4.24E-03	1.06E-04	5.77E-04	0.0076	4.54E-02	3.45E-04
Isabel	800	2.61 E-05	0.0357	2.06E-03	7.34E-05	5.50E-04	0.0076	4.33E-02	3.29E-04
CEM	800	9.33E-07	0.189	7.35E-05	1.39E-05	6.35E-04	0.0073	5.00E-02	3.65E-04
Bertini preequilibrium	800	5.39E-05	0.0249	4.24E-03	1.06E-04	5.77E-04	0.0076	4.54E-02	3.45E-04
Results from Measurement	800			6.50E-03	2.40E-04			2.95E-02	1.00E-03

Neutron Yield and Spectrum Tests

Initial target irradiation began in December, with one foil packet mounted on the LBE target (20 cm dia, 50 cm length) with beam for ~60 nA-hrs. Following removal of the first foil, initial gamma spectroscopy measurements began, and 10 additional foil packets were mounted with beam on target for ~100 nA-hrs. Figure 28 shows the target in the Blue Room with foils mounted. Once the foil irradiations were completed, high-energy and low-energy time-of-flight measurements were conducted for three different target locations.

A preliminary report is being drafted. Initial results from activation foil analysis and time-of-flight measurements indicate that both types of measurements produce useful results. It will take time to analyze the results and compare the two counting methods. Some preliminary findings and results are presented here.



Fig. 28. Foils mounted on the LBE target in the Blue Room.

Foil Counting

Foil counting was performed in December 2001 and will continue into January 2002. Initial data analysis has begun. Although each foil packet contained a dozen elements, the initial analysis concentrated on bismuth and lutetium. Figure 29 shows details of a small slice of the gamma energy range. The same foil was counted shortly after the irradiation (upper curve) and about 20 hours later (black-filled curve). The spectra being compared were taken with two different detectors, counted for different times, and normalized using two peaks belonging to longer-lived ^{206}Bi , at 803 keV and 881 keV.

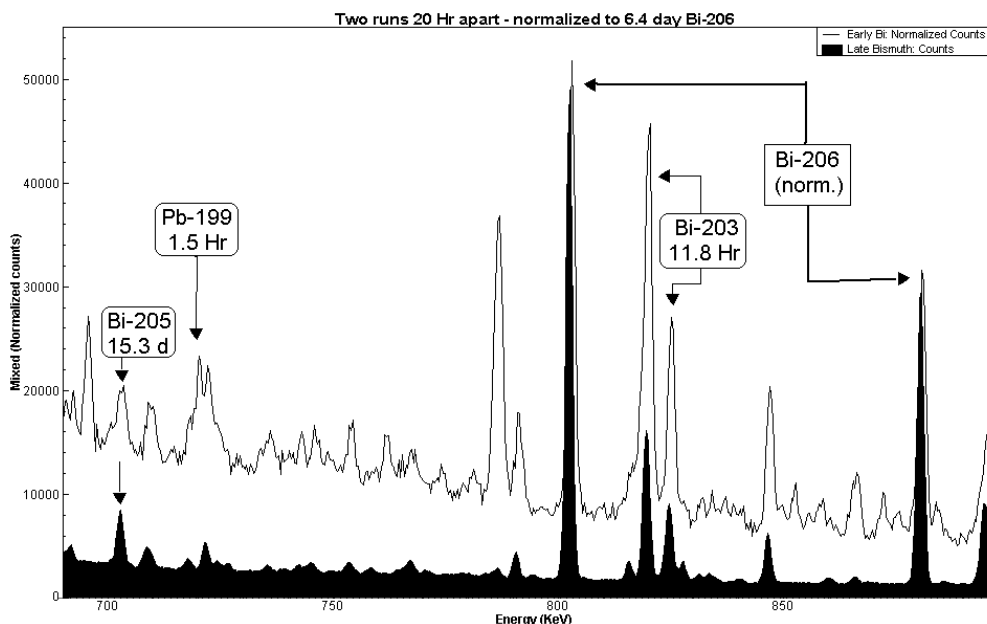


Fig. 29. Bismuth foil measured twice at about 20-hr interval in the 700–900-keV region.

Most peaks can be attributed to nuclides produced by neutrons interacting with the ^{209}Bi nuclei in the foil. Peaks are labeled with the corresponding nuclide and its accepted half-life. The disappearance or decrease in intensity of the peaks belonging to the short-lived activities (a few hours) reinforces confidence in the identification obtained from multiple gamma peaks. In the future, quantitative half-life determination (or consistency) can be performed for many of the samples.

For the time-of-flight measurements, two data acquisition sequences were performed at each of the three target positions. The first data acquisition sequence used plastic detectors to obtain data in the high-energy neutron region ($\sim 0.5\text{--}800\text{ MeV}$). This required about 1.5 hours of beam ($\sim 20\text{ nA}$) on target at each target position and used $20\text{-}\mu\text{s}$ spacing for the beam pulses. The second sequence used lithium-loaded glass detectors to obtain data in the lower energy region ($\sim 0.01\text{--}1\text{ MeV}$). About 8 hours of beam time ($\sim 25\text{ nA}$) were required for each target position having a beam-pulse spacing of $40\text{ }\mu\text{s}$.

Helium and Hydrogen Production Tests

Hydrogen and helium are produced when energetic neutrons interact with materials, and these gases can lead to significant changes in material properties such as embrittlement and swelling. Such effects have been seen in fission reactors, and a significant effort has been made for the development of fusion reactors where the effects are expected to be larger because of higher neutron energy when gas production rates per neutron (proportional to the production cross-sections) are higher. For AAA, which has neutrons of even higher energy, there could be even greater effects from neutron-induced gas production. Because of the paucity of data for neutron energies above 20 MeV , we are measuring gas production cross-sections for materials of interest from $20\text{--}100\text{ MeV}$, which should cover much of the higher-energy region of importance.

In the first quarter of FY02, we commissioned the detector station to measure hydrogen and helium production cross-sections as functions of incident neutron energy. These gases are produced initially from nuclear reactions as energetic protons, deuterons, and alpha particles. When these charged particles slow down and stop (with ranges of mm to cm), they acquire electrons from the material and become hydrogen (protons and deuterons) or helium (alpha particles). Our method is to measure the protons, deuterons, and alpha particles that escape from thin foils as illustrated in Fig. 30.

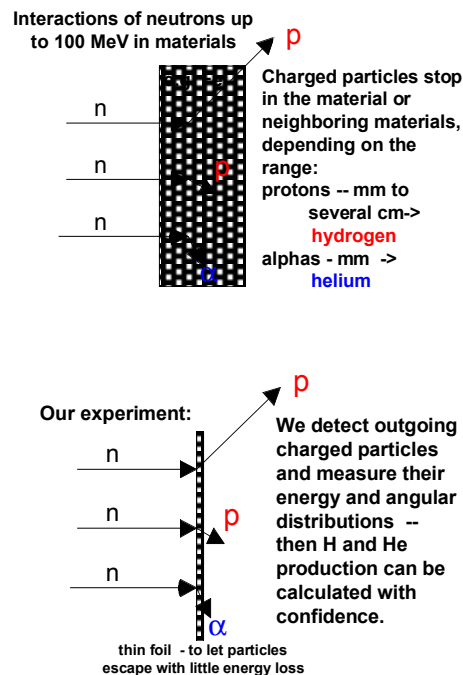


Fig. 30. Interactions of neutrons with materials produce charged particles that stop either in the material or in neighboring materials.

In our experiment, we use a thin foil of the material so charged particles can escape and be detected. We are measuring charged particles with detector systems at many angles. Each detector system consists of two or three detectors in coincidence and arranged so the charged particles pass through the first detector and stop in the second or third. We do this to identify the protons, deuterons, and alpha particles and also the small numbers of tritons and ^3He .

Our commissioning experiments included a test run on an iron sample. Data from our first run are shown in Fig. 31 to illustrate the good identification of the charged particles and, qualitatively, the good counting rate. The data also have a good signal-to-background ratio (much of our effort this quarter was focused on reducing the background).

In performing the commissioning runs, we identified several experimental improvements that should be made before the production runs begin in July 2002, when the LANSCE accelerator begins operations again after the scheduled outage. These improvements in detectors and data acquisition are not expensive and will further

improve the quality of the data. We expect to run Fe and one other material (either SS or Cr) in July and August of this year and to provide cross-sections shortly thereafter. Because the data will also include energy spectra and angular distributions of the charged particles, the data will provide further constraints on nuclear model calculations, which can be used to predict gas production when experimental data are not available.

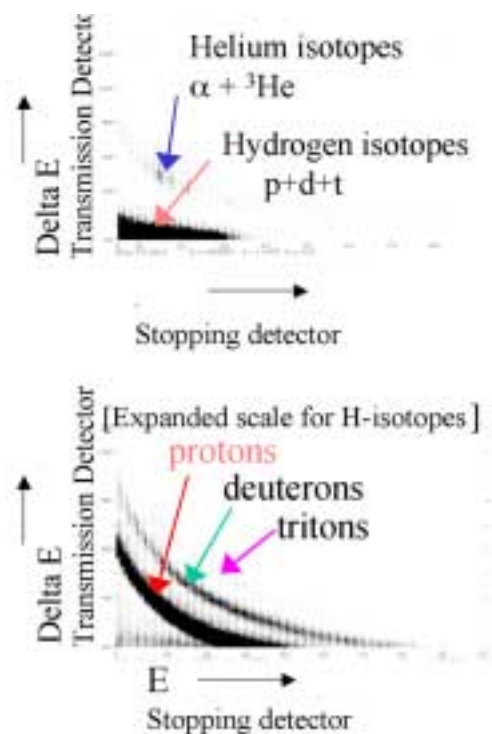


Fig. 31. Identification of protons, deuterons, tritons, ${}^3\text{He}$, and alpha particles from this quarter's experiment of neutron interactions with iron.

Corrosion Studies

In preparing for the July 2002 LANSCE irradiation experiments, we designed an experiment set that will allow us to characterize the physical and electrical properties of the oxide film on stainless and martensitic steels. To do this, it is necessary to expose samples to prototypic environments, so we are examining oxide scales that will likely form in an LBE loop. We have chosen to expose our samples in a small scale LBE furnace used to test the DELTA Loop oxygen sensor. The first 300-hr exposure is currently underway and scheduled for completion in late January. To accomplish this immersion experiment, we successfully designed and fabricated a fixture to hold corrosion sensors for extended exposure periods. We also procured and metallographically prepared an array of corrosion samples for the exposure. Characterization of the oxide film that forms on these samples will take place in the second quarter of FY02.

3.5 High-Energy Physics

The major objective of high-energy physics activities is to improve and maintain the computer codes used in the analyses of accelerator-driven transmutation systems. As part of the improvement, the nuclear data accuracy will be reevaluated to match the desired objectives.

Scope

MCNPX Code Development

MCNPX code development consists of the following activities:

- Development of the *mix and match* capability within MCNPX, which requires production of a version of MCNPX in which evaluated data libraries with different upper-energy limits may be used within the same MCNPX run. This will allow the new LA150n data tables to be used simultaneously with the standard 20-MeV data tables for those isotopes that do not appear in LA150n. (LA150n refers to Los Alamos generated nuclear data library, extending up to 150 MeV.)
- Incorporation of the Cugnon intranuclear cascade and Schmidt evaporation models into MCNPX, which will be carried out in collaboration with CEA-Saclay under the CEA-AAA collaboration framework. CEA will install the models in MCNPX with LANL oversight. LANL will perform a quality check of this work and incorporate the code changes into the official release.
- MCNPX maintenance and beta testing, which involves maintaining an approved list of beta testers for the code and fixing bugs as beta testers report them. Regular releases of MCNPX will be transmitted to the Radiation Safety Information Computational Center (RSICC) as significant improvements to the code are made.

Nuclear Data Evaluations

The nuclear data activities include production of new neutron fission and capture ENDF evaluations to 150 MeV for two actinide isotopes of highest priority. This involves the following:

- Calculating fission barrier and ν -bar¹¹ data to 150 MeV;
- Using the results of GNASH (nuclear reaction code) to generate model-based cross-sections; and
- Using advanced statistical methods to combine discrepant experimental data in the adjustment of the GNASH-generated results to produce new evaluated cross-sections.

As part of these activities, NJOY data processing of new ENDF evaluations and generation of data files of the new ENDF evaluations using the NJOY code will be performed.

¹¹ Average number of neutrons released per fission.

The nuclear data tasks also include improving ^{208}Pb inelastic scattering ENDF cross-section and production of a new version of ENDF ^{208}Pb neutron cross-section that improves the inelastic scattering in the few MeV energy regions.

Initially, an effort was started to upgrade the CINDER90 activation libraries to 150 MeV. This effort was terminated in November due to budget limitations.

Highlights

- MCNPX version 2.3.0 was released to the Radiation Safety Information Computational Center in December.
- MCNPX version 2.4.d was released as an alpha test version in December.

MCNPX Code Development

MCNPX version 2.3.0 was released to the RSICC in December. This is a major update to the current public version, 2.1.5 (released November 1999), although it is still based on the MCNP4B code. New code features include the capability to use proton and photonuclear libraries, as well as the secondary particle-biasing variance-reduction technique needed to efficiently model high-energy hadronic showers. AAA applications have special problems in simulating these since the low-energy neutrons produced in the shower will greatly multiply in the transmuter blanket. Improvements were also made to mesh and radiography-tally capabilities as well as energy deposition tallies. The full set of 150-MeV neutron, proton, and photonuclear libraries now available was also included in the code release, along with an updated User's Guide.

In December, MCNPX version 2.4.d was released as an alpha test version. The 2.4 series of MCNPX is fully integrated with MCNP4C and is regularly released to AAA collaborators. Version 2.4.d implemented some code speed-up suggestions, made corrections to an F8 energy-deposition tally, corrected a criticality bug needed for transmuter blanket analysis, and implemented a warning statement for improper use of one input card. Two bugs identified in the base MCNP4C code related to delayed neutrons were also fixed.

In November and December, version 2.4.e was released, which incorporated two additional bug fixes, and also added recent changes made to the MCNP4B version of the code, 2.3.0. That ensures that the developmental 2.4 series is now consistent with all recent changes incorporated into the RSICC release.

In November, we met with staff from Saclay to discuss implementation of the Cugnon Intranuclear Cascade model and the Schmidt evaporation model into MCNPX. A draft Memorandum of Understanding was produced that outlines the responsibilities of all parties and how updates to and distributions of the software will be handled.

Arrangements for an MCNPX class at the University of Nevada-Las Vegas were completed. Twenty-six students registered for the class, scheduled for January. More than half of these students are directly connected with the AAA Program, including 14 UNLV faculty and students, and 2 Idaho Accelerator Center staff. A class was also taught in Knoxville Tennessee, primarily for the benefit of the Oak Ridge National Laboratory (ORNL) accelerator community. ORNL has long been a collaborator on MCNPX development, beginning with the APT Program. ORNL has also finalized the

inclusion of the latest version of the CEM code in MCNPX, and this is now available for implementation into the next code release. Part of this work included addition of physics modules to do photonuclear interactions above the 150-MeV library limit.

Nuclear Data

We have focused on modeling nuclear reactions up to 150 MeV for neutrons incident on actinides, particularly Pu and U. The GNASH nuclear-reaction code provides a modeling tool to produce 150-MeV ENDF evaluations. For actinide targets, a number of advancements need to be made, and we have begun this work. This includes setting up Hauser-Feshbach calculations, in which numerous (50-100) excited nuclei may be populated and estimating fission barriers and fission properties for these nuclides; modeling preequilibrium reactions at higher energies; and developing a high-energy optical potential for calculating the scattering and the transmission coefficients. We also began investigating CEM intranuclear cascade code methods to calculate neutron production and spectra from the hundreds of decaying fission fragments that play an important role in the 150-MeV evaluation. These techniques will allow us to generate ENDF evaluations that can be used in MCNPX for more accurate predictions of fission, criticality, transport, and radiation damage. Significant advances have been made in benchmarking models for fission neutron spectra.

In November, P. Lisowski provided his $^{239}\text{Pu}(n,f)$ data from LANSCE (actually ratio data to ^{235}U fission), allowing us to finalize our evaluation of the neutron-induced fission cross-section reaction on ^{239}Pu up to 20-MeV incident energies using a statistical Bayesian method. Incorporating recent experimental data from Lisowski,¹² Shcherbakov,¹³ and Staples,¹⁴ this new evaluation allowed us to significantly reduce the associated error bars on the evaluated cross-section. This work also demonstrated the strong influence of the ENDF/B-VI standard $^{235}\text{U}(n,f)$ cross-section on the $^{239}\text{Pu}(n,f)$ one, since most experimental data on $^{239}\text{Pu}(n,f)$ are considered in ratio to $^{235}\text{U}(n,f)$.

CINDER90 Update

Initially, we made significant progress in developing an activation library up to 150 MeV for CINDER transmutation calculations, using model calculations with the HMS-ALICE code that include isomer production. However, AAA support for this effort was terminated due to limited budget.

3.6 Reactor Physics

The reactor physics task involves the codes and methods used to assess the transmutation process. The objective also includes defining and designing long-term experiments needed to advance the TRL in this area.

¹² Los Alamos Neutron Science Center, 2001.

¹³ Petersburg Nuclear Physics Institute, 2000.

¹⁴ Los Alamos Neutron Science Center, 1998.

Scope

Experiment and Safety Analysis

This task consists of analyzing physics experiments and developing a safety analysis strategy applicable to accelerator-driven system (ADS) design. Part of the physics experiment work consists of providing high-quality experimental data; and for this purpose, ANL personnel will participate in collaboration with CEA to perform the critical and subcritical experiments of the MUSE4 configuration. To validate data and methods for the neutronic design of an ADS, an analysis of the experimental results obtained in the MUSE4 program will be performed using both deterministic and stochastic codes with different data files (e.g., JEF2 and ENDF/B-VI). Additionally, the irradiation experiments PROFIL-1 and -2 will be analyzed, in which samples of actinide isotopes have been irradiated in the French Phenix reactor. The objectives for safety analysis are to develop the conceptual safety design basis and criteria for ADS reactors, to develop and verify the computational safety analysis methods and computer codes necessary for safety assessment of ADS reactors, and to perform initial scoping analyses of design basis and bounding accident sequences for an ADS reactor conceptual design.

Physics Needs and Methods Development

Physics needs will be assessed by performing uncertainty evaluations and developing new capabilities for computational tools used for the neutronic analysis of ADS. Work will be performed to define physics needs and needs related to cross-section data uncertainties. In a first phase, sensitivity and uncertainty analyses will be performed for minor-actinide-dominated fuel compositions. A significant effort will be devoted to extend the present field of applicability of deterministic tools to energies >20 MeV, taking into account phenomena (e.g., gas productions) that can be affected by uncertainties in this energy range. Code and methods upgrades are needed to improve our capability to correctly calculate coupled systems with deterministic tools. The iteration strategies for equilibrium concentrations in the REBUS-3 burnup code will be modified to eliminate instabilities observed for subcritical and deep burnup conditions. Implementation of multivariate cross-section fitting capability will be also performed. Coupling with high-energy (spallation) source calculation has to be extended to the 3-D geometries (Cartesian and hexagonal) and needs to be implemented in a more flexible manner. Considerations will also be given to the possibility of developing an entirely deterministic coupled calculation (i.e., spallation and high-energy charged-particle transport treated deterministically).

Physics Experiment Planning

The purpose of this task is the definition of an experimental plan conceived to support the needs of the neutronic design of an ADS. To simulate the physics and dynamic behavior of accelerator-driven systems and to support their design, an action will be taken to investigate the possibility of using the TREAT and ZPPR facilities located at ANL-W. The information coming from the potential experiments performed at these facilities will play a critical role in validating data, codes, and methods needed for reducing uncertainties and margins for the actual design of a power ADS. These experiments will be planned to be complementary of existing and future experimental programs (e.g., MUSE, TRIGA) carried out by foreign partners. The scope of this work is to provide an experimental plan, to perform sensitivity analysis for justification of the program, and to define the objectives and the feasibility of the experiments.

Highlights

- A preliminary analysis of the MUSE benchmark, corresponding to the critical configuration of the MUSE4 experiment, has been performed.
- An uncertainty assessment quantifying the impact of nuclear data on integral parameters relevant to the neutronic design of an ADS was completed for systems with fuels having a high content of minor actinides.

MUSE Benchmark

Work has started for the calculation of the MUSE benchmark. The configuration is very similar to that of MUSE4, and it corresponds to the real MUSE4 critical configuration, without the 0.8-cm-thickness buffer at the fuel/reflector interface. A first parametric series of calculations has been performed, and preliminary results (in terms of subcriticality levels) are shown in Table 10 for the critical configuration of the COSMO and MUSE4 experiments. VARIANT (three-dimensional nodal transport) and BISTRO (two-dimensional discrete ordinates) codes were used with JEF2.2 data and different energy group (NG) structure. The influence of the angular approximation, simplified spherical harmonics (HS), against full P3 expansion (Legendre polynomial) has been found not important ($>0.1\%$). On the contrary, the number of groups has quite an impact. In the future, this issue will be studied, along with a more accurate treatment of the reflector cross-sections. In the same table we show some results with ENDF/B-VI data processed by MC²-2. As observed in the past, a huge discrepancy exists when compared to the results obtained by JEF2.2 data. Also in this case, we notice the big impact of the number of energy groups on the results.

Table 10. Subcriticality Levels Expressed in PCM with Different Methods and Data

Case	NG	COSMO		MUSE4 reference			Comments
		VARIANT		VARIANT		BISTRO	
		HS*	P3	HS*	P3		
A.1	33	26	-103	-333	-282	831	Subcritical Flux No Step 1968 Gr
A.2	172	-159		-505		No	
		-161	-381	-511	-558		
E.1	33	ENDF/B-VI		2851		3822	Subcritical Flux
E.2	231			2105		3111.5	

Uncertainty Assessment

An uncertainty assessment task has been initiated to provide indications on physics needs for improvement in cross-section data evaluation. This task will focus on data related to minor actinides. For this latter purpose, we have used the core calculated in the ATW system point design employing a sodium-cooled blanket defined by R.N. Hill and H. Khalil. The core considered corresponds to the once-through option. A cylindrical model was derived and a neutron spallation source was computed using MCNPX. All subsequent neutronic and perturbation calculations were performed using ERANOS in conjunction with JEF2.2 cross-section and dispersion data. The main results are shown in Figs. 32-37.

As usual, the integral parameters that are ratios of neutron flux functionals (i.e., K_{eff} , F^* , and the helium-production-to-dpa ratio) present lower uncertainties than functionals that are linear on the flux (dpa, He, and H production), which are more sensitive to the neutron flux level through their dependence on K_{eff} . The total uncertainty of K_{eff} is on the order of $\leq 1.7\%$ of what was found in a previous study. This is to be attributed to the use of sodium coolant that eliminates one large component of the uncertainty coming from the contribution of Pb and Bi coolants. We note that ^{240}Pu is the isotope with the largest component of uncertainty. The contribution of the reactions $\text{Pb}(n,xn)$ and $\text{Bi}(n,xn)$ are the largest for the helium-production-to-dpa ratio.

Subsequently, the core proposed for the OECD/NEA ADMAB (Accelerator-Driven Minor Actinide Burner) benchmark.¹⁵ has been considered. This core fuel is predominantly composed of minor actinides. Fuel composition and the r - z model are given in Table 11 and Fig. 38. The uncertainties obtained for the different integral parameters, broken down by isotopes and reactions, are given in Figs. 39-44.

As can be observed, uncertainties are relatively high. Subcriticality level uncertainty, for instance, carries out a total value of 3%. This is three times that normally calculated for a standard fast reactor. As expected, most of the uncertainty is coming from minor actinides such as ^{237}Np , ^{241}Am , and ^{243}Am . For these isotopes, capture and fission cross-sections are the main contributors. In addition to these isotopes, for gas production and damage (dpa), Pb and Bi provide a significant contribution, especially through their inelastic and (n,xn) cross-sections. A quite high value of uncertainty is found for the helium-production-to-dpa ratio, indicating a significant spectral sensitivity at high energy. However, because these calculations were performed with a library starting at 20 MeV, a likely significant contribution due to helium production coming from the higher energies has not been included. Future studies will use new available cross-section files extended up to 150 MeV.

¹⁵ Na, B.C., Wydler, P., and Takano, H., "OECD/NEA Comparison Calculations for an Accelerator-Driven Minor Actinide Burner: Analysis of Preliminary Results," *Proceedings: Second Workshop on Utilization and Reliability of High-Power Proton Accelerators*, OECD Nuclear Energy Agency, Aix-en-Provence, France, November 22-24, 1999.

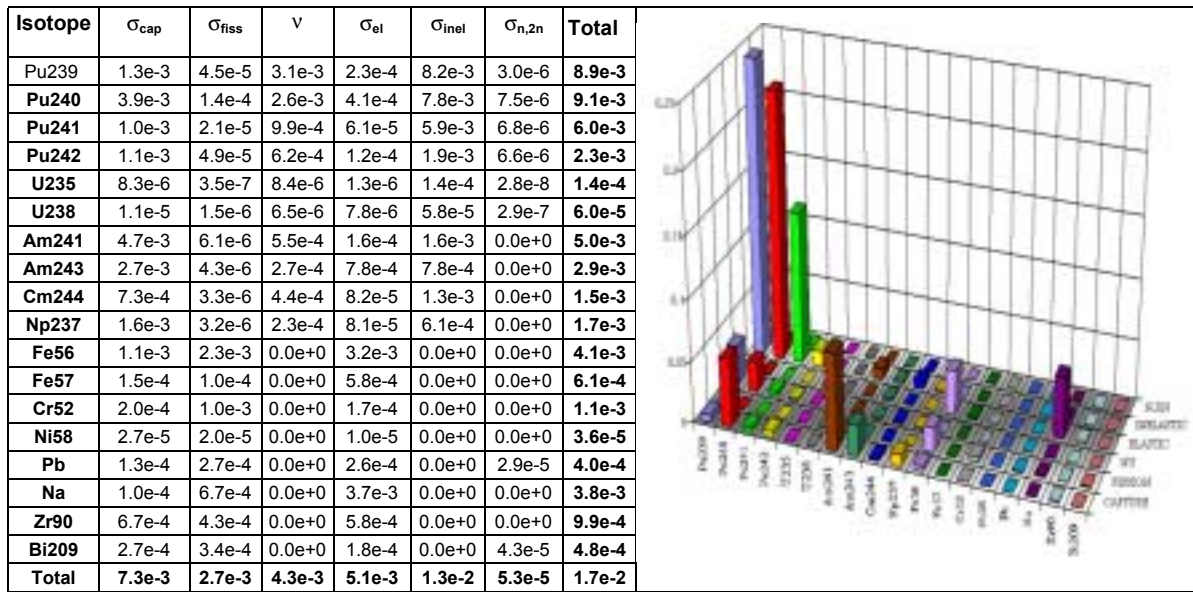


Fig. 32. Uncertainties by isotopes on K_{eff} , where $K_{eff}=0.96922$.

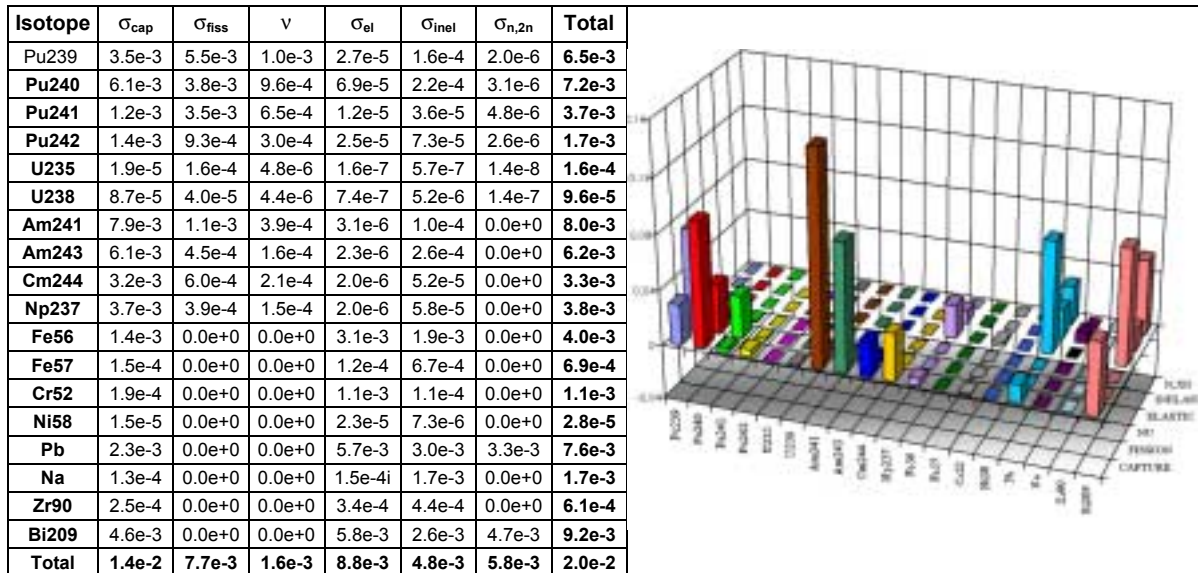


Fig. 33. Uncertainties by isotopes on ϕ^* , where $\phi^* = 8.21E-1$.

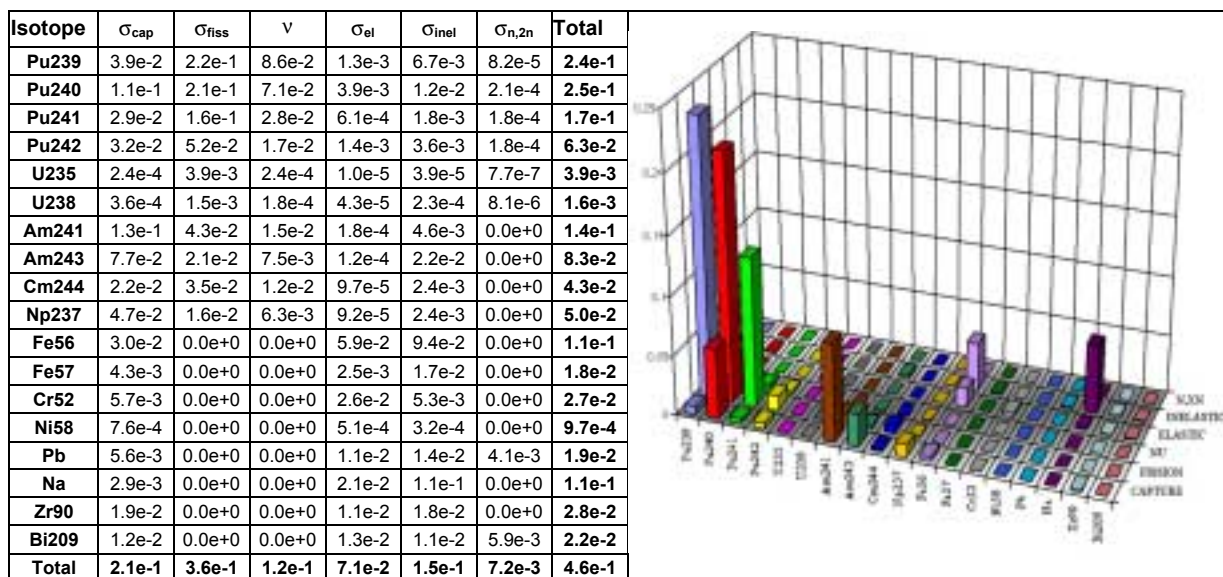


Fig. 34. Uncertainties by isotopes on dpa at the boundary between the core and buffer.

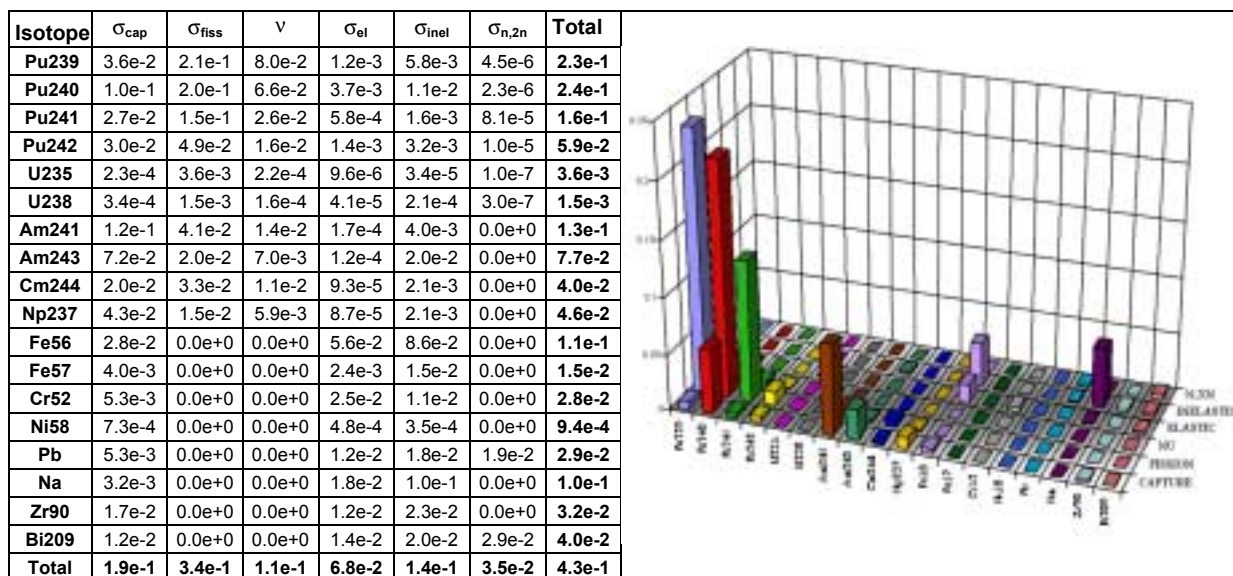


Fig. 35. Uncertainties by isotopes on helium production at the boundary between the core and buffer.

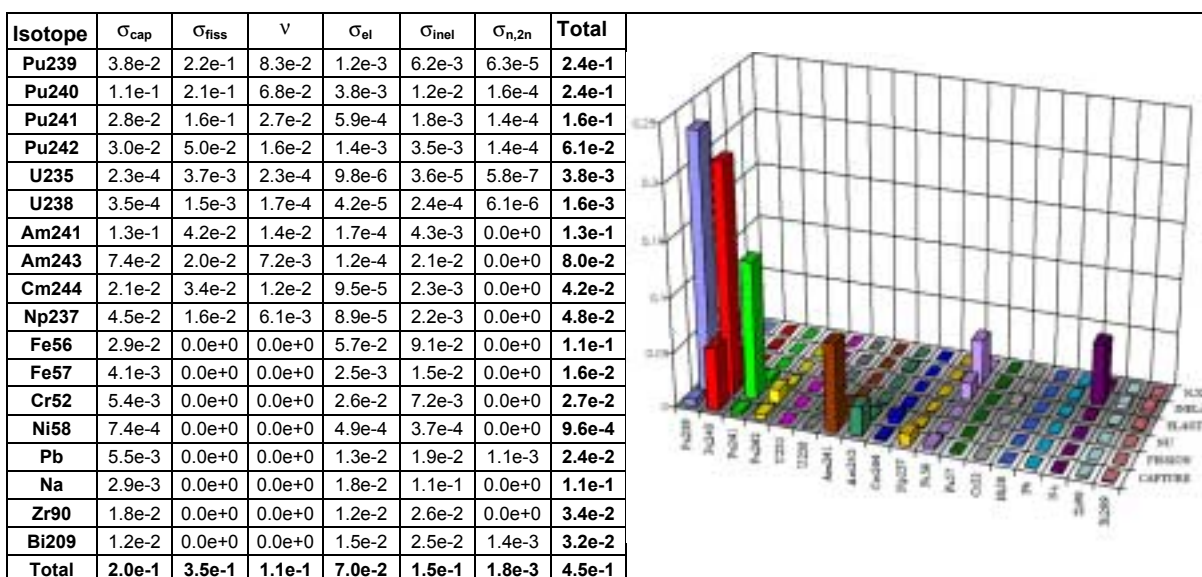


Fig. 36. Uncertainties by isotopes on hydrogen production at the boundary between the core and buffer.

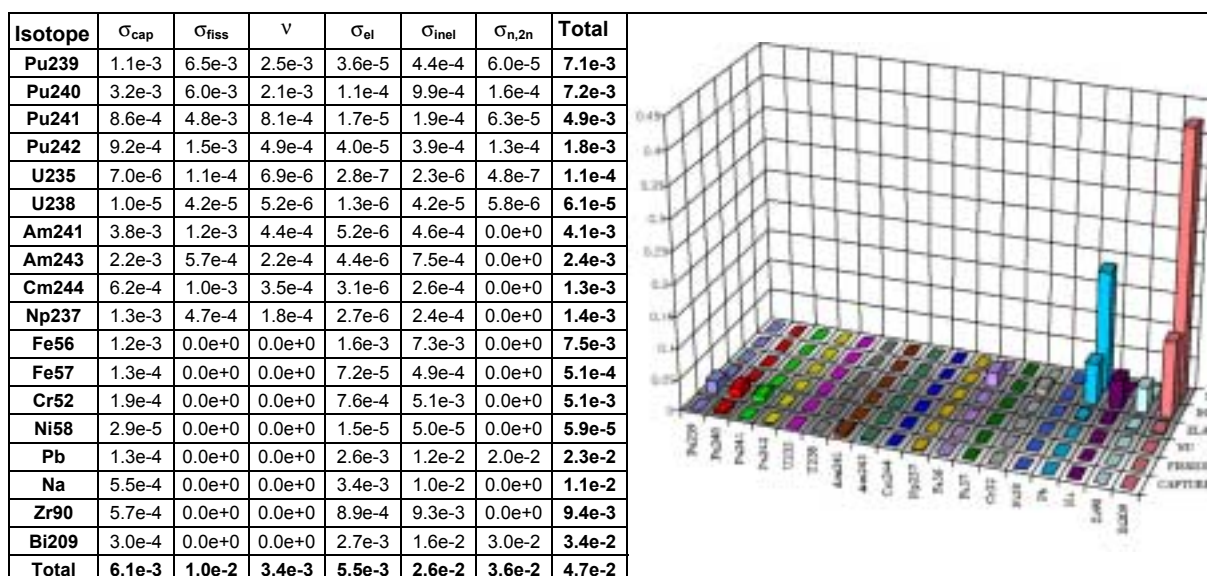


Fig. 37. Uncertainties by isotopes on helium production to DPA ratio at the boundary between the core and buffer, where $(n,\alpha)/DPA = 1.84E-01$.

**Table 11. Fuel
Composition of ADMAB
Benchmark**

	Fuel
	Equilibrium
'U232'	1.00E-10
'U233'	1.00E-10
'U234'	1.00E-10
'U235'	1.00E-10
'U236'	1.00E-10
'U237'	1.00E-10
'U238'	1.00E-10
'NP237'	4.38E-04
'NP238'	1.00E-10
'NP239'	1.00E-10
'PU238'	4.23E-05
'PU239'	5.05E-04
'PU240'	2.32E-04
'PU241'	1.23E-04
'PU242'	9.10E-05
'AM241'	8.08E-04
'AM242M'	1.09E-05
'AM242F'	1.00E-10
'AM243'	5.83E-04
'CM242'	4.08E-08
'CM243'	3.33E-06
'CM244'	2.37E-04
'CM245'	3.16E-05
'CM246'	5.36E-07
'CM247'	1.00E-10
'CM248'	1.00E-10
'ZR90'	3.85E-03
'ZR91'	8.47E-04
'ZR92'	1.29E-03
'ZR94'	1.29E-03
'ZR96'	2.06E-04
'N15'	1.06E-02
'FE54'	9.76E-04
'FE56'	1.49E-02
'FE57'	3.51E-04
'FE58'	4.39E-05
'CR50'	1.13E-04
'CR52'	2.10E-03
'CR53'	2.33E-04
'CR54'	5.68E-05
'NI58'	6.45E-05
'NI60'	2.38E-05
'NI61'	1.02E-06
'NI62'	3.17E-06
'NI64'	7.79E-07
'MO'	1.16E-04
'MN'	1.11E-04
'W182'	6.98E-06
'W183'	3.77E-06
'W184'	8.05E-06
'W186'	7.44E-06
'PB'	6.36E-03
'BI209'	7.87E-03
'SFPU235'	1.00E-10
'SFPU238'	1.00E-10
'SFPPU239'	1.00E-10
'SFPPU240'	1.00E-10
'SFPPU241'	1.00E-10
'SFPPU242'	1.00E-10

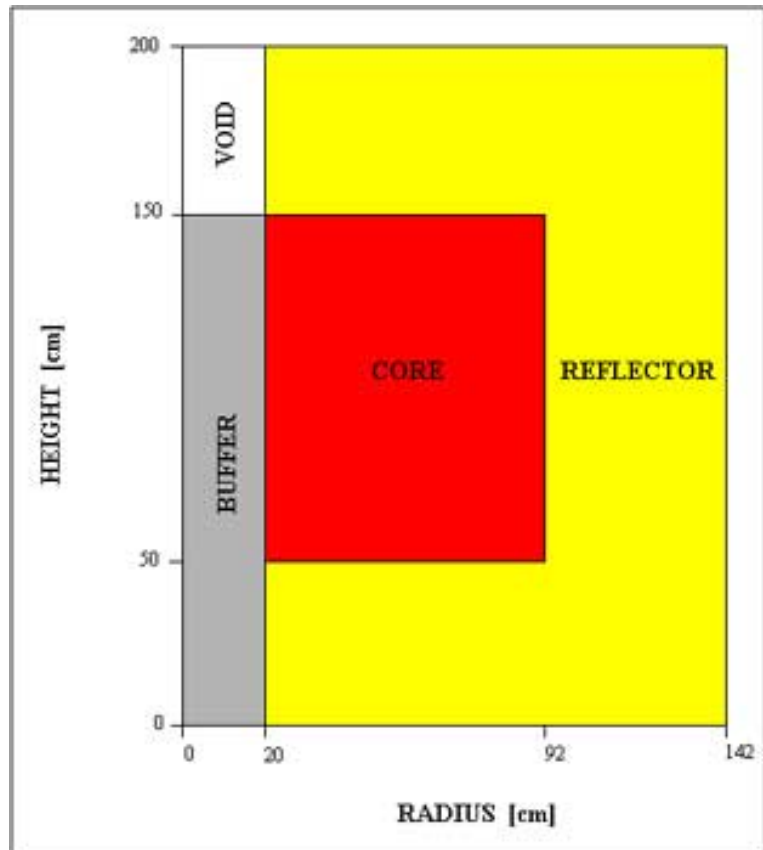


Fig. 38. ADMAB benchmark R-Z model.

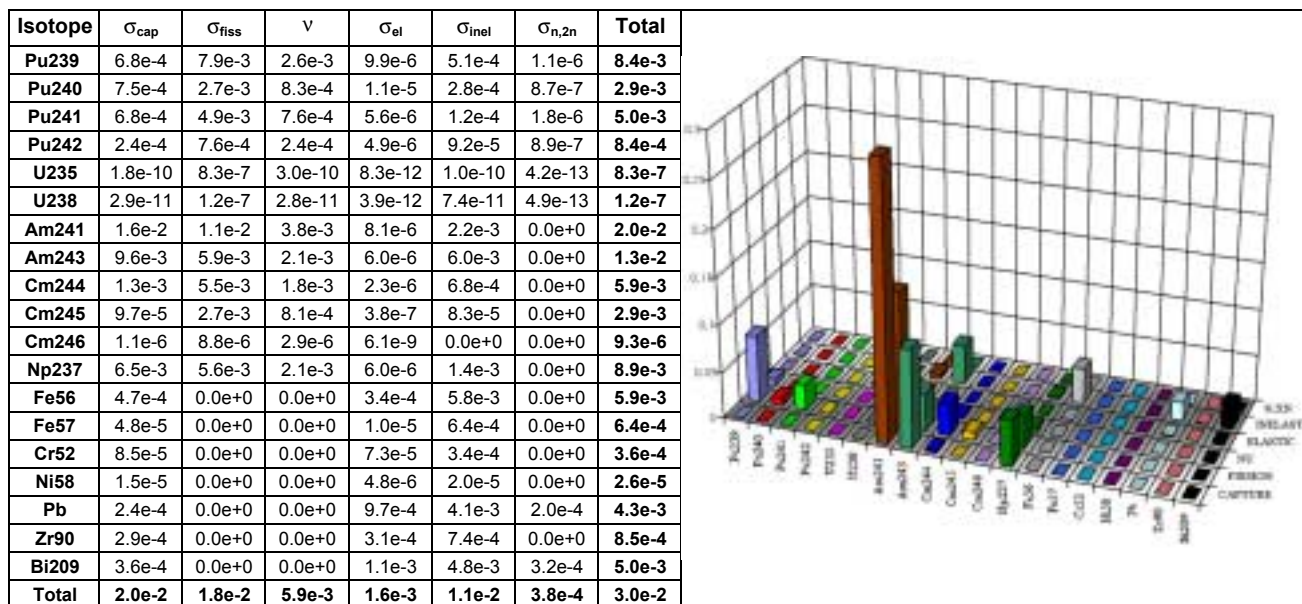


Fig. 39. Uncertainty on reactivity level of the ADMAB benchmark, where $K_{eff} = 0.94930$.

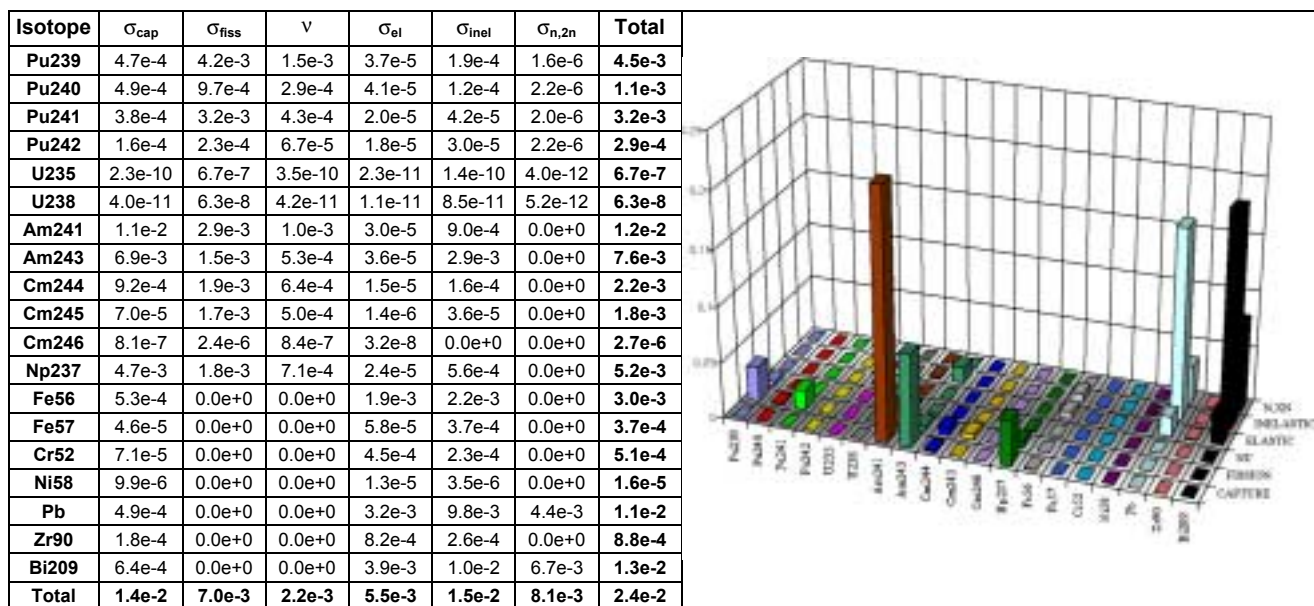


Fig. 40. Uncertainty on source importance factor of the ADMAB benchmark, where $\phi^* = 0.8941$.

Isotope	σ_{cap}	σ_{fiss}	V	σ_{el}	σ_{inel}	$\sigma_{n,2n}$	Total
Pu239	9.1e-3	1.0e-1	3.4e-2	1.8e-4	7.1e-3	1.7e-5	1.1e-1
Pu240	1.0e-2	3.4e-2	1.1e-2	2.0e-4	4.0e-3	1.4e-5	3.8e-2
Pu241	9.3e-3	6.5e-2	1.0e-2	1.0e-4	1.7e-3	2.4e-5	6.6e-2
Pu242	3.3e-3	9.8e-3	3.1e-3	8.8e-5	1.3e-3	1.4e-5	1.1e-2
U235	2.6e-9	1.1e-5	4.1e-9	1.4e-10	1.6e-9	9.0e-12	1.1e-5
U238	4.0e-10	1.7e-6	4.1e-10	6.7e-11	1.1e-9	1.1e-11	1.7e-6
Am241	2.2e-1	1.4e-1	5.0e-2	1.5e-4	3.0e-2	0.0e+0	2.7e-1
Am243	1.3e-1	7.6e-2	2.7e-2	1.1e-4	8.6e-2	0.0e+0	1.7e-1
Cm244	1.7e-2	7.1e-2	2.4e-2	3.9e-5	9.4e-3	0.0e+0	7.7e-2
Cm245	1.3e-3	3.6e-2	1.1e-2	7.0e-6	1.2e-3	0.0e+0	3.8e-2
Cm246	1.5e-5	1.1e-4	3.8e-5	1.1e-7	0.0e+0	0.0e+0	1.2e-4
Np237	8.8e-2	7.2e-2	2.7e-2	1.1e-4	2.0e-2	0.0e+0	1.2e-1
Fe56	5.9e-3	0.0e+0	0.0e+0	4.9e-3	8.0e-2	0.0e+0	8.1e-2
Fe57	6.0e-4	0.0e+0	0.0e+0	2.0e-4	8.4e-3	0.0e+0	8.4e-3
Cr52	1.1e-3	0.0e+0	0.0e+0	7.9e-4	4.8e-3	0.0e+0	5.0e-3
Ni58	2.1e-4	0.0e+0	0.0e+0	5.5e-5	2.8e-4	0.0e+0	3.5e-4
Pb	3.8e-3	0.0e+0	0.0e+0	1.4e-2	7.1e-2	6.7e-3	7.3e-2
Zr90	4.0e-3	0.0e+0	0.0e+0	3.6e-3	1.0e-2	0.0e+0	1.2e-2
Bi209	5.6e-3	0.0e+0	0.0e+0	1.7e-2	8.4e-2	1.0e-2	8.6e-2
Total	2.7e-1	2.3e-1	7.8e-2	2.3e-2	1.7e-1	1.2e-2	4.0e-1

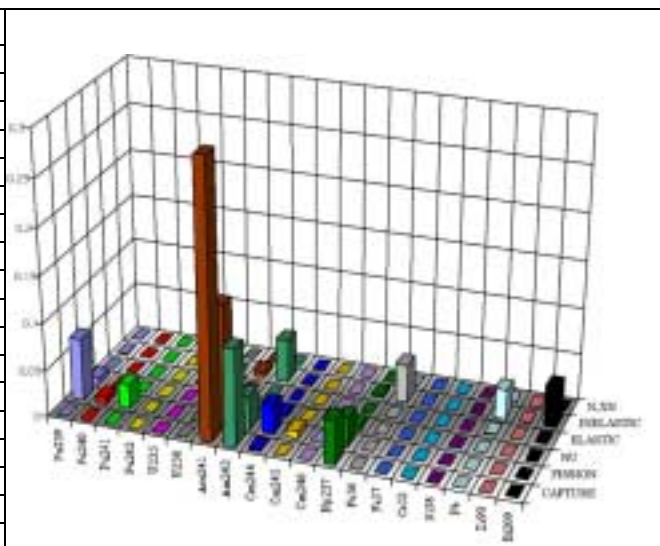


Fig. 41. Uncertainty on max DPA of the ADMAB benchmark, where $\text{dpa}=4.48 \times 10^{-3}/\text{s}$.

Isotope	σ_{cap}	σ_{fiss}	V	σ_{el}	σ_{inel}	$\sigma_{n,2n}$	Total
Pu239	5.3e-3	6.3e-2	2.0e-2	1.1e-4	3.9e-3	4.4e-5	6.6e-2
Pu240	5.8e-3	2.1e-2	6.5e-3	1.2e-4	2.2e-3	3.4e-5	2.3e-2
Pu241	5.3e-3	3.9e-2	6.0e-3	5.8e-5	9.6e-4	4.0e-5	4.0e-2
Pu242	1.9e-3	6.0e-3	1.8e-3	5.2e-5	7.4e-4	3.1e-5	6.6e-3
U235	1.5e-9	6.8e-6	2.5e-9	8.3e-11	8.6e-10	3.2e-11	6.8e-6
U238	2.3e-10	1.0e-6	2.4e-10	4.0e-11	6.6e-10	4.9e-11	1.0e-6
Am241	1.3e-1	8.7e-2	3.0e-2	9.0e-5	1.7e-2	0.0e+0	1.6e-1
Am243	7.5e-2	4.6e-2	1.6e-2	6.7e-5	4.6e-2	0.0e+0	1.0e-1
Cm244	1.0e-2	4.3e-2	1.4e-2	2.7e-5	5.2e-3	0.0e+0	4.7e-2
Cm245	7.6e-4	2.2e-2	6.3e-3	4.1e-6	6.4e-4	0.0e+0	2.3e-2
Cm246	8.9e-6	6.9e-5	2.3e-5	6.9e-8	0.0e+0	0.0e+0	7.3e-5
Np237	5.1e-2	4.4e-2	1.6e-2	6.4e-5	1.1e-2	0.0e+0	7.0e-2
Fe56	3.5e-3	0.0e+0	0.0e+0	2.6e-3	4.6e-2	0.0e+0	4.7e-2
Fe57	3.5e-4	0.0e+0	0.0e+0	8.3e-5	4.4e-3	0.0e+0	4.4e-3
Cr52	6.5e-4	0.0e+0	0.0e+0	5.7e-4	6.0e-3	0.0e+0	6.0e-3
Ni58	1.3e-4	0.0e+0	0.0e+0	2.9e-5	1.9e-4	0.0e+0	2.3e-4
Pb	2.1e-3	0.0e+0	0.0e+0	8.7e-3	7.5e-2	9.4e-2	1.2e-1
Zr90	2.3e-3	0.0e+0	0.0e+0	2.1e-3	8.4e-3	0.0e+0	9.0e-3
Bi209	3.2e-3	0.0e+0	0.0e+0	1.0e-2	9.3e-2	1.4e-1	1.7e-1
Total	1.6e-1	1.4e-1	4.6e-2	1.4e-2	1.4e-1	1.7e-1	3.1e-1

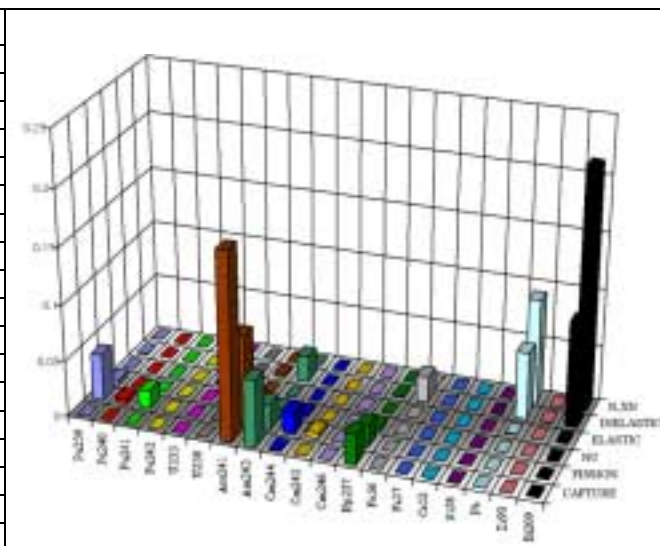


Fig. 42. Uncertainty on max helium production of the ADMAB benchmark, where $(n,\alpha)=1.16 \times 10^{-3}/\text{s}$.

Isotope	σ_{cap}	σ_{fiss}	V	σ_{el}	σ_{inel}	$\sigma_{n,2n}$	Total
Pu239	7.9e-3	9.3e-2	3.0e-2	1.6e-4	6.1e-3	9.6e-7	9.9e-2
Pu240	8.7e-3	3.1e-2	9.7e-3	1.8e-4	3.4e-3	1.7e-6	3.4e-2
Pu241	7.9e-3	5.8e-2	8.9e-3	8.5e-5	1.5e-3	1.0e-5	5.9e-2
Pu242	2.8e-3	8.9e-3	2.8e-3	7.6e-5	1.2e-3	2.1e-6	9.8e-3
U235	2.2e-9	1.0e-5	3.7e-9	1.2e-10	1.3e-9	2.1e-12	1.0e-5
U238	3.5e-10	1.5e-6	3.6e-10	5.9e-11	1.1e-9	3.9e-12	1.5e-6
Am241	1.9e-1	1.3e-1	4.4e-2	1.3e-4	2.6e-2	0.0e+0	2.3e-1
Am243	1.1e-1	6.8e-2	2.4e-2	9.8e-5	7.0e-2	0.0e+0	1.5e-1
Cm244	1.5e-2	6.4e-2	2.1e-2	3.8e-5	8.2e-3	0.0e+0	7.0e-2
Cm245	1.1e-3	3.2e-2	9.5e-3	6.0e-6	1.0e-3	0.0e+0	3.4e-2
Cm246	1.3e-5	1.0e-4	3.4e-5	1.0e-7	0.0e+0	0.0e+0	1.1e-4
Np237	7.6e-2	6.5e-2	2.4e-2	9.4e-5	1.7e-2	0.0e+0	1.0e-1
Fe56	5.1e-3	0.0e+0	0.0e+0	4.1e-3	7.0e-2	0.0e+0	7.1e-2
Fe57	5.2e-4	0.0e+0	0.0e+0	1.2e-4	6.6e-3	0.0e+0	6.6e-3
Cr52	9.5e-4	0.0e+0	0.0e+0	8.6e-4	5.5e-3	0.0e+0	5.7e-3
Ni58	1.9e-4	0.0e+0	0.0e+0	4.2e-5	2.8e-4	0.0e+0	3.4e-4
Pb	3.1e-3	0.0e+0	0.0e+0	1.2e-2	9.7e-2	9.5e-3	9.8e-2
Zr90	3.4e-3	0.0e+0	0.0e+0	3.1e-3	1.3e-2	0.0e+0	1.4e-2
Bi209	4.8e-3	0.0e+0	0.0e+0	1.5e-2	1.3e-1	1.4e-2	1.3e-1
Total	2.3e-1	2.1e-1	6.9e-2	2.0e-2	1.9e-1	1.7e-2	3.7e-1

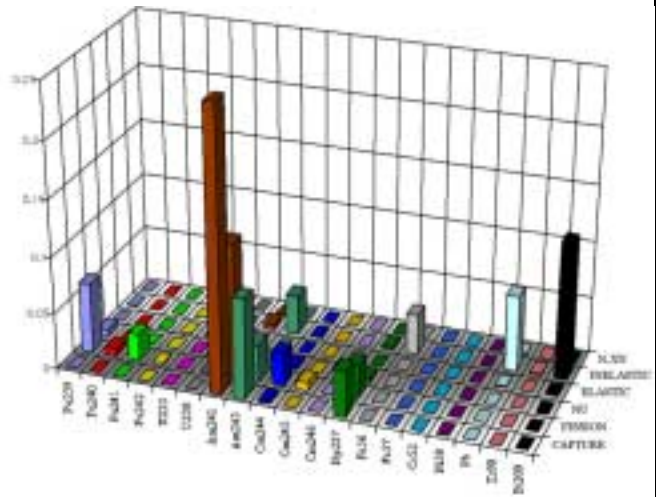


Fig. 43. Uncertainty on max hydrogen production of the ADMAB benchmark, where $(n,p)=3.49 \times 10^{-8}/s$.

Isotope	σ_{cap}	σ_{fiss}	V	σ_{el}	σ_{inel}	$\sigma_{n,2n}$	Total
Pu239	2.6e-3	3.1e-2	9.9e-3	5.1e-5	2.1e-3	4.5e-5	3.2e-2
Pu240	2.9e-3	1.0e-2	3.2e-3	5.6e-5	1.2e-3	3.6e-5	1.1e-2
Pu241	2.6e-3	1.9e-2	2.9e-3	2.7e-5	5.6e-4	3.6e-5	1.9e-2
Pu242	9.3e-4	2.9e-3	9.1e-4	2.4e-5	4.4e-4	3.3e-5	3.2e-3
U235	7.4e-10	3.4e-6	1.2e-9	4.1e-11	4.7e-10	3.0e-11	3.4e-6
U238	1.1e-10	4.9e-7	1.2e-10	1.9e-11	4.5e-10	4.5e-11	4.9e-7
Am241	6.2e-2	4.2e-2	1.5e-2	4.4e-5	9.3e-3	0.0e+0	7.7e-2
Am243	3.7e-2	2.2e-2	7.9e-3	3.2e-5	2.3e-2	0.0e+0	4.9e-2
Cm244	5.0e-3	2.1e-2	7.0e-3	1.3e-5	3.0e-3	0.0e+0	2.3e-2
Cm245	3.7e-4	1.1e-2	3.1e-3	2.0e-6	3.6e-4	0.0e+0	1.1e-2
Cm246	4.4e-6	3.3e-5	1.1e-5	3.4e-8	0.0e+0	0.0e+0	3.5e-5
Np237	2.5e-2	2.1e-2	7.9e-3	3.1e-5	6.2e-3	0.0e+0	3.4e-2
Fe56	1.6e-3	0.0e+0	0.0e+0	1.6e-3	2.4e-2	0.0e+0	2.4e-2
Fe57	1.7e-4	0.0e+0	0.0e+0	4.3e-5	2.2e-3	0.0e+0	2.2e-3
Cr52	3.1e-4	0.0e+0	0.0e+0	2.9e-4	2.0e-3	0.0e+0	2.1e-3
Ni58	5.6e-5	0.0e+0	0.0e+0	1.4e-5	1.0e-4	0.0e+0	1.2e-4
Pb	1.0e-3	0.0e+0	0.0e+0	4.4e-3	5.5e-2	8.4e-2	1.0e-1
Zr90	1.1e-3	0.0e+0	0.0e+0	1.1e-3	6.0e-3	0.0e+0	6.2e-3
Bi209	1.6e-3	0.0e+0	0.0e+0	5.2e-3	7.3e-2	1.3e-1	1.5e-1
Total	7.6e-2	6.8e-2	2.3e-2	7.1e-3	9.9e-2	1.5e-1	2.1e-1

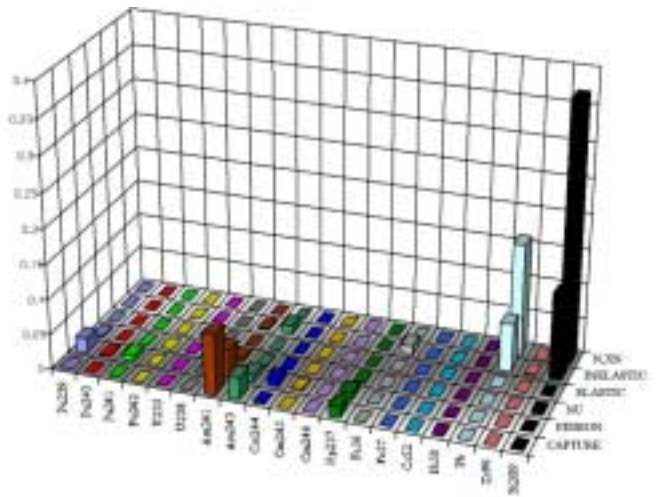


Fig. 44. Uncertainty on max helium/dpa of the ADMAB benchmark, where $(n,\alpha)/DPA=0.260$.

3.7 International Support

International support and collaboration is a strong part of the research conducted under transmutation science. A major collaborator is CEA in France. However, this collaboration is defined at the basic research level, and there are no tasks specifically conducted or funded in support of CEA's efforts. All the tasks outlined above directly or indirectly benefit this collaboration.

Some tasks are specifically funded in support of the MEGAPIE Project at Paul Scherrer Institute (PSI) in Switzerland, as well as the import of the Russian IPPE (Institute of Physics and Power Engineering) LBE target. Those tasks are discussed below.

Scope

MEGAPIE is a 1-MW LBE spallation target experiment being set up at PSI in Switzerland. DOE signed a partnership agreement on the MEGAPIE Project that includes having a US engineer participate in the MEGAPIE design and analyses on change-of-station at PSI. The objective is to provide technical support to the MEGAPIE Project and to transfer knowledge gained and related research on the Project to US laboratories to advance the TRL for the US LBE target development.

We will provide analysis support to MEGAPIE in US laboratories. The specific scope of this support has not yet been determined, but it will be defined soon in collaboration with PSI scientists and engineers.

The IPPE LBE target was designed and built in Russia with the initial objective of irradiating it at LANSCE (LANL). However, because of the unavailability of the irradiation facility, the target will be used as another LBE loop for basic research. Currently, the objective is to bring the target to the US, to deliver it to UNLV, and to set it up as another research loop.

Highlights

- The contract for the Russian scientists at IPPE was completed, and the target is being prepared for shipment to the US. The expected shipment date is in March 2002.

MEGAPIE

The MEGAPIE support tasks were not started in the first quarter.

For the IPPE target import, the contract was awarded to the IPPE scientists and engineers to prepare the target for shipment to the US. Preparation has started, and shipment is expected in March 2002. Also, a number of bids were received for the shipping contract and an initial selection was made. Details of the contract are being worked out.

4. SYSTEMS TECHNOLOGIES

Scope

Accelerator-Driven Test Facility

The scope of work covers both preconceptual and conceptual design phases of the Accelerator-Driven Test Facility (ADTF) project and includes the Target and Materials Test (TMT) Station, the Subcritical Multiplier (SCM), the accelerator, and the balance of facility segments. The preconceptual design will support a Critical Decision 0 (CD-0), *Approval of Mission Need*, for the Project. The conceptual design will commence thereafter, ultimately leading to CD-1, *Approval of Preliminary Baseline Range*.

The scope for ADTF under Systems Technologies also includes collaboration with CEA for this year, and has been determined as follows:

- Completion of the ADTF reference design documentation;
- Development of an ADS reference design—US will work on liquid-metal-cooled designs (Na and LBE) and CEA will work on a gas-cooled design;
- Proof-of-performance (POP) coupling tests—a work plan for experimental POP of the coupling between an accelerator and a multiplier will be developed; and
- POP for accelerator reliability and accelerator development.

Integration activities include:

- Development of functional and performance requirements for the ADTF project;
- Definition and control of design interfaces between major facility segments;
- Coordination of internal and external design reviews;
- Technical risk assessment; and
- Cost estimating.

ADS Preconceptual Reference Design

The purpose of this task at ANL is development of a preconceptual design for a sodium-cooled, accelerator-driven system. LANL will lead the reference design for a lead-bismuth-cooled system.

This work involves development of a preconceptual design for a large-scale ($\sim 800 \text{ MW}_{\text{th}}$) ADS with liquid-sodium cooling and a lead-bismuth eutectic target. In FY02, we will concentrate on defining a set of top-level requirements for the ADS engineering design concept for the facility as a whole, including:

- (1) Identifying the containment structure with ingress and egress routes for personnel, services, and radioactive and nonradioactive equipment;
- (2) Routing and shielding of the accelerator beam;

- (3) Configuring the subcritical multiplier, the vessel in which it is housed and its cover, and all other in- and ex-vessel ancillary components and systems; and
- (4) Handling schemes for all of the above.

The ADS design will be used to update, as necessary, requirements developed for the ADTF.

Accelerator-Driven Coupling Proof-of-Performance Experiments

This task will investigate the use of an experimental facility such as the Transient Reactor Test (TREAT) reactor, located at ANL-W, for the study of accelerator-driven systems control issues related to the coupling of the multiplier to the external source. The feasibility of using the TREAT reactor coupled with an accelerator-driven external source to be part of a POP for ADS will be assessed. The dynamic behavior of the experimental coupled system will provide useful information that can be used for simulation of operation of an actual ADS power system.

Highlights

Target and Material Test Station

- Additional layouts of the TMT irradiation chamber illustrating details of the trolley system and materials irradiation thimbles were produced.
- The annular target concept produced an improved peak neutron flux in the central core region that is about a factor of two greater than other conventional target geometries. The introduction of a buffer between the target and fuel test region will allow designers to tailor the neutron spectrum in the fuel test region to meet users' demands. For an annular target driven by a 14-MW, 500-MeV beam, peak fast fluxes exceeding 3×10^{15} n/cm²/s can be realized in the fuel test region.

Subcritical Multiplier

- A draft preconceptual system design description for the SCM-100 was prepared.
- Three major activities under Systems Technologies have been identified and the scope of work under each activity defined.
- A coordination meeting between DOE and CEA was held. The work package on ADTF and Systems Technologies was discussed with CEA, and a scope agreement for the collaboration under Systems Technologies was reached.

Balance of Facility

- Three conceptual design layouts were completed, one for each cost estimate configuration.

Target and Materials Test Station

The TMT station is uniquely designed to provide a test environment for materials and fuels experiments, coolant and target technology, and the potential for isotope production. Its design centers around an evacuated irradiation chamber that contains the

spallation neutron source (target), reflectors, moderators, and closed test loops. A continuous wave proton beam, operating at an energy of 500-600 MeV and 10-30 mA of current is also directed into the irradiation chamber, where it impacts the spallation neutron source and produces the cascade of neutrons. The irradiation chamber is surrounded by 5 meters of steel and concrete shielding, which protects equipment and workers located in adjacent areas.

As depicted in Fig. 45, the irradiation chamber is centrally located with two adjacent hot cells. These two hot cells allow for horizontal insertion of both the spallation target trolley and the closed test-loop trolley. The proton beam is also brought into the chamber horizontally, which provides a simple, straightforward beam transport system from the accelerator to the irradiation chamber.

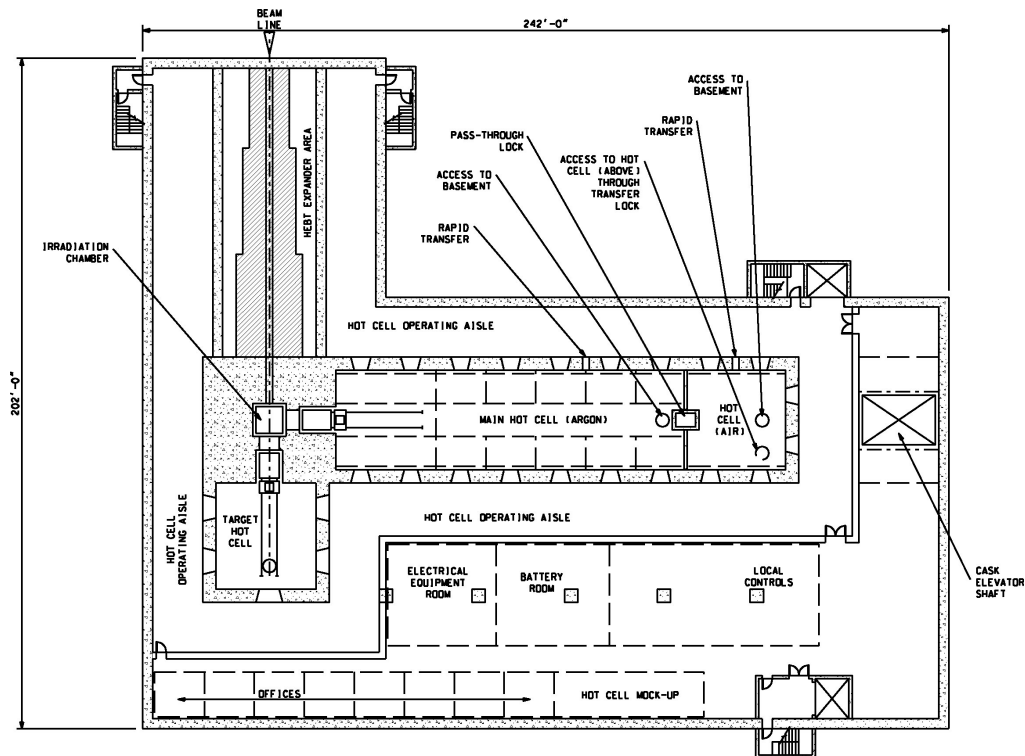


Fig. 45. TMT first floor plan view.

The target and test-loop trolleys rely upon proven technologies based on existing and planned facilities. Figures 46 and 47 depict the target trolley mechanism in both the inserted and withdrawn positions. Once the irradiation cycle is complete, the trolleys would be withdrawn into their adjoining hot cells, allowing the target or test loops to be removed and replaced. This trolley concept provides the capability to test different materials, geometries, and coolants for both the spallation target and the experimental loops. One important trolley design feature is that the primary heat-removal systems are located on the trolley itself, with the secondary heat-removal systems brought into the hot cells. This allows for safe operation and maintenance of the coolant system, while it also permits the primary coolant system to be changed by swapping out coolant loop components or by utilizing another trolley inside the hot cell.

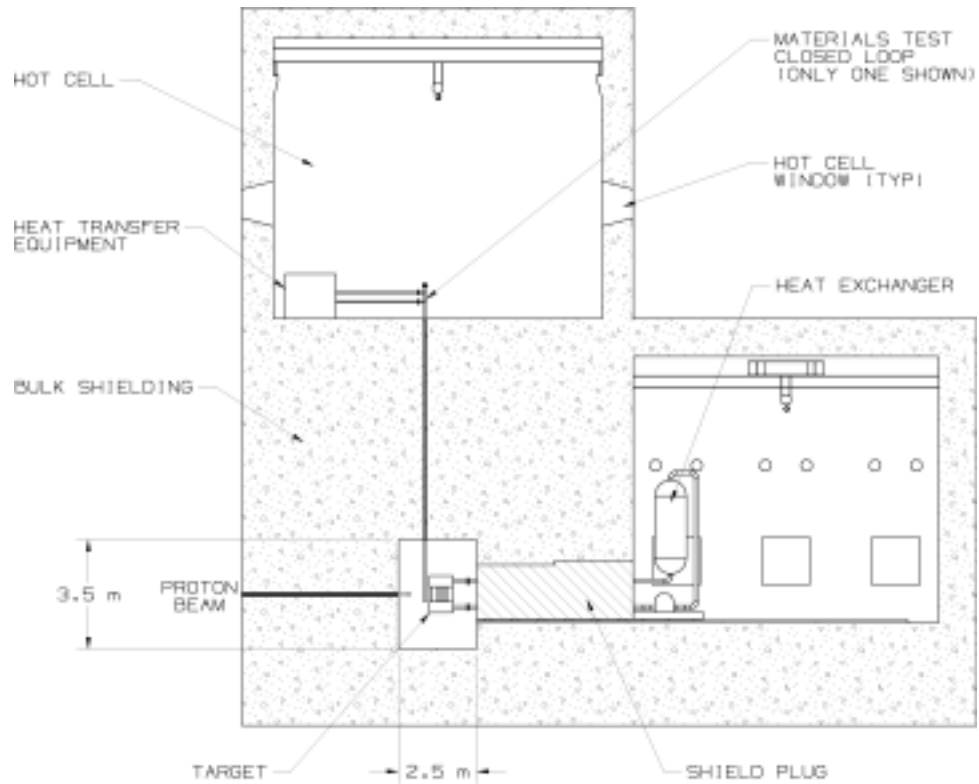


Fig. 46. Irradiation chamber elevation view.

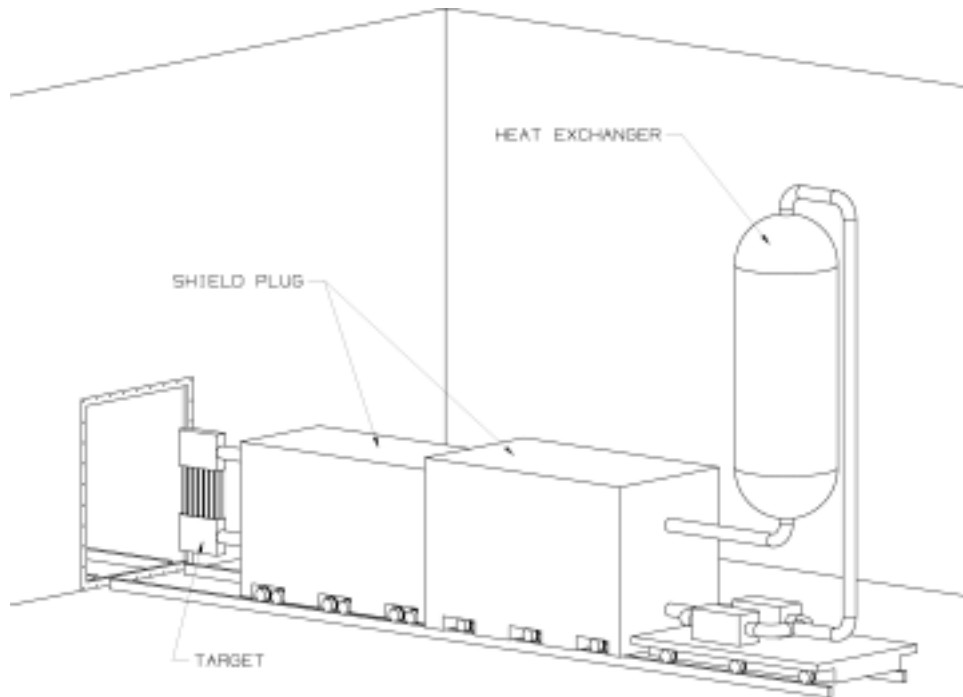


Fig. 47. Target trolley isometric view.

Target Design

As described in the previous *AAA Quarterly Report*, two target/reflector/moderator configurations, the wing and annular geometries, were developed. Together, these two configurations provide flexibility for fast-spectrum and thermal-spectrum irradiations. Additional progress was made on improving the neutronic performance of the annular target geometry.

Annular Target Geometry Option — The annular target concept is similar to an annular core reactor, except that spallation (rather than fission) is the primary source of neutrons. In this geometry, the target is an annulus, with the high-flux test volume located in the *hole* of the annulus. The annular proton beam spot on target is produced using raster magnets. Uniform current density on target can be realized using an appropriate raster pattern.

The benefit provided by this innovative geometry is a higher neutron flux in the test volume, as compared to more classical target concepts such as wing geometry. This higher flux is due to source neutrons entering the test volume from all directions, rather than from only one direction, as is the case for the wing geometry. For equivalent beam powers, calculations have shown the annular target concept provides a neutron flux in the test volume that is about a factor of two greater traditional target concepts.

Figure 48 shows proton and fast (>0.1 MeV) neutron flux spatial distributions for an annular target geometry. These results were obtained using MCNPX version 2.2.3. Proton beam energy and current are 500 MeV and 28 mA, respectively, for a total beam power of 14 MW. The proton beam spot area is 400 cm^2 , giving a uniform beam current density on target of $70\text{ }\mu\text{A}/\text{cm}^2$. The figures show flux spatial distributions in r - z geometry. The test volume extends from $0 < r < 1.78\text{ cm}$, which gives an area equivalent to the cross-sectional area of a 19-rod bundle of fuel whose dimensions match the fuel used in the Fast Flux Test Facility. A 1-mm-thick stainless steel tube encloses this fuel volume. Another 1-mm-thick tube starts at $r=2.22\text{ cm}$. Between these two tubes is a return channel for the fuel coolant, which is sodium. A 0.68-cm-thick vacuum gap exists between this central assembly and the target region, which in this example, is liquid LBE (44.5 atm% Pb, 55.5 atm% Bi, with a mass density of $10.236\text{ g}/\text{cm}^3$ at 644 K). The target zone extends from $3 < r < 14.34\text{ cm}$. The proton beam spot is 2 cm smaller on both the inner and outer edges, extending from $5 < r < 12.34\text{ cm}$. This extra 2 cm of target radial dimension accommodates beam blowup from multiple scattering while traversing the target, as well as small (\sim few mm) beam misalignment on target. Outside of the target is a reflector region, composed of 30.8 vol% nickel, 21.6 vol% stainless steel, and 47.6 vol% sodium.

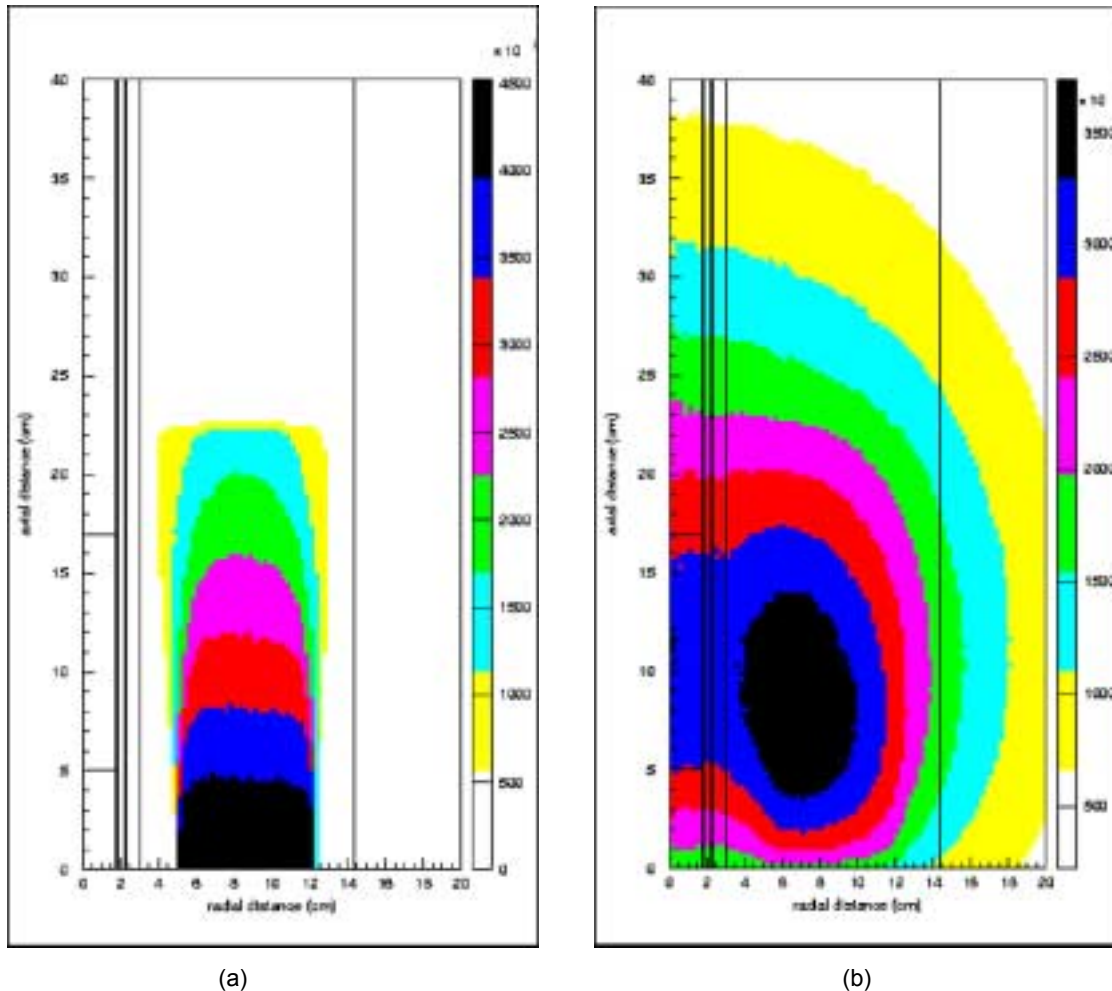


Fig. 48. (a) Proton and (b) fast (>0.1 MeV) neutron flux spatial distributions for an annular target.

As seen in Fig. 48(a), the protons are well contained within the LBE target region, ranging out after traversing about 22 cm of LBE. As expected, the fast neutron flux peaks in the LBE target where most of the neutrons are born (Fig. 1(b)). But the flux is nearly as high in a segment of the fuel test region. Averaged over a 12-cm axial length (5–17 cm) of this region, the fast neutron flux is 3.1×10^{15} n/cm²/s. This high flux produces high burn rates: 14.5%/FPY for ²³⁵U, 18.5%/FPY for ²³⁹Pu, and 11.7%/FPY for a minor actinide fuel whose composition is given in Table 12. The very hard spectrum produced by spallation not only yields a high fuel burn rate, it also has the undesirable effect of a high helium production rate (470 appm/FPY) in steel located in the fuel test region. This is clearly evident in Fig. 49, where the relative contribution to neutron-induced atomic displacements and helium production are plotted as a function of neutron energy. It shows that neutrons with energies less than 10 MeV are responsible for more than 80% of atomic displacements, but less than 20% of helium production. The atomic displacement rate in steel in the fuel test region is 71 dpa/FPY, which gives a He/dpa ratio of 6.6 appm/dpa.

Table 12. Composition of Representative Minor Actinide Fuel

Isotope	Fraction (a%)
U-235	0.018
U-236	0.009
U-238	2.185
Np-237	22.980
Pu-238	0.436
Pu-239	18.246
Pu-240	7.386
Pu-241	1.297
Pu-242	1.607
Am-241	41.007
Am-242	0.064
Am-243	4.235
Cm-243	0.009
Cm-244	0.476
Cm-245	0.041
Cm-246	0.005

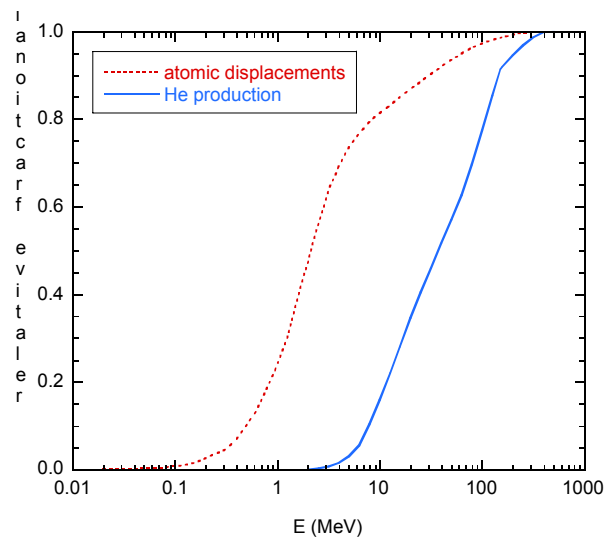


Fig. 49. Energy dependence of neutrons responsible for atomic displacements and helium production in stainless steel located in the fuel test region.

The high helium production rate is undesirable because steels in the fuel regions of an ADS system are expected to have helium production rates around 150 appm/FPY, which is a factor of three lower than what is calculated for the fuel test region of the annular target concept. Since neutrons with energies greater than 10 MeV are primarily responsible for helium production, attenuating these high-energy neutrons by inserting a buffer between the target and fuel test region should reduce He production in the test region. An ideal buffer material in this application is ^{238}U because it has high mass density and an appreciable fission cross-section ($\sim 0.6 \beta$) above 1 MeV. The function of the buffer is to soften the spectrum of neutrons entering the fuel test region without significant loss of total neutron flux. Because ^{238}U fissions above 1 MeV, some of the high-energy neutrons attenuated by the buffer will produce useful lower-energy fission neutrons, thereby boosting total neutron production in the

system. This additional production helps offset the loss of neutron flux in the test region brought about by introduction of the buffer.

The effect of a buffer on the helium production rate is shown in Table 13. A 6-cm-thick depleted uranium buffer yields reduction at a factor of four in helium production and reduction at a factor of two in atomic displacements, with only a 24% reduction in fast neutron flux. The change in the neutron spectrum within the fuel test region resulting from the introduction of a buffer is shown in Fig. 50. The softening of the spectrum with the introduction of a buffer is clearly evident. Without a buffer, the mean neutron energy in the fuel test region is 4.1 MeV, whereas it is 1.6 MeV with a 6-cm-thick depleted uranium buffer. These results show that a buffer may be used to tailor the spectrum to meet specific irradiation requirements.

Table 13. Impact of ^{238}U Buffer Thickness on Fast Neutron Flux, He Production Rate, and Atomic Displacement Rate in the Fuel Test Region

Buffer Thickness (cm)	Fast (>0.1 MeV) Neutron Flux (10^{15} n/cm ² /s)	He Production Rate (appm/FPY)	Atomic Displacement Rate (dpa/FPY)	He/dpa ratio (appm/dpa)
0	3.06	467	71.3	6.55
1	3.04	358	63.8	5.62
2	2.95	277	56.8	4.89
3	2.81	224	50.4	4.44
4	2.64	175	44.6	3.92
6	2.32	115	35.6	3.23

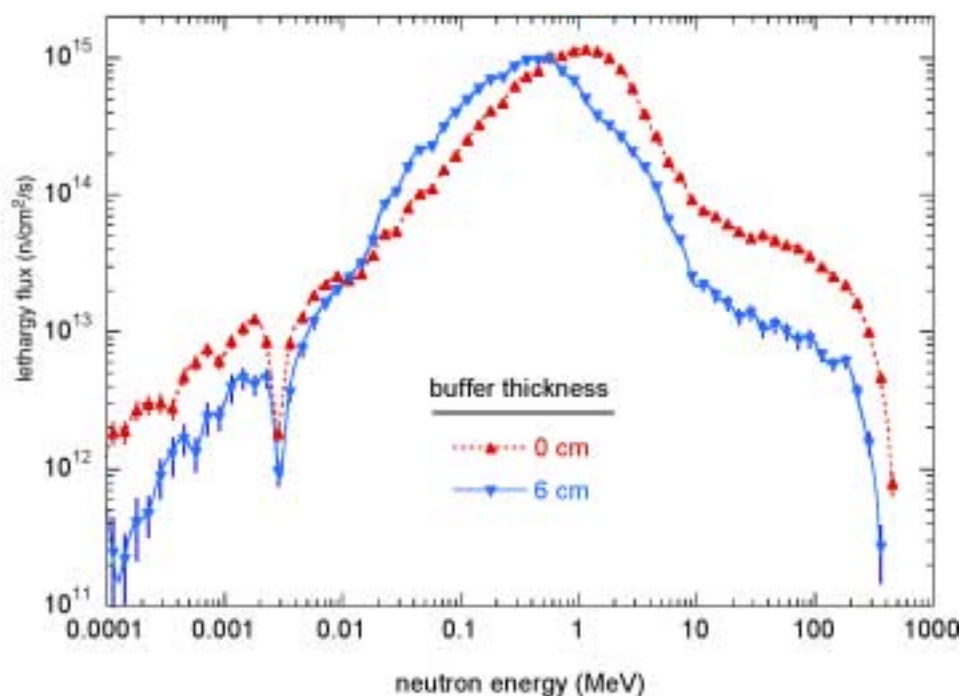


Fig. 50. Softening of the neutron flux spectrum in the fuel test region through the use of a depleted uranium buffer.

The major drawback to using a buffer is the reduction in the neutron flux observed in the fuel test region. One method for boosting this flux without increasing the accelerator beam power is to use an actinide target material (such as depleted uranium) instead of a subactinide LBE target. For a target that is 60 vol% depleted uranium and 40 vol% LBE (for cooling), neutron production is 36% greater than for a pure LBE target. This translates into a flux that is 37% higher in the fuel test region. The spatial distribution of the proton and fast neutron fluxes for such a system is shown in Fig. 51. Here the 6-cm-thick buffer is composed of 80 vol% ^{238}U and 20 vol% LBE, while the target material is 60 vol% ^{238}U and 40 vol% LBE.

The annular target geometry can be easily changed to accommodate larger fuel test volumes with only a small penalty in fast flux. As an example, increasing the fuel test region radius from 1.78 cm to 3.76 cm, which increases the number of fuel pins in a hex array from 19 to 91 pins, degrades the total neutron flux in the fuel test region by only 9.5%. Performance characteristics for these two configurations are shown in Table 14. Here, the buffer is 7 cm thick and composed of 80 v% ^{238}U and 20 v% LBE, while the target material is 60 v% ^{238}U and 40 v% LBE.

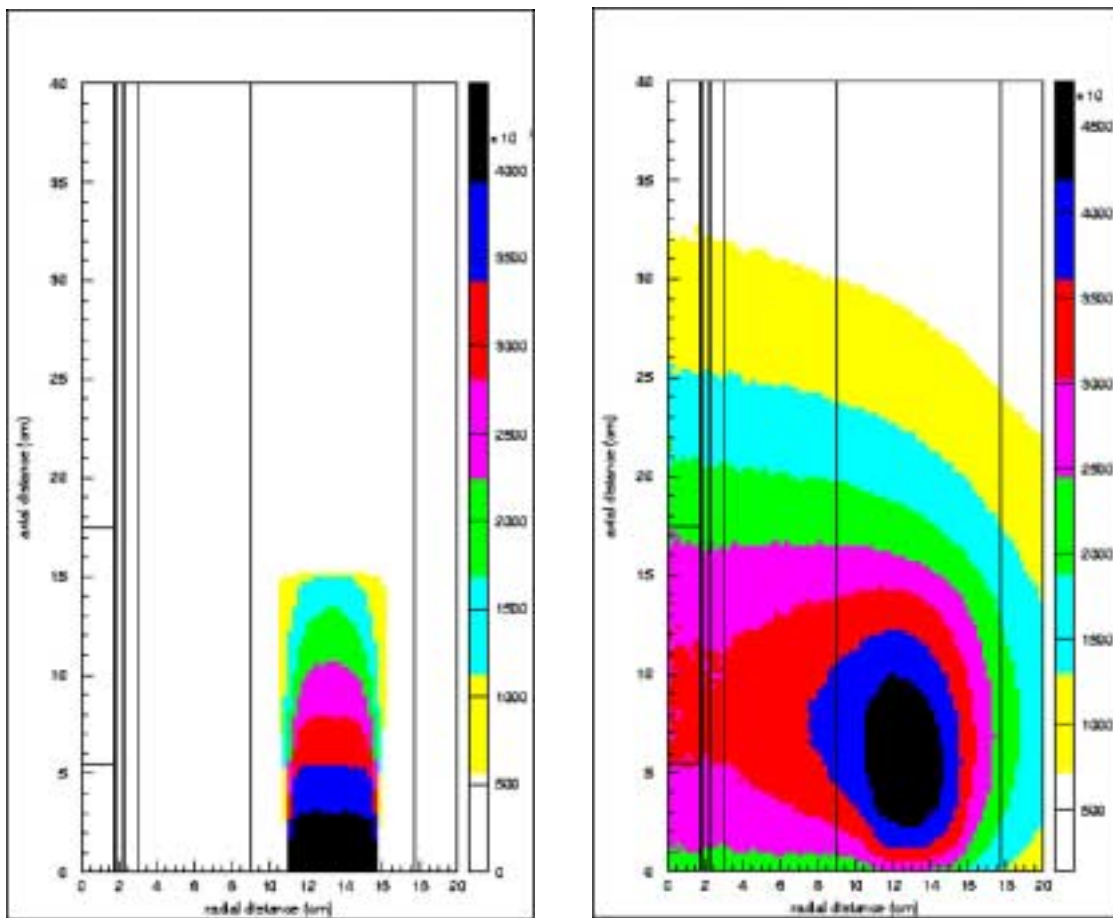


Fig. 51. Proton and fast neutron flux spatial distributions for a depleted uranium target and buffer.

**Table 14. Performance Characteristics of Annular Target Concepts
for 19- and 91-Pin Fuel Assemblies.**

Parameter	19-Pin Array	91-Pin Array
Fuel test region radius (cm)	1.78	3.76
Fuel test region volume in 12-cm length (cm ³)	119	533
Volume-averaged fuel test region neutron flux (10 ¹⁵ n/cm ² /s)		
fast	2.62	2.36
high-energy (>20 MeV)	0.019	0.013
total	3.25	2.95
Representative fuel burn rates (%/FPY)		
²³⁵ U	14.3	13.0
²³⁹ Pu	16.5	15.0
minor actinide	6.5	6.0
He production rate in steel in fuel test region (appm/FPY)	96.9	75.0
Atomic displacement rate in steel in fuel test region (dpa/FPY)	36.4	33.3
He/dpa ratio (appm/dpa)	2.66	2.25

In summary, the annular target concept produces a peak neutron flux in the central core region that is about a factor of two greater than other conventional target geometries. The introduction of a buffer between the target and fuel test region allows designers to tailor the neutron spectrum in the fuel test region to meet user demands. Large target volumes can be accommodated, if needed. For an annular target driven by a 14-MW, 500-MeV beam, peak fast fluxes exceeding 3×10^{15} n/cm²/s are realized in the fuel test region.

Subcritical Multiplier — 100 MW

Systems Technologies involves a similar team at ANL that works on a preconceptual reference design for an SCM to be used in a full-scale (~800 MW_{th}) accelerator-driven system for transmutation of LWR spent fuel and generation of electricity. An expanded team, including facility expertise, will study the feasibility of performing accelerator-driven transmutation proof-of-performance experiments in the TREAT reactor at ANL-W.

Representatives of the ANL Systems Technologies team participated in the coordination meeting between DOE and CEA held in Phoenix, Arizona, in early December. The reference design for the SCM-100 was presented, emphasizing the differences with respect to the design status presented at the previous coordination meeting in June 2001. The status of other joint activities in the DOE-CEA collaboration for the ADTF design (comparison of oxide and metal fuels and development of the experimental plan) were also reported during the meeting. Joint DOE-CEA activities in the ADTF area were discussed under the redirected program.

Accelerator-Driven Coupling Proof-of-Performance Experiments

The issues that can be studied in coupling experiments of TREAT and an external source have been investigated. The most relevant items are as follows:

- It will be possible to perform a study of startup and shutdown procedures for an ADS and to validate the instrumentation needed for monitoring such a procedure. These procedures have not yet been defined; they can consist of

variations of source levels or subcriticality levels, or more likely a combination of both.

- It will be possible to study the domain of reliable operation of an ADS system at different levels of subcriticality. Optimal level of subcriticality for operating an ADS could be a source-dominated regime, a middle of the road regime, or an almost critical (beta-compensated) feedback-dominated regime.
- It will be possible to simulate different fuel irradiation (burn-up swings) situations by control-rod movements. In an actual power ADS, the burn-up swing will be compensated either by an increase of the beam power (this means a financial penalty due to the increase in the size of the accelerator), or by reactivity compensation of control rods (this would have a safety implication due to the large reactivity reserve present in the system).
- It will be possible to validate different techniques of subcriticality measurements in a power system. Techniques proposed are modified source method, pulsed neutron source, transfer function with source modulation, or power spectral density.
- It will be possible to study the correlation between power and current. This is very important for the operation of an ADS and an indirect measurement of the reactivity level.

An assessment in the use of TREAT in the coupling experiments has been initiated. A set of subcritical transients has been studied. A modified version of the computer code TREKIN (point kinetics for TREAT), which includes the external neutron source, has been used. The initial study includes transients induced by the change in control-rod positions. The initial reactor power was fixed at 80 kW. The reactor operates at this power until a control rod is pulled out to introduce reactivity in the core.

Three different transients introducing 1000 pcm of reactivity in a steady power state were studied. The results indicate that at subcriticality levels far from $k_{\text{eff}}=1$, the response of the system is mostly dominated by the external neutron source. As criticality is approached, the dynamics is mostly governed by the feedback of the core. The temperature of the core and the integrated power values in studied transients do not exceed the safety requirement limits for a relatively broad range of subcriticality. Transients induced by the change in the accelerator power were also analyzed. At very slight subcritical levels, reactor feedback plays a more important role than in deep subcritical situations.

The choice of external source was also investigated. Theoretical estimates indicate that an external neutron source of $\sim 1.4 \times 10^{14}$ n/s would be needed for the desired coupling experiments. Three different possibilities were considered: (1) proton-induced spallation source (base choice for ADS), (2) $\text{Be}^9(\text{d},\text{n})\text{B}^{10}$ reactions, and (3) use of an electron accelerator to ignite photoneutron reactions.

Studies of the proton-based spallation source with an initial choice of metal tungsten for the spallation target indicate that a beam current of 0.1 mA and proton energies of 100 MeV will be the best option to satisfy the need in the external neutron feed for the coupling experiments.

With a deuteron-induced source and a metal beryllium target, it was concluded that to reach the required level for the external source, deuteron beam currents of several dozens of milliamps would be necessary, which is not practical.

In general, the required neutron yield can be easily achieved by utilizing a linear accelerator system ($E_e=50$ MeV with intensity of 1 mA, resulting in 50 kW of beam power). The possibility of using the available linear accelerator at the Idaho Accelerator Center (IAC), Pocatello, Idaho, has been considered. This machine is capable of producing an average beam current of 300 mA, thus resulting in a beam power of 9 kW (at 30 MeV beam energy). The electrons directly release relatively few neutrons: the most copious yields are produced by the interaction of photons, which are emitted by electrons in an electromagnetic cascade within the target. The neutron yields from high-Z materials, such as Ta ($Z=73$), W ($Z=74$), or Pb ($Z=82$) whose neutron separation energies are about 6-7 MeV, exhibit a swift rise with energy in the 10-30 MeV range. After 30 MeV, the yields saturate due to the fall in the photo neutron cross-sections beyond the Giant Dipole Resonance region. Additional gain in flux can be achieved by surrounding the high-Z target with Be, owing to the low neutron separation energy of Be ($B_n=1.7$ MeV). The typical yield for a composite W-Be target is about 0.01 n/e⁻ ($E_e=34$ MeV). Further increase in neutron flux can be achieved by using a target from fission material, due to the additional emission of delayed, post-fission neutrons. Using a composite ²³⁸U/Be target, the highest total neutron flux expected from the 30-MeV linac at IAC would be 3.7×10^{13} n/s; additional increase (up to 10%) in the neutron flux can be achieved by optimizing the target thickness and geometry. The availability and relatively low operating cost of this system, when compared to the other neutron source options, make it an attractive choice for an external neutron source for the coupling experiments.

ADTF Documentation

SCM Preconceptual System Design Description

To complete the reference preconceptual design of the SCM-100, work on the layout of the SCM-100 containment building's operating floor was finalized. In particular, routing of the piping runs for the secondary Na cooling system, the NaK shutdown heat-removal system, and the Pb-Bi liquid-metal target received considerable attention. Difficulties in this layout led to reconsideration of the entire concept. The original design always had the SCM tank off-center in the building, which leaves a larger free area on the floor for work. However, this design, which had the high-energy beam transport (HEBT) system on the long side of the floor, is different from the Burns and Roe facility layout, which has the HEBT on the short side. A preliminary drawing of the HEBT showing the placement of magnets was received from accelerator specialists at LANL. The horizontal section of the HEBT is longer than the 10-m original estimate, which was hardly more than a guess at the envelope required for the system, indicating that centering the SCM within the containment building may be an optimal choice. However, the new drawing shows breaks in the string of magnets, so some may be placed external to the building. On these bases, the layout of the containment building's operating floor was completed. Routing of the piping runs is shown in Fig. 52 for the new configuration. Figure 53 shows the HEBT location in containment.

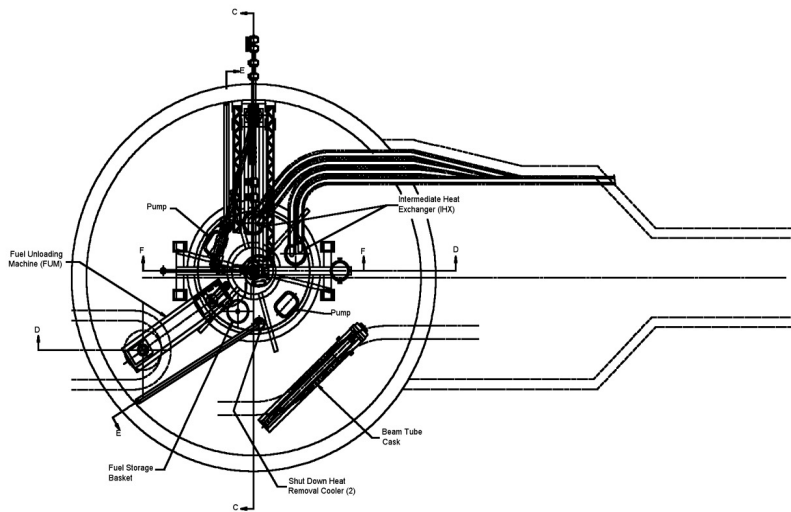


Fig. 52. SCM plan view.

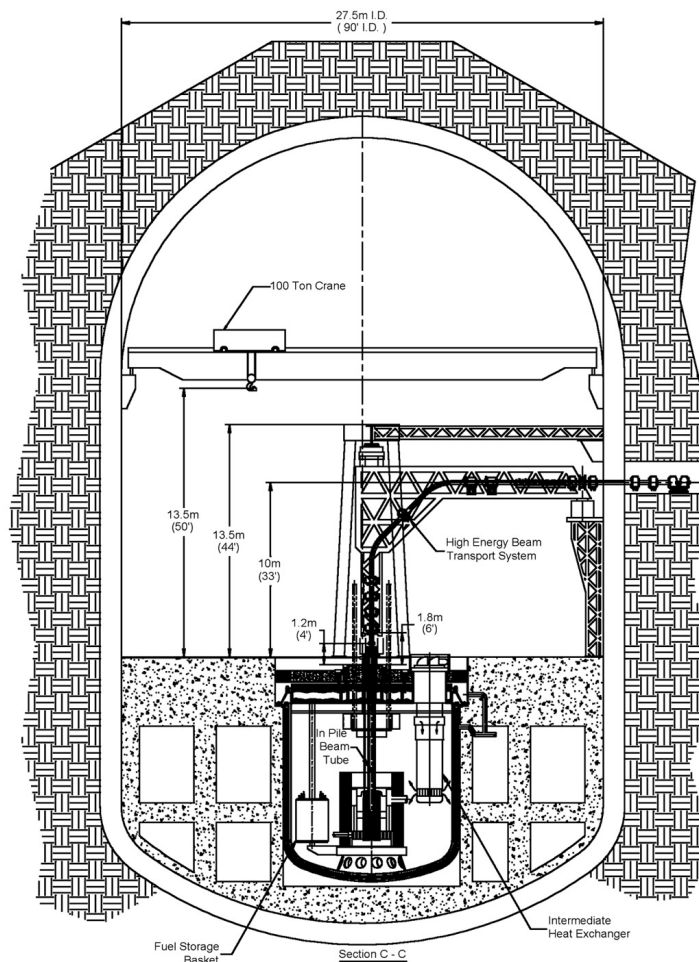


Fig. 53. SCM elevation.

A draft preconceptual system design description has been prepared to indicate the state of the SCM-100 design at the end FY2001. The report includes sections on the mechanical systems, core, and target design. Documentation on alternatives options studied in support of the SCM has also been prepared. The documentation will be completed next quarter.

SCM Target Design Completion and Documentation

LBE Spallation Target Design — A draft report on the LBE spallation target design concept for the subcritical multiplier was written to document the work performed during FY01. Contributions from BNL and GA were included in the report. The target design is based on a coaxial geometrical configuration, which has been carefully analyzed and designed to achieve an optimum performance. The report gives the target design description, results from the parametric studies, and design analyses including neutronics, heat-transfer, hydraulics, structure, radiological, and safety analyses.

A paper on the LBE spallation target design concept was written and submitted at the ANS Winter 2001 Meeting. The target design is based on a coaxial geometrical configuration, which has been carefully analyzed and designed to achieve an optimum performance. In the paper, the target design description, results from the parametric studies, and design analyses including neutronics, heat transfer, and hydraulics analyses are presented.

Sodium-Cooled Tungsten Target Design — Models of the beam window cooling system were developed for the proposed ADTF solid target concepts. The thermal hydraulics analyses used the Star-CD and CFX computer programs. The models include the beam window wall, fluid between the beam window wall and the cooling channel guide, and fluid within the inlet channels from the body of the solid target design. These models do not fully represent the full target design, but the results can be used to optimize the heat transfer coefficient along the surface of the beam window wall. A parametric study considering beam window wall thickness, window cooling channel width, and different flow distributions from the body of the solid target design were completed to provide data for the design of the beam window cooling.

Balance of Facility Design

Three ADTF conceptual design layouts were completed, one for each cost estimate configuration. The three designs are as follows:

- A multi-station ADTF that has both a TMT and SCM stations coupled to a 600-MeV, 13-mA accelerator;
- A single-station ADTF with only the TMT station initially constructed, but with the capability to append an SCM sometime in the future; and
- A TMT station constructed at LANL and coupled to an upgraded LEDA facility.

International Support

A memo documenting the SCM-100 neutron-physics design performed in the framework of the international collaboration with CEA was prepared and distributed in November. Presentation materials for the SCM-100 physics design were prepared for the USDOE/CEA collaboration meeting held in Phoenix in December.

Earlier ERANOS (computer modeling code) calculations for the SCM-100 under this effort were performed with homogeneous transport theory (i.e., without taking into account the external source). More refined calculations using the source-driven (inhomogeneous) option of the ERANOS code system have now been completed. The results of the two approaches have been compared. The power-peaking factors were found to be relatively higher (by ~7%–10%) when the external source is taken into account. Differences in zonal power-sharing are less than 2%. The power density distribution computed in the core mid-plane shows a stronger gradient in the power distribution close to the interface between the target-buffer zone and the core. The comparison suggests that the homogeneous calculation give a sufficiently accurate representation of the power density distribution in the core region, particularly for scoping studies.

5. PROJECT INTEGRATION

Scope

System and Technology Integration coordinates all technical elements in defining requirements, performing system-level evaluations, developing preconceptual designs, and establishing technology development activities in a comprehensive research and development/proof of performance effort. Overall system objectives, system performance requirements, and POP requirements are used to correlate R&D needs, data quality objectives, experimental facilities, resources, and materials. System-level modeling evaluates the performance of multi-strata options in establishing a technically feasible spent nuclear fuel management program, especially with regard to proliferation, economics, environment, safety, and institutional issues. Likewise, preconceptual designs serve as fundamental bases in defining critical R&D and focusing POP testing. Woven together, System and Technology Integration activities can provide a solid foundation for focused and coordinated AAA research and development.

5.1 Systems and Technology Integration

A detailed work plan has been completed to further evaluate the various multi-tier scenarios and rank them through a formal decision process. In FY01, three base cases were analyzed, including (1) plutonium consumption in thermal spectrum reactors (both water and gas cooled) and the residue fed to fast spectrum transmutation systems, (2) partial transuranic consumption in thermal reactors (water and gas) and the residue fed to fast spectrum systems, and (3) stand-alone fast spectrum systems. Basic assumptions were made about the reference separations techniques and fuel forms, although considerable uncertainties remain regarding each. More detailed planning on the scope of the Systems Approaches Analysis (SAA) for the three reference multi-tier transmutation systems has been completed. The SAA FY02 work plan includes development of a comprehensive list of criteria such as life-cycle costs, technology maturity, infrastructure readiness, and relative ease by which these technologies can be tested and demonstrated, as well as deployment schedules. These criteria will be structured in a formal multi-attribute, multi-variate decision process to determine a relative ranking of the preferred alternatives.

The SAA FY02 work will provide the basis for more detailed evaluations and help set AAA programmatic priorities in the short term. A year-end report will be prepared by September 30, 2002, to document these analyses to form the basis for further defining AAA long-term and FY03 tasks.

5.2 University Programs

Scope

University Programs consists of four major aspects: the University of Nevada-Las Vegas (UNLV) University Participation Program (UPP), AAA Program at the Idaho Accelerator Center (IAC) of Idaho State University (ISU), University Fellowships Program (UFP), and AAA Directed University Research.

- **UNLV AAA University Participation Program** — The University of Nevada supports the AAA Program through “research and development of technologies for economic and environmentally sound refinement of spent nuclear fuel...”¹⁶ The UNLV Program has four components: student-based research, infrastructure, international collaborations, and support.
- **Idaho Accelerator Center** — The IAC at Idaho State University received \$1.5 M in FY02 for unspecified research. They will develop a long-term plan and a research program to conduct a variety of investigations that depend on high-energy electron accelerators.
- **University Fellowships Program** — The Amarillo National Research Center (ANRC) acts as the executive agency for the AAA Program to select, award, and administer fellowships for 10 graduate students who were selected last year and 10 more to be selected in FY02.
- **AAA Directed University Research** — Three universities currently support R&D and technology development: the University of Michigan, the University of California-Berkeley, and the University of Texas-Austin.

In addition, the scope of this effort involves coordination between other AAA activities and academia.

Highlights

American Nuclear Society Winter Meeting, Reno, NV

- A total of 32 presentations based on AAA-sponsored university programs were given at the ANS Winter Meeting and Student Mini-Conference held in Reno, NV, in November. Students gave 24 of the presentations in the mini-conference, and eight others were given during the regular AccApp/ADTTA’01 embedded topical meeting. In addition, four technical presentations were given on AAA-related work by faculty and students from the Universities of Michigan and California-Berkeley.

AAA University Participation Program

- UNLV hired a research scientist in the Center for Environmental Studies to develop a new laboratory to conduct scientific studies in support of AAA R&D missions.

¹⁶ ref. H.R. 5483, P.L. 106-377.

- ANL technical staff conducted AMUSE training at UNLV (training on the Argonne Model for Universal Solvent Extraction separations process modeling).
- UNLV AAA students displayed a large AAA poster at the Pahrump (the city nearest Yucca Mountain) Harvest Festival, which was attended by ~60,000 people.
- Two UNLV students won awards for best presentation at the ANS Winter Student Mini-Conference held in Reno, Nevada.
- A group from UNLV traveled to Russia and Eastern Europe to visit IPPE and other nuclear science institutes to discuss future collaborations within the AAA Program and potential research, as well as to recruit scientists and students for AAA research at UNLV.
- A third-quarter summary report describing the progress and technical status of the university research projects was completed.
- UNLV initiated an intercollegiate collaboration with ISU on computing dose conversion coefficients for hundreds of radioisotopes that would be created in spallation targets.

AAA Idaho Accelerator Center

- AAA management visited Idaho State University to view their equipment and capabilities and begin planning for IAC participation in FY02.
- IAC submitted a draft plan, statement of work, milestones, and deliverables for ISU-IAC participation in the AAA Program.
- ISU and UNLV initiated an intercollegiate collaboration to use positron annihilation spectroscopy to examine bulk samples for determining residual stresses of cold-worked and welded engineering materials.

AAA University Fellowship Program

- Seven Fellows attended the ANS Student Mini-Conference, and four made oral presentations.
- Research topics and abstracts were submitted by all 10 AAA Fellows to the Amarillo National Research Center.
- ANRC issued an announcement and call for applications for 10 fellowships available in the 2002 AAA University Fellowship Program.

AAA Directed University Research

- Contract extensions were initiated for Directed University Research at the University of Michigan, UC-Berkeley, and UT-Austin.

Technical Progress

Technical progress of ongoing investigations by direct university research projects is reported under appropriate technical areas (e.g., Transmutation Science). Some technical progress made under the UNLV program has been reported separately (e.g., quarterly progress reports by primary investigators).

5.3 Collaborations

Scope

There is great potential for beneficial international collaborations, with more than a dozen nations currently evaluating nuclear waste partitioning and transmutation. The AAA Program, primarily through the technical community, has informal contacts with many of these programs; however, formal international collaborations, which are in the best interests of the AAA Program, must be carefully developed so as to avoid over-commitments or other programmatic challenges. The scope of collaborative activities include the following:

- Participation in technical collaborations with the French CEA in developing technologies related to materials, fuels, physics, safety, and a proposed accelerator-driven test facility. Also under discussion are separations, accelerator technology, and systems.
- Participation in a Working Party on Partitioning and Transmutation (WPPT) under the auspices of the OECD/NEA (Organization for Economic Cooperation and Development/Nuclear Energy Agency).

Other collaborative efforts under consideration include work by the European Union, work under the auspices of the IAEA (Austria), and work by JAERI (Japan). Several other national programs are also of interest, and discussions on collaborations need to be pursued.

5.4 Report to Congress

As a result of budget uncertainties that were not resolved until late in the quarter, much effort was spent drafting and redrafting work plans on the Report to Congress. Once the work plan was completed, a consensus was quickly developed on the format, content, level of detail, and task and writing assignments. The primary tasks required for the report include the calculation of life-cycle costs, proliferation risk, and characterization of the waste stream. Only life-cycle costs and proliferation risk are addressed here.

A review of life-cycle costing and proliferation-risk assessment methodologies indicated that a discrete, time-dependent simulation of the nuclear fuel cycle (NFC) was required for accuracy; however, this was not possible in the time allotted for analysis in FY02. Even the development of a static (equilibrium) NFC systems model was not possible. Instead, an existing equilibrium NFC systems model developed as part of the recently completed *OECD Comparative Study of P&T Approaches Using Fast Reactors (FR) and Accelerator-Driven Systems (ADS)* was modified as needed. While many of the NFC scenarios considered by the OECD effort are applicable to the current round of AAA-driven systems studies, differences do exist. These differences are reflected in the mass-balance algorithms that drive the systems model, as well as in the technological and neutronic databases. Analytical mass- and energy-balance algorithms needed to describe AAA-specific algorithms were developed, implemented, and verified; database issues will be resolved next quarter using the results from both the AAA Roadmap Study and the Multi-Tier Study. The majority of modeling effort this quarter was devoted to advancing and aligning the equilibrium OECD model with the requirements of the AAA Program.

Supplemental Analyses

A review was conducted of past efforts on nuclear-fuel-cycle assessment methodologies, various approaches to multi-criteria analysis (MCA), and a full range of proliferation metrics for possible inclusion in the AAA Program. An effort has been initiated to apply MCA to the equilibrium OECD model discussed above to combine resource, economic, waste, and proliferation metrics in a way that can be used to assess the relative merits of NFC scenarios.

The development of a time-dependent capability required for an accurate assessment of life-cycle costs and proliferation risk was initiated. Significant progress has been made in developing the NUCSim code that, in its infancy, is now able to simulate shutdown of currently operating US nuclear power plants as a function of time under various assumptions regarding the length of possible extensions of their operating licenses. Typical results are shown in Fig. 54.

Past work regarding the radiotoxicity of long-lived spallation products from various targets has been reviewed, and codes have been modified to analyze this radiotoxicity.

A preliminary analysis of a possible extension of transmutation capability has been initiated. The extension considers using mixed-oxide (MOX) fuel with a plutonium-neptunium mix instead of just Pu or all minor actinides (previous cases 1X and 2X) in a Tier-1 light-water reactor. Preliminary calculations assumed that the heavy metal in the MOX was mainly comprised of depleted U with some TRU (Pu+Np) and that the Pu and Np were recycled after each cycle and mixed with some *fresh* spent nuclear fuel and depleted U for the next cycle. After four cycles, 50% of the TRU (60% of the Pu+Np) was burned up; more cycles would yield even greater burnup. This fuel cycle would also require the use of an Am extraction step before electro-metallurgic separations to remove a majority of the Am, Cm, and lanthanides from the spent nuclear fuel mixture.

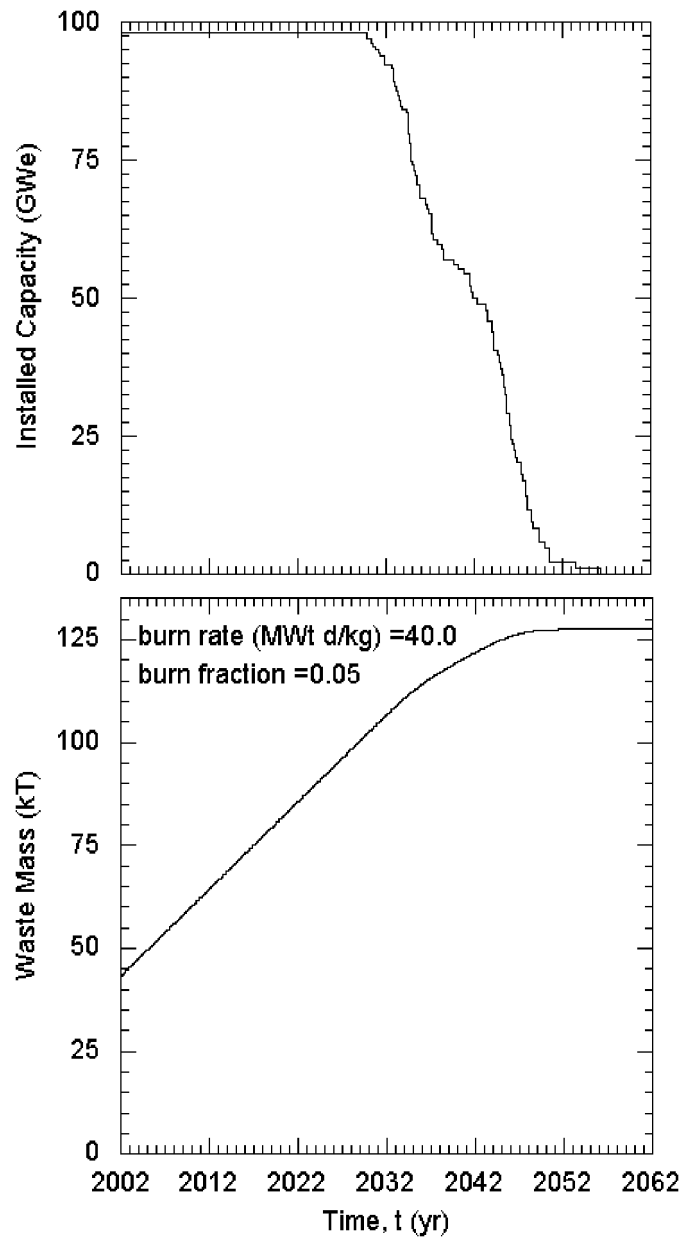


Fig. 54. Time-dependent simulation of the shutdown of the installed capacity of the present fleet of commercial reactors and the buildup of waste in cooling ponds (a 60-year plant-life is assumed).